Groundwater Recharge Modelling: Linkage to Aquifers and Implications for Water Resources Management and Policy

By

Kibreab Amare Assefa

A Thesis submitted to
the Faculty of Graduate Studies of
The University of Manitoba
in partial fulfilment of
the requirements for the degree of

Doctor of Philosophy

Department of Civil Engineering
University of Manitoba
Winnipeg

Abstract

The main goal of this research is to develop and test a groundwater recharge estimation method that can address some of the key research priorities in groundwater. In this context use is made of various modelling tools including ArcGIS^{TM}, field data (in situ observations of soil temperature and soil moisture), and soil physics as represented by a physically based vadose zone hydrologic model (HYDRUS-1D). The research is conducted in a pilot watershed in north Okanagan, Canada.

The public version of HYDUS-1D and another version with detailed freezing and thawing module are first used to investigate seasonal distribution of heat and water movement in the vadose zone. Model performance is evaluated in different scales by using field data, the gradient-based optimization algorithm of HYDRUS-1D, and ROSETTA derived prior information about soil hydraulic parameters. The latter are fitted to statistical distributions and used in Monte-Carlo experiments to assess the potential uncertainty in groundwater recharge due to model parameters. Next, the significance of the recharge estimation method for catchment scale transient groundwater modelling is demonstrated by applying uniform and variable flux boundary condition to a saturated zone transient groundwater model, MIKESHE. The results showed that the traditional uniform recharge assumption can lead to misleading decisions related to water resources management and pumping well network design.

The effect of pumping well network and the provincial Water Act on water resources sustainability are further examined in an evolving climate. The results suggest potential water resource problem in the basin, which can possibly be attributed to the previously installed pumping well network (depth and screen level), and the provincial water use policy. The findings of this study demonstrate that such problems related to inappropriate well network and water resource management can greatly be minimised with the use of the recharge estimation method developed in this study.

Acknowledgments

First and foremost, I would like to express my utmost gratitude to my advisor, Dr. Allan Woodbury. I am very thankful for his advices, critical comments, kind support and patience throughout the entire process.

I am highly grateful to Dr. Peter Rasmussen and Dr. John Hanesiak for their crucial comments on shaping my research, and for the valuable discussions at different stages of my research, to Dr. Hartmut Hollaender for his input in developing Chapter 5 and journal papers, to Kasun Nanayakkara and Idris Adelakun for the great companionship.

I would like to thank Dr. Adam Wei for offering me the opportunity to work on the "one-water" research project in collaboration with DHI-Cambridge, Dr. C. Nichol and Dr. Wei for their logistics supports, Mike, Mesfine and Getnet for their assistance in field works.

I am grateful to Dr. Sitotaw, Dr. Seifu and their families and friends for comforting me during my trying time, to all friends and family back home for taking care of all the important things on my behalf, and to Mariamawit, Luladai and Dagmawi, for all the love and joy they brought. My special thanks go to my wife Fana Gebrehiwot, Dr. Sitotaw and Belaynesh Ayine. Last but not least, I thank and honour the almighty God.

Dedication

This thesis is dedicated to my sister Dr. Birhan Amare and my mother Haymanot Gebre-egziabher (EMAYE), who respectively passed away just before and after I embarked upon this PhD journey, with all loving memories. I will always miss you!!!

Without you, the journey has been rough and tough… my heart is broken but I am doing my job, I believe you are still watching over me.

EMAYE: I would not be where I am now without your enriching love, care and unconditional support in all stages of my life…

Contents

List of Tables

List of Figures

List of Acronyms

125Fd : Number of frost days

BC MoE : British Columbia Ministry of Environment

BMP : Best Management Practice

DHI: Danish Hydraulic Institute

EPA : United States Environmental Protection Agency

GCM: Global Climate Model

GHG : Greenhouse gas

IPCC: Intergovernmental Panel on Climate Change

m a.s.l: meter above sea level

mslpna: Surface meridional velocity

O.G.L : Original ground level

p5_vna: 500 hPa V-component

p5zhna: 500 hPa Divergence

p8_u: 850 hPa U-component

p500: 500 hPa Geopotential height

p850: 850 hPa Geopotential height

p_una: 1000 hPa U-component

r500: 500 hpa relative humidity

r850na: relative humidity at 850 hPa pressure levels

rhum: Near surface relative humidity

SDSM: Statistical Downscaling Model

shum: Near surface Specific Humidity

tempna : Mean temperature at 2m

T_{min}: Minimum temperature

T_{max}: Maximum temperature

Tmax90p: Threshold value of the 90th percentile of maximum daily temperature

Tmin10p: Threshold value of the 10th percentile of the minimum daily temperature

UTM: Universal Transverse Mercator

VGM : Van Genuchten – Mualem

WSA : Water Sustainability Act

List of Appendices

Chapter 1

Introduction

1.1 Thesis Objectives

- To develop a method for recharge estimation that can address some of the key research priorities in groundwater, and to demonstrate the significance of the method for catchment scale fully saturated transient groundwater modelling.

- To evaluate the robustness of the developed method in a plot scale by looking at the effect of different parameterization schemes on soil moisture and groundwater recharge under changing climate.

- To prove the need for improved water resources management and policy for sustainable use of water resources in an evolving climate.

- To evaluate aquifer sustainability under the existing pumping well network in a strategically important watershed in British Columbia, Canada.

1.2 Research Rational and Overview of Thesis

Groundwater is the main source of direct water supply for about 40% of the world's population and the major source of irrigation water for about 50% of the global food production [Seiler and Gat, 2007]. Sustainable use and management of this crucial resource highly depends on the amount of water that actually replenishes groundwater aquifers; this is often simply referred to as recharge.

Recharge is primarily determined by precipitation. The incoming precipitation may be intercepted by plant canopies and evaporate back to the atmosphere. Part of the precipitation that reaches the ground may be stored in depressions, infiltrate to the soil and/or runoff depending on the rainfall intensity and land cover. The infiltrated water might be used by plants and eventually transpire to the atmosphere or it may continue seeping into deeper soil layers to become recharge. There can be no question that recharge quantities are probably the most important quantities for groundwater budgets. However, recharge estimation is a very difficult task [Scanlon et al., 2002] and determined values are often associated with a high degree of uncertainty. This chapter summaries some of the outstanding issues in groundwater research related to recharge and sets the stage for all of the research contained in this thesis.

Generally, there are four methods to evaluate recharge: (i) direct measurements, (ii) derivation from the water budget, (iii) groundwater table fluctuation (purely analytical), and (iv) numerical and analytical methods related to infiltration processes. Direct

measurements often rely on point measurements using lysimeters, isotopes, and tracers or on catchment scale by stream gauging [e.g. Lerner et al., 1990; Scanlon et al., 2002]. However, direct methods are susceptible to measurement errors and spatial variability, and are often limited by their cost [Jyrkama et al., 2002]. Recharge may be derived from the water budget if other components in the hydrologic cycle are known with sufficient accuracy. These methods are often used for studies where meso to large scale area recharge is needed on a gridded basis (e.g. the river Elbe basin, Kunkel and Wendland [2002]). However, these estimations are generally highly uncertain at the local scale [Varni and Usunoff, 1999]. Groundwater table fluctuation is another widely applied method in basins where observation wells are available. However, this method comprises a high uncertainty due to inaccuracies in porosity estimation especially when working in (semi-) conducting aquifers [Hollaender et al., 2009b]. Analytical and numerical methods, on the other hand, intend to predict the soil water movement. The first approach mainly started before the 1990s. For instance, Gardner [1962] showed that for water contents above field capacity the discharge out of a soil column is roughly proportional to the square of the water content. Although similar water balance models such as the Hydrologic Evaluation of Landfill Performance (HELP) code are still in use [Liggett and Allen, 2010; Jyrkama and Sykes, 2007], they are known to be less accurate particularly in semi-arid and arid regions [Scanlon et al., 2002]. HELP has been cited by various comparative studies [Loukili et al., 2008; Khire et al., 1997; Gogolev, 2002] mainly for its overestimation of the ‘true’ recharge. Chapters 2, more fully reviews the pertinent literature related to the research work and focuses on unsaturated zone processes.

This thesis develops and tests a new methodology for recharge estimation (see esp. Chapter 4). In this context use is made of various modelling tools including ArcGIS [ESRI, 2011], field data (in situ observations of soil water content and soil temperature), and soil physics as represented by a physically-based finite element code (HYDRUS-1D) [Simunek et al., 2005]. This particular combination of codes and approaches represents a novel way forward to better represent the land surface contributions, particularly in an evolving climate (see Chapter 5). To the writer's knowledge, such an approach of combining all these facets has not been attempted before.

The Okanagan Basin is noted as having the lowest supply of water per capita in Canada [Summit Environmental Consultants, 2010]. Yet, water demand is anticipated to increase in the future due to population growth and agricultural development [Van der Gulik and Neilson, 2008]. The water resource problem in the basin is further complicated by the provincial water policy which considers surface and groundwater as separate water sources (B.C. Reg. 204/88 O.C. 889/88). The north Okanagan valley is selected here as a pilot watershed to investigate the outstanding water resource issues because of its diverse topography and complex groundwater aquifers as well as the significant variations in climate, land covers, and soil type (Chapter 3).

The question of soil heterogeneity and uncertainty in soil hydraulic parameters is one of the known problems in hydrology. For instance, a recent study by Hollaender et al. [2009a] has conducted a priori water budget modelling of a small artificial catchment using ten different modellers and hydrological models. The recharge estimates were

generally not close to one another. One major problem in the modelling attempts by the different modellers was related to the definition of soil hydraulic parameters and the soil heterogeneity within the catchment. To address the problem of heterogeneity and to estimate the uncertainty of recharge estimations, this study has evaluated water movement in the vadose zone using ROSETTA derived and calibrated soil hydraulic parameters at plot scale (Chapter 5). The motive here is to evaluate the reliability of ROSETTA derived parameters for plot scale vadose zone hydrologic modelling. To this end, the impact of model parameterization on soil moisture and groundwater recharge is evaluated by using the historical climate data. While the conclusion derived from the past water movement modelling results can be used to comment on the performance of the ROSETTA derived soil hydraulic parameters, an additional effort is expended to verify the results under different climate data.

The verification attempt requires synthesising future climate data necessary to force the vadose zone hydrologic model (HYDRUS-1D). To this end, daily climate data (precipitation, minimum temperature and maximum temperature) are synthesised by using predictor variables from a Global Climate Model (GCM) known as the Hadley Center Coupled Model, Version 3 (HadCM3). Note here that the use of GCM in Chapter 5 evolves out of the basic objective of the chapter, namely that evaluating the robustness of the recharge estimation method and government soil data for plot scale vadose zone hydrologic modelling. The downscaled climate scenarios are then forced to two versions of the vadose zone hydrologic model (HYDRUS-1D) and multiple runs are completed. The two versions of HYDRUS-1D are developed using ROSETTA derived soil hydraulic

parameters, and a different set of parameters derived from calibration. While the model outputs (i.e., recharge projections) are used primarily to verify the reliability of the government soil data for plot scale hydrologic modelling, the analyses can be exemplary to show the benefit of the groundwater recharge estimation method for climate change studies. Note that the climate model used in here is one of the major GCMs in the IPCC Third Assessment Report [IPCC, 2001]. HadCM3 has also been successfully used in various studies in the Okanagan Basin [e.g., Toews and Allen, 2009; Merritt et al., 2006]. However, there are several other GCMs, the most common models include [Sivakumar, 2011]: CM2.1 (A coupled general circulation model developed at the NOAA Geophysical Fluid Dynamics Laboratory in the United States), CCCma CGCM3 (Canadian Center for Climate Modelling and Analysis Coupled Global Climate Model), ECHAM5 (Max Planck Institute of Meteorology Model, Version 5), NCAR-CCSM (National Center for Atmospheric Research Community Climate System Model), PCM1 (National Center for Atmospheric Research Parallel Climate Model). Each of these models has its own limitations and advantages, and may also give importance to specific climate processes [Sivakumar, 2011]. However, processes in the climate system are often chaotic in nature that exclusion of a single factor can significantly affect GCM outputs [Sivakumar 2009]. Thus, selection of the best model among the various GCMs remains to be a challenge [Sivakumar, 2011]. In this regard, various climate change studies tend assume that the skill of GCMs in reproducing future climate is the same [e.g., Woldemeskel et al., 2012]. Other studies attempt to introduce weights to account for varying accuracy of GCMs prediction skills based on the past accuracy of GCMs [e.g., Hawkins and Sutton, 2009]. However, the past accuracy of GCMs may not be repeated

for future climate conditions [Power et al., 2012; Jun et al., 2008]. The GCM selection attempt is further complicated by lack of an accurate "GCM skill measurement framework" and limitation of length of verification data [Woldemeskel et al., 2012]. To this end, typical climate change studies attempt to understand the impact of climate change by using multiple GCMs and emission scenarios [e.g., Merritt et al., 2006; Toews and Allen, 2009; Déqué et al., 2007]. The study by Déqué et al. [2007], which was aimed at identifying the respective role of the various sources of uncertainties (e.g., GCMs and SRES scenarios), reports that the uncertainty due to GCM scenarios is generally larger than the other sources of uncertainties such as the SRES scenarios. IPCC [2001] also suggest to using at least three GCM outputs before making conclusions on climate change studies [IPCC, 2001].

The research in Chapter 7 of this thesis requires the use of multiple GCM outputs as it is aimed at assessing the water resources potential of the basin with respect to the provincial water use policy. Note that the British Columbia (B.C.) water act has conservatively focused on surface water resources only without regulating groundwater extraction from shallow and deep aquifers (B.C. Reg. 204/88 O.C. 889/88). The implication of the water policy on water resource sustainability is assessed using four GCM scenarios with high (A2), medium (B2) and low (B1) emission scenarios [Section 2.2.2]; the third generation Canadian global coupled model (CGCM3), HadCM3, CM2.1, and ECHAM5. The climate data were prepared by Neilsen et al. [2010] using a statistical downscaling algorithm called "TreeGen" [Stahl et al., 2008]. Van der Gulik et.al [2010] reported that these GCM scenarios provide a wide range of scenarios to examine a number of possible

impacts of climate change in the Okanagan. Note also that all of these models have been successfully used in previous climate change studies in British Columbia (e.g., CGCM3 and HadCM3 in Toews and Allen [2009]; ECHAM5, CM2.1, and HadCM3 in Flower et al. [2013]). The consistency of the aforementioned GCM scenarios in predicting future events is evaluated in Chapter 6 before applying them for hydrological assessment in MIKESHE (Chapter 7). MIKESHE is a fully integrated hydrologic model that can simulate surface and groundwater processes [Abbott et al., 1986]. In addition to climate change scenarios, potential changes in hydrological model parameter distributions and sources and sinks in groundwater aquifers are considered in conducting the hydrological assessment. Model outputs are then analyzed to examine water resources sustainability and the provincial water use policy. It is however important to note that the four GCM scenarios used in this thesis cannot cover the whole spectrum of values for the hydrological variables of interest. Therefore, continuous experimentation with multiple GCM scenarios is needed to better understand the water resources challenges in the basin.

Chapter 8 is the final synthesis chapter; it presents and summarizes the major findings of the thesis.

Chapter 2

Literature Review

2.1 Modelling Subsurface Processes

2.1.1 Groundwater Recharge Modelling

Accurate representation of groundwater recharge in groundwater models is necessary for effective water resources management. For example, the current water resource regulation policy in British Columbia, Canada, is designed for surface water sources without considering groundwater storage (details on provincial water use policy are discussed in Chapter 7). However, groundwater and surface water are in continuous dynamic interaction. This interaction predominantly occurs as discharge of groundwater to surface water and recharge of groundwater by surface water [Winter, 1999]. Note that recharge has generally been defined as soil water in excess of the soil moisture deficit and evapotranspiration [Lerner et al., 1990]. However, all the excess soil water does not necessarily reach the saturated zone due to the storage property of the vadose zone or

because the groundwater system may not be able to accommodate additional recharge. For example, the infiltrated water might be obstructed by semi pervious materials and drain as lateral subsurface flow [De Vries and Simmers, 2002]. In cases of shallow aquifers on the other hand, recharge may lead to local seepage discharge by initiating a rise of the water table; and /or the recharge that joins the groundwater storage might subsequently be extracted by evapotranspiration [De Vries and Simmers, 2002].

Recharge may be estimated by various methods. Frequently used techniques include direct measurement by lysimeters, tracer techniques and stream gauging [Lerner et al., 1990]. Recharge may also be estimated using temperature logs [Ferguson et al., 2003; Vandenbohede and Van Houtte, 2012]. However, these methods are susceptible to measurement errors and spatial variability, and are often limited by their cost [Jyrkama et al., 2002]. Groundwater models may also be used to estimate recharge if other components in the hydrologic cycle are known to sufficient accuracy. However, as groundwater hydraulic parameters are also highly uncertain, recharge is often crudely estimated as a lumped fitting parameter together with other uncertain parameters during calibration [Varni and Usunoff, 1999; Ping et al., 2010]. Consequently, it can be argued that an improved calibration can be achieved only if known values of recharge can be supplied as input to a groundwater model. In recognition of this fact, recent studies in the Okanagan Basin, and other parts of North America, have used the Hydrologic Evaluation of Landfill Performance [HELP] code for recharge estimation [Jyrkama et al., 2002; Liggett and Allen, 2010; Toews and Allen, 2009; Jyrkama and Sykes, 2007]. However, water budget models such as HELP [Schroeder and Ammon, 1994] are known to be less

accurate particularly in semi-arid and arid regions, because recharge in these regions is smaller than the other water balance components and thus the recharge term in the water balance equation accumulates the errors in all the other terms [Scanlon et al., 2002]. HELP has further been found in various comparative studies [Loukili et al., 2008; Khire et al., 1997; Gogolev, 2002] to estimate the 'true' recharge. Besides, none of the previous studies that used HELP for recharge estimation attempted to verify the performance of their model.

2.1.2 Recharge and Transient Groundwater Modelling

Water movement in the groundwater system is generally affected by three factors [Winter, 2001]: Climate, topography as a medium of infiltration from the land surface to the groundwater system, and geologic framework particularly in deep aquifers. Climate plays a significant role, together with the other two factors, in choosing an appropriate upper boundary condition in groundwater models. In humid climates, where high precipitation and water content are expected, the geologic conditions constrain the rate of recharge. As a result, constant head boundary condition may be represented in groundwater models. However, this type of boundary condition may lead to significant over estimation as it has an implied assumption of infinite water source with constant water table. On the other hand, climate and topography determine the available infiltration for recharge in arid regions where precipitation is generally low. Subsequently, specified flux should be supplied as upper boundary condition. Indirect recharges are, however, commonly represented by using mixed boundary conditions which link an externally specified head through a hydraulic conductivity to the head in

the aquifer. In this type of boundary condition, the direction of the boundary flux is determined in the model in response to the position of water levels. The interaction of the nature between surface water features and groundwater is formulated based on the well-known Darcy's law [McDonald and Harbaugh, 1988]. This involves the hydraulic conductivity of the medium linking the surface water feature and the groundwater, and the head difference between the two bodies - and such is the bases for the river-aquifer flow calculation in the MIKESHE saturated zone groundwater model [Abbott et al., 1986]. MIKESHE is a fully integrated hydrologic model that can simulate all the major land-based water balance components such as evapotranspiration (ET), overland flow, snow melt, channel flow, unsaturated flow, and saturated zone groundwater flow. It can also be dynamically linked with a hydrodynamic surface water model, MIKE 11, for a complete representation of the hydrologic system [DHI, 2007].

2.2 Climate Change

2.2.1 General

Climate comprises the statistics of precipitation, temperature, humidity, atmospheric pressure, wind and other meteorological variables in a certain region of interest over long periods. Change in climate is caused by various natural processes and anthropogenic activities within the Earth's environment. Until the industrial revolution (a period from about 1760 to sometime between 1820 and 1840), natural processes related with solar variations, circulation of oceans and volcanic eruption were considered the sole causes of climate variability [Alfonso et al., 2004]. After the industrial revolution however, the

increasing atmospheric concentration of greenhouse gases due to anthropogenic activities were found to be the primary causes of global warming [IPCC, 2001]. This finding was further validated by Meehl et al., [2004] who evaluated the relative contribution of natural and anthropogenic forcing to global warming. The results showed that greenhouse gases are in fact primarily responsible for global warming. A recent review paper by Sivakumar [2011] presented that the global atmospheric concentration of carbon dioxide, which already increased by about 35% from the pre-industrial era value of about 280 ppm, is still increasing at an average rate of 0.5% per year. Among others, Miller et al. [2005] have also advised that greenhouse gas emissions will likely continue to aggravate global warming for the next several decades. Thus, impacts of climate change need to be properly addressed in water resources studies.

2.2.2 Global Climate Models and Emission Scenarios

Global climate models (GCMs) have been developed to simulate the present climate and predict the future by representing various earth systems [IPCC, 2001]. The modelling processes include analysing the magnitude and direction of feedback processes in the atmosphere, oceans, land surface and sea-ice [IPCC, 2001]. One example of this is the ice-albedo feedback in which warming tends to decrease ice cover, resulting in increased amount of solar energy being absorbed, and hence increased warming. The description of such processes and the various Earth systems in climate models is conducted by using different models. Atmospheric General Circulation Models (AGCM) and Oceanic General Circulation Models (OGCM) are the major building blocks of GCMs. For consistency among various GCMs (see Chapter 1), the IPCC (Intergovernmental Panel on

Climate Change) has defined four emission scenarios as reasonable pathways of greenhouse gases development [IPCC, 2000]. The emission scenarios provided by the Special Report on Emissions Scenarios [SRES] are: A1 which represents fast economic and population growth with rapid and more efficient technological change - population is assumed to decline after mid-century; A2 which assumes high population growth, slow economic and technological development ; B1 assumes population growth that peaks in mid-century with rapid changes in economic structures toward a service and information economy; B2 intermediate population and economic growth. Note however that the future levels of atmospheric concentration of trace gases depend on several factors that may not even be foreseen at the present time (e.g., assumptions about the rate of population growth, technological and structural change) [Sivakumar, 2011]. Nonetheless, one or more SRES scenarios are typically used in climate change studies despite the uncertainty in the underlying fundamental assumptions [Sivakumar, 2011].

2.2.3 Climate Change and Water Resources

It is well known that climate change impacts the water budget, and thus nearly all aspects of human activities such as water demand and supply, agricultural productivity, extreme weather events, and so on. Although exact predictions of these impacts are difficult, the overall worldwide impacts of climate change on water resources are projected to be undesirable [Sivakumar, 2011]. For example, Kleinen and Petschel-Held [2007] have projected that, by the 2080's, up to 20% of the world's population that live in river basins are likely to be at increased flood risk. Several other studies [e.g., Pancura and Lines, 2005; Kundzewicz et al., 2008] have also suggested significant increases in the frequency

and magnitude of extreme events such as floods and droughts. These findings and the recent intensifications in climate extremes around the world have put climate change studies at the forefront of scientific research today [Woldemeskel et al., 2012; Towler et al., 2010; Obeysekera et al., 2011].

Typical studies of climate change and hydrological change rely on hydrologic models [Merritt et al., 2006; Toews and Allen, 2009; Jyrkama and Sykes, 2007]. However, hydrological models, like any other model, are simplified representation of the reality, and can generally be classified in to three-groups based on the underlying physical processes [Refsgaard, 1996], namely physically based, conceptual, and Black Box. The former are designed to describe the natural system using mathematical formulations of the fundamental physical processes. Such models attempt to use physically significant parameters that can be evaluated by independent measurements [Refsgaard, 1996]. On the other hand, conceptual models - also known as Grey Box models - are developed on the basis of physically sound structures, but the physical significance of model parameters is not usually quite clear that they have to be determined from calibration. The third group of hydrological models, empirical or Black Box, are developed based on analysis of concurrent input and output time series without consideration of the physical processes.

This thesis utilizes physically based hydrologic models. Note however that, lack of sufficient input data and model parameters may always limit to fully implement the discussed concept of physically based models. Data in hydrological models are typically

intrinsically deterministic (e.g., geological formations). However, their properties (parameters) are usually observed at only few locations despite the fact that they exhibit a high degree of spatial variability. Physically based models may also introduce errors due to one or more of the following structure related reasons [Abbaspour, 2008]: a) processes occurring in the watershed but not included in the model, b) processes that are included in the model, but their occurrences in the watershed are unknown to the modeller, and c) processes unknown to the modeller and not included in the model either.

In the use of hydrological models for climate change studies, additional uncertainty is introduced due to scale mismatches between GCMs and hydrological models [Wilby et al., 2002] – notwithstanding the inherent uncertainties in GCMs and SRES scenarios (Section 2.2.2). GCMs generally provide a reliable estimate of future climate change, particularly at continental scales and above [IPCC, 2007]. However, they are restricted in their usefulness for catchment scale applications due to their coarse spatial resolution. Typical GCM resolutions are between 1 and 5 degrees in latitude or longitude, for example the Hadley Centre model HadCM3 uses 2.5° in latitude by 3.75° in longitude [Gordon et al., 2000]. The problem of scale mismatches between GCMs and hydrological models is typically minimised by using dynamical or statistical downscaling techniques. The former involves the use of Regional Climate Models (RCMs) nested within a global-scale model at a horizontal resolution close to that of watershed models [Xu, 1999]. RCMs are, however, limited in use mainly because of their computational cost [Hay and Clark, 2003]. On the other hand, statistical techniques can provide reliable results with minimum requirements in computing resources [Hay and Clark, 2003]. Statistical

methods are developed by using empirical relationships between atmospheric predictor variables and ground station variables (predictands) [e.g., Schoof and Pryor, 2001]. The classifications and detailed descriptions of statistical downscaling methods can be found in Fowler et al. [2007]. A regression based downscaling technique called Statistical Downscaling Model (SDSM) [Wilby et al., 2002] is commonly used in climate change impact assessment of hydrological processes [Chen et al., 2011; Gebremeskel et al., 2004]. The assumption here is that the statistical relationship formulated under the observed climate conditions would remain valid under the future climate conditions, and this remains one of the known limitations in statistical downscaling techniques [Fowler et al., 2007].

The above points indicate the existence of too many uncertainties in each step of the modelling hierarchy, starting from GCM, to emission scenarios, to downscaling and hydrological modelling. In an attempt to account for some of these uncertainties, climate change impact studies typically use multiple GCMs and SRES scenarios [e.g., Flower et al., 2013; Toews and Allen, 2009; Déqué et al., 2007].

In summary, the knowledge gaps indicated in this chapter, particularly regarding recharge estimation and water use policy (Section 2.1.1) plus the presented theories have prompted me to: i) develop a method for recharge estimation that can address some of the key research priorities in groundwater (Chapter 4), ii) evaluate the robustness of the developed method on a plot scale by looking at the effect of different parameterization schemes on soil moisture and groundwater recharge under changing climate (Chapter 5);

iii) to conduct preliminary assessment of climate change impacts on extreme weather events (Chapter 6); iv) and assess yield of groundwater aquifers under changing climate, evaluate water resource sustainability under the existing pumping well network conditions and provincial water use policy (Chapter 7).

Chapter 3

Study Area and Data

3.1 The Deep Creek Watershed

The Okanagan Valley is situated in the semi-arid southern interior of British Columbia. Deep Creek is one of the many watersheds located in the Northern part of the Okanagan valley approximately between 334538 and 348739 m (latitude) and 5577752 and 5611646 m (longitude). It covers about 245 km^2 and consists of a relatively narrow flat valley bottom bounded by undulating mountain. The elevation of the bottom part of the basin ranges between 340 – 520 meters while upper part ranges from 370 – 1620 meters above sea level. Two small urban areas, Armstrong and Spallumcheen are located in the watershed [Figure 3-1].

The Okanagan valley is selected as a pilot watershed because of its diverse topography and complex groundwater aquifers as well as the significant variations in climate, land

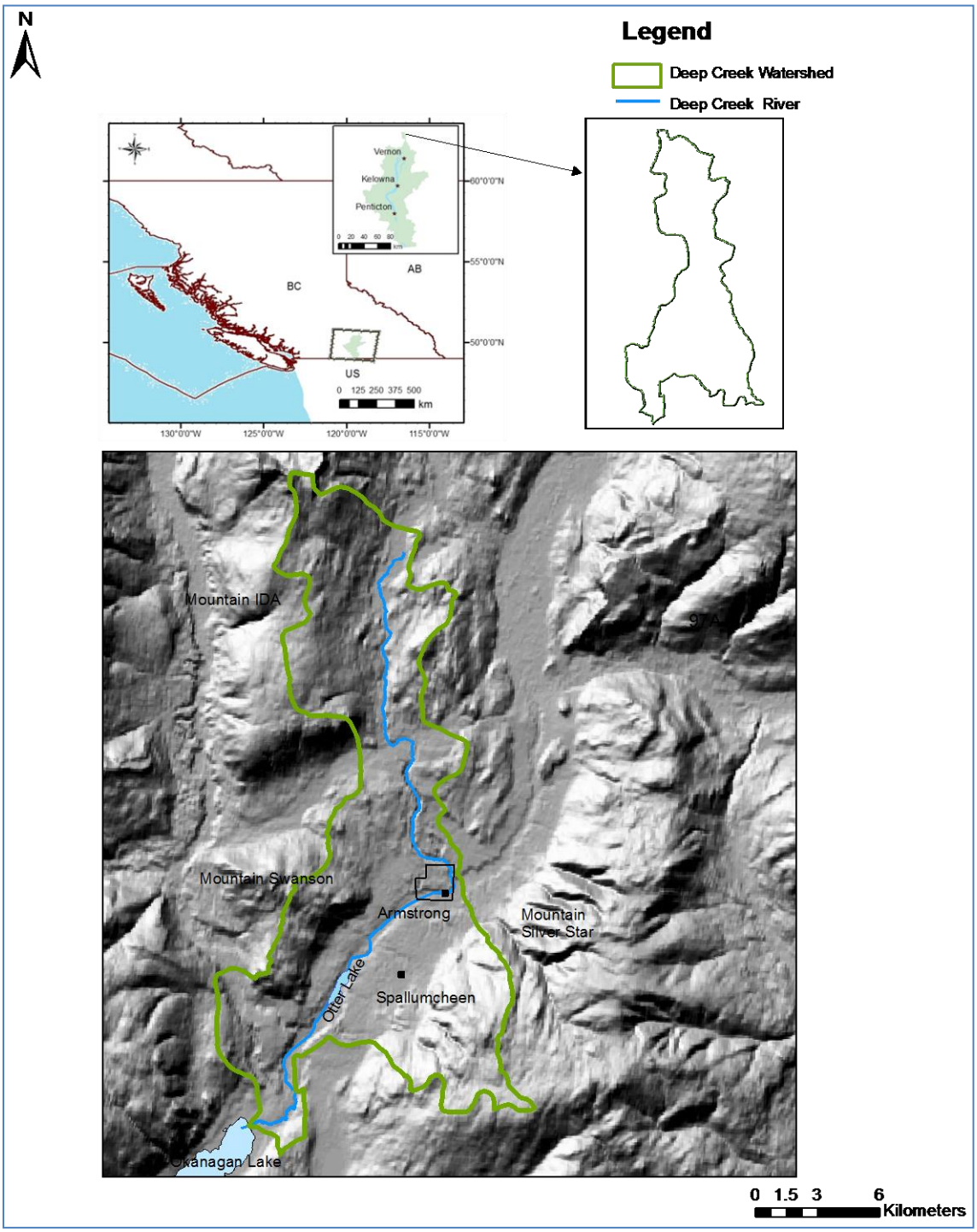

Figure 3-1 Location and topography of study area

covers, and soil type. The complex nature of the watershed provides an ideal environment to evaluate and test the robustness of the method developed in this study, and to better demonstrate the need to consider groundwater-surface water interaction before devising water resource management strategies.

3.1.1 Climate Data

A climate data set was prepared in gridded format for the entire Okanagan Valley through collaboration between Environment Canada, Agriculture and Agri-foods Canada, the British Columbia Ministry of Agriculture, and the University of Lethbridge as part of a basin-wide assessment of agricultural irrigation requirements [Neilsen et al., 2010]. The gridded data was prepared by making use of meteorological data from various sources such as the Canadian Daily Climate Data [CDCD] [Environment Canada, 2002] and data from other weather data networks including the BC Environment Snow Pillow stations; BC Ministry of Transportation Highways Network and the BC Ministry of Forests Fire Weather Network. The data acquired from the above sources were used to generate basin-wide 500 m × 500 m gridded surfaces using a GIS interpolation methodology [Neilsen et al., 2010]. Figure 3-4 shows the location of the Environment Canada stations within the study watershed. Note however that the gridded climate data was prepared by making use of additional data from the aforementioned sources. In total, data from 182 stations were used [Neilsen et al., 2010]. The quality of the climate data set may be improved, in the long run, by installing additional weather stations in the basin. The dataset are stored in a standard ESRI ASCII grid file format using single precision values, and consists of 46 years (1960 to 2006) of daily minimum, maximum temperatures, precipitation and

potential evapotranspiration. The latter was calculated using the Penman-Monteith method [Monteith, 1965]. Hence, the climate data for study area are contained in a total of 68,631 files (the product of the number of variables and number of days in 47 years). Time series data are extracted from this database using a MATLAB code and the values are assigned to each grid (500 m × 500 m) of the watershed in ArcGIS ™. These data are used to represent the spatial distribution of precipitation and evapotranspiration in the study watershed. Spatial and temporal analysis of the extracted climate data is conducted. Based on this analysis, long term average annual precipitation and potential evaporation over the Deep Creek watershed is estimated at 496.5 ± 77.9 mm and 749.6 ± 23.8 mm respectively.

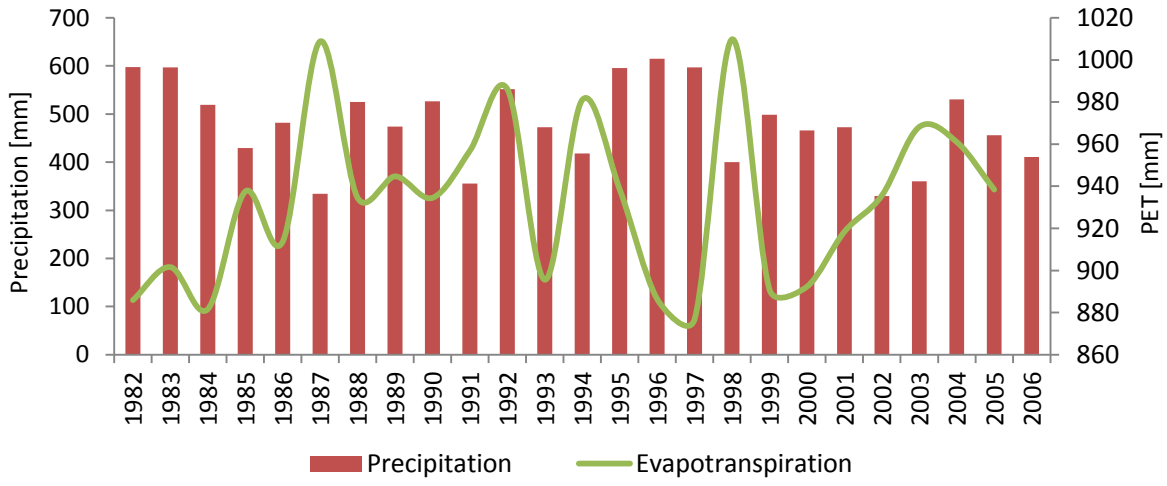

Figure 3-2 Annual precipitation and potential evapotranspiration (PET)

The large standard deviations indicate the fact that the climate data exhibit large spatial variability throughout the watershed. Next, the spatially variable climate data are prepared to be input to the HYDRUS-1D code at different areas of interest in the watershed. Daily weather data (precipitation and PET) are used in HYDRUS-1D. More coarse time averaging of weather data (weekly or monthly) generally leads to lower recharge estimates. The climate data are further analysed by aggregating the spatially averaged daily data into annual values. Average annual precipitation and evapotranspiration plots are shown on the same graph [Figure 3-2]. Seasonal proportion of rain/snow is estimated based on climate data from environmental Canada station known as Vernon North [Table 3-1].

In addition to that shown in the temporal analysis [Figure 3-2], evapotranspiration is also calculated here by using the Hargreaves formula [Samani, 2000]. This method is integrated to HYDRUS-1D to calculate potential evapotranspiration (ET0) with minimal user input: minimum temperature and maximum temperature. The long term average annual evapotranspiration results are found to be 733.4± 35 mm/annum (Hargreaves) and 741.6±31 mm/annum (Penman-Monteith). Further comparative analysis between the two datasets showed a good agreement with high degree of correlation estimated at $r \approx 0.99$ [Figure 3-3]. This comparison shows that the Hargreaves method is worthwhile provided adequate data is available. Although the two ET0 estimates are statistically close to each other, I decided to use the gridded ET0 data for groundwater recharge modelling based on Penman-Monteith as it has a stronger physical foundation [Simunek et al., 2005].

Table 3-1 Seasonal rain/snow proportion.

	Winter	Spring	Summer	Fall
Rain[mm]	18	106	93	69
Snow[mm]	124	20	0	19
Precipitation [mm]	142	126	93	88
% (proportion of rain)	12	84	100	78

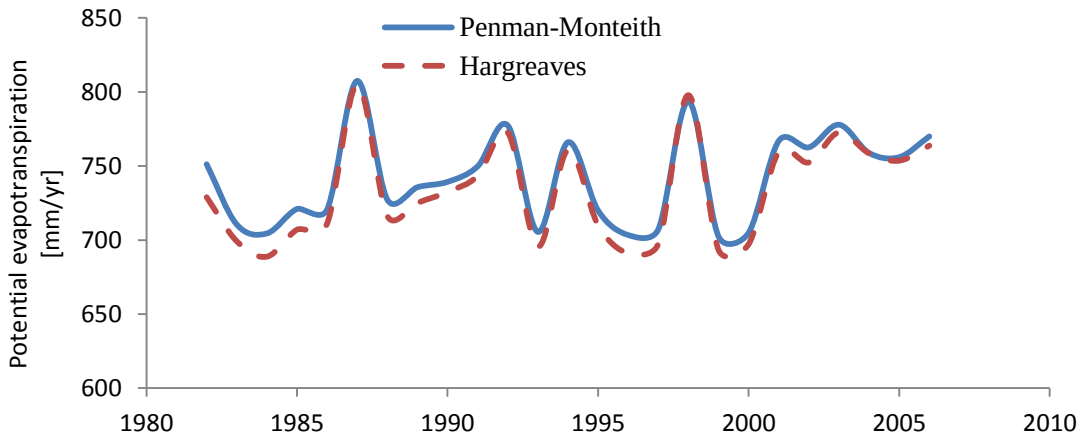

Figure 3-3 Potential evapotranspiration estimates, Hargreaves and Penman-Monteith

3.1.2 Land use Data

The majority of the Deep Creek watershed is covered by agricultural land that covers about 45% of the total watershed, followed by forests which make up 43%. The remaining 12% of the study area is covered by rangelands, bare lands, water bodies and urban areas. The land use map shown in Figure 3-4 was prepared by the Province of British Columbia [2008] and is available from GeoBC [http://geobc.gov.bc.ca/]. The information from this land use map is used to retrieve additional data required to partition potential evapotranspiration into potential evaporation and potential transpiration

Table 3-2 Monthly LAI

Land use	LAI											
	Jan	Feb	March	April	May	June	July	Aug	Sept	Oct	Nov	Dec
Forest	5.8	6.0	6.4	6.9	7.6	8.4	8.3	8.0	7.6	6.7	6.1	5.8
Rangeland	1.8	1.9	2.0	2.2	2.6	3.6	4.0	3.8	2.9	2.3	2.0	1.8
Cropland	0.8	0.9	1.0	1.1	1.8	3.7	4.8	4.2	2.0	1.2	1.0	0.9
Barren surfaces	0.0	0.0	0.0	0.0	0.0	0.0	0.0	0.0	0.0	0.0	0.0	0.0

[Section 4.2.4]. Time-variable leaf area index (LAI) values, representative of the land uses in the watershed are shown in Table 3-2. The monthly average LAI values were organized by Rodell [2010] available from the NASA data assimilation systems [http://ldas.gsfc.nasa.gov/]

3.1.3 Groundwater Levels

Ground water levels are also important for recharge modelling. Well locations in the Deep Creek watershed are shown in Figure 3-4. Detailed investigation of the wells in the watershed was conducted by the University of British Colombia [Ping et al., 2010]. According to that groundwater study, water levels, in most cases, were found to be at much deeper depths than the bottom of the soil column in most cases. For instance, soil data at the majority of the agricultural areas in the valley bottom is available only up to a depth of 90 cm, whereas the groundwater level as approximated from nearby wells is at a depth greater than 15 m. This fact was an important consideration in deciding the type of lower boundary conditions necessary for recharge modelling [Section 4.2.3].

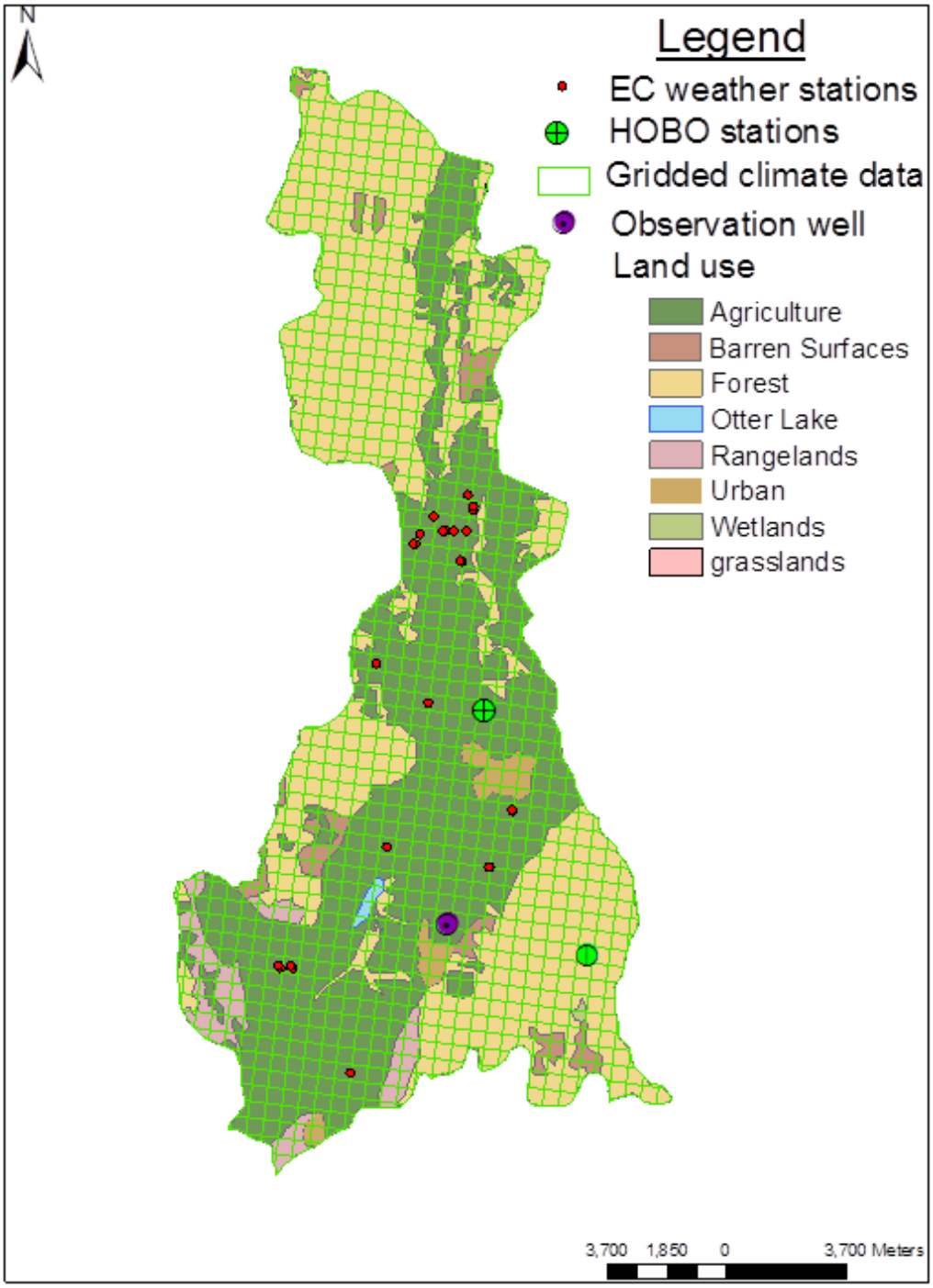

Figure 3-4 Combined inputs to HYDRUS-1D across the watershed: EC (Environment Canada], pixel size 500 m x 500 m, HOBOTM stations on Silver Star Mountain and valley bottom.

3.1.4 Soil Data

A vector data map of spatially distributed soil types was found from the Okanagan Plus Project of Agriculture and Agri-Food Canada [Kenney and Frank, 2010]. The soil map contains soil texture data that, of course, vary vertically at each grid location as well as horizontally from grid to grid. Soil codes indicated in Figure 3-5 are used to retrieve spatially varied soil texture data for soil columns of variable depth (0.6 m - 1.5 m) across the study area. The legends shown in the soil code represent soil texture data across the basin and are shown in Table 3-3.

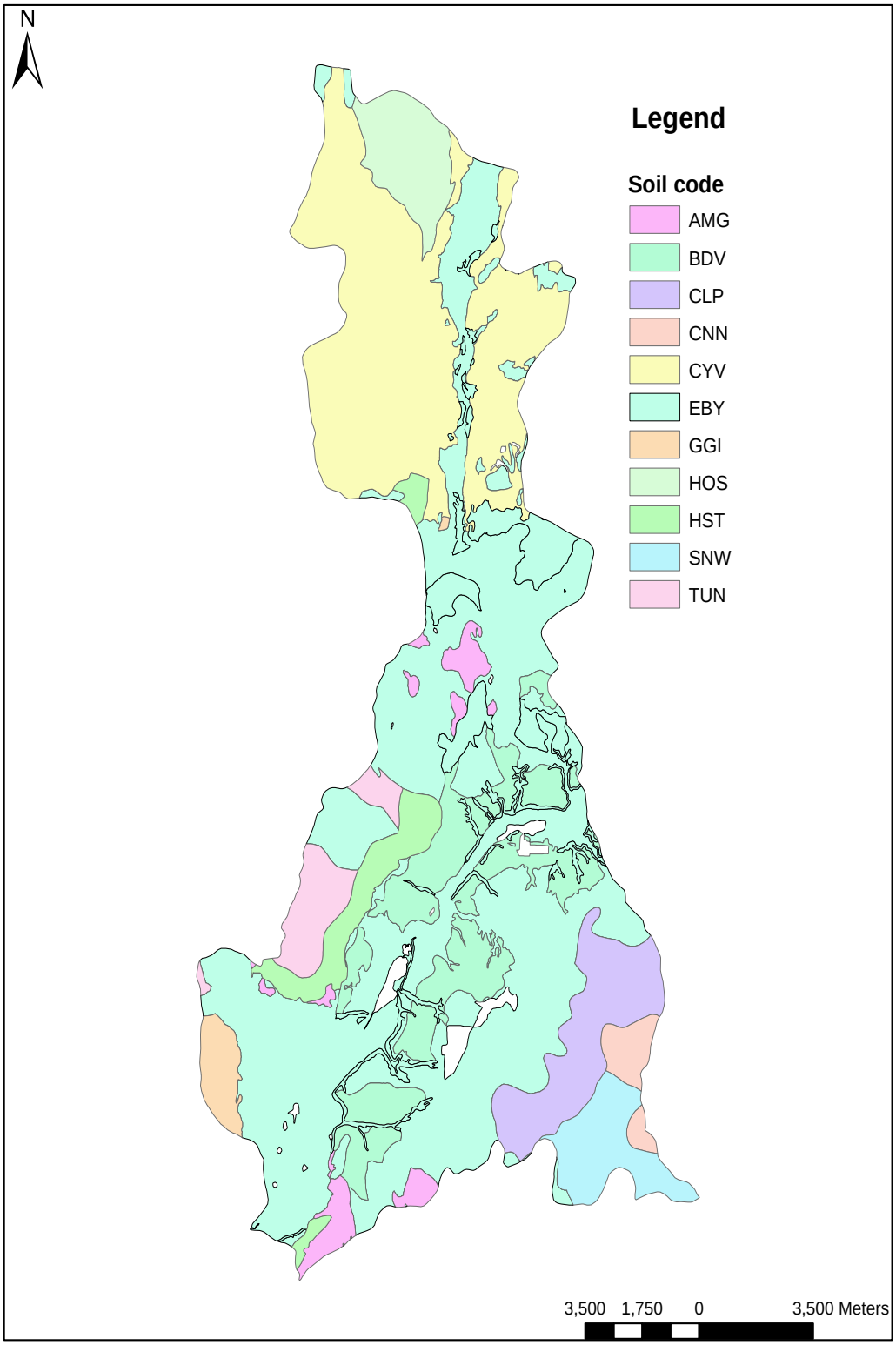

Figure 3-5 Soil map, Soil codes to retrieve spatially varied soil texture data for soil columns of variable depth (0.6 m - 1.5m) across the Deep Creek watershed.

Table 3-3 Attributes of the soil code [Kenney and Frank, 2010]

Soil Code	DEPTH [cm]	SOIL TEXTURE [%]		
		SAND	SILT	CLAY
AMG	0-18	54	36	10
	18-31	53	36	11
	31-46	54	37	9
	46-91	56	35	9
	91-126	52	39	9
BDV	0-10	5	26	69
	10-24	2	17	81
	24-39	0	18	82
	39-64	0	17	83
	64-90	1	11	88
CLP	0-10	52	38	10
	10-20	56	36	8
	20-41	57	33	10
	41-83	58	30	12
	83-135	60	31	9
EBY	0 - 15	12	68	20
	15 - 24	12	70	18
	24 - 39	10	70	20
	39 - 64	7	70	23
CNN	0 - 10	64	31	5
	10 - 24	59	33	8
	24- 38	59	33	8
	38 - 68	65	28	7
TUN	0 - 15	39	54	7
	15 - 41	37	55	8
	41 - 61	31	38	31
	61 - 110	36	55	9
SNW	0 - 10	56	39	5
	10-17	58	38	4
	17 - 33	67	28	5
	33 - 89	61	36	3

3.1.5 Field Work

While the above dataset was fundamental to derive recharge values, an additional effort had to be expended to evaluate the performance of the groundwater recharge model in the study area. To this end, two portable state-of-the art HOBO™ weather stations were installed in in the valley bottom and Silver Star Mountain of the Deep Creek watershed in the summer of 2010 and 2011 respectively. The stations at the valley bottom and mountain will be referred to as Station 1 and Station 2, respectively. The HOBO™ U30 stations have the capability to log data at a user defined time step (logging interval), set twice a day for the two stations. The single logged measurements are calculated by averaging readings at fine sampling interval of about 1 minute. Both weather stations contain plug-and-play smart sensors for soil temperature, soil moisture and climate data including temperature, radiation, wind speed, relative humidity and pressure. Trenches were excavated to install soil temperature and FDR (Frequency Domain Reflectometry) soil moisture probes. The sensors were installed horizontally into a vertical trench face to record soil moisture and soil temperature data at different depths. While the sensors at the valley bottom (Station 1) were installed at a depth of 10 and 50 cm, the ones at high elevation (Station 2) were installed at 20 cm depth. The two sites are characterised by different soil type and vegetative cover [Figure 3-4]. Information about the HOBO™ sensors is given in Table 3-4.

Table 3-4 Sensors specification

Parameter	Instrument	Installation	Range	Accuracy
Barometric Pressure	S-BPB-CM50	1 m height	600 - 1070 mbar	±3.0 mbar
Solar Radiation (Spectral Range):	S-LIB-M003 300 to 1100 nm	2 m height	0 - 1280 W/m²	± 10 W/m²
Air temperature	S-THB-M008	2 m height	-40 - 75°C	±0.13°C
Relative humidity	S-THB-M008	2 m height	0 – 100%	±2.5%
Soil temperature	S-TMB-M006	-10 cm depth -20 cm depth -50 cm depth	-40 - 100°C	±0.2°C
Water content	S-SMC-M005	-10 cm depth -20 cm depth -50 cm depth	0 - 0.55 m³/m³	±3.1%
Wind speed	S-WSA-M003	2 m height	0 – 45 m/s	±1.1 m/s

Chapter 4

Subsurface Water and Heat Movement

4.1 Vadose Zone Processes

Vadose zone processes determine the amount of water that percolates through the unsaturated zone to reach the groundwater table. It also affects the pathways of a contamination plume before it reaches aquifers. A wide range of computer programs are available to simulate water and/or heat movement processes in the vadose zone. As described in chapter 1, groundwater recharge may be estimated using analytical methods such as water table fluctuation methods and water balance based numerical models such as HELP [Ligget and Allen, 2010]. However, these methods are reported to be unreliable due to imprecision in porosity estimation and over estimation of the 'true' recharge [Loukili et al., 2008; Khire et al., 1997; Gogolev, 2002; Hollaender et al., 2009b]. On the other hand, physically based models can fully describe the natural system using mathematical formulations of the fundamental physical processes. Based on current understanding, the Richards equation for vadose zone water movement, and the Fickian-based advection-dispersion type equation for heat transport are believed to appropriately

describe the underlying physical processes. HYDRUS is one of such software package that uses the above concepts for simulating water and heat movement in the vadose zone [Simunek et al., 2005]. Besides the physical foundation of the model, other reasons for choosing HYDRUS -1D for this modelling experiment are listed below.

- HYDRUS-1D represents "the cutting edge" of research developments in the unsaturated zone hydrology. It is developed by leading scientists in the field of vadose zone hydrology. Details on the historical development and various application of HYDRUS-1D can be found in Simunek et al. [2008, 2012].

- HYDRUS-1D has been extensively verified and used by thousands of users around the world, including leading research centers and regulatory agencies (e.g., Pacific Research Center, EPA, Campbell Scientific, US Army Engineer Research and Development Center, and several universities around the world). Complete lists can be found in the HYDRUS official website [www.pc-progress.com]. Recent applications of HYDRUS for recharge calculations can be seen in Jimenez et al. [2009], Mastrociccoa et al. [2010], Kurtzman and Scanlon [2011], and Lu et al. [2011].

- HYDRUS-1D has two versions [Simunek et al., 2005; Hansson et al., 2004], which provide an ideal platform to experiment with one of the objectives of this chapter, namely that evaluating the impact of freezing and thawing on water and heat movement in the vadose zone.

The basic form of Richards equation may be described in three forms: the " ψ - based" form, the "θ -based" form, and the "mixed form" [Celia et al., 1990]. The same study by Celia et al. [1990] showed that " ψ - based" formulations are subject to large mass balance errors. On the other hand, the "θ -based" formulations have known limitations associated with the discontinuous nature of moisture content, and cannot be used in wet regions near saturation. The "mixed form" on the other hand can minimize the mass balance error without affecting modelling capability near saturation [Celia et al., 1990]. HYDRUS-1D solves the "mixed form" equation [equation 4-1] by using Galerkin-type linear finite element schemes [Simunek et al., 2005].

$$\frac{\partial \theta}{\partial t} = \frac{\partial}{\partial z}\left[K(\psi)\left(\frac{\partial \psi}{\partial z} + \cos\alpha\right)\right] - S \qquad 4\text{-}1$$

where ψ is the pressure head [L], which is a measure of the degree of suction pressure in the unsaturated zone, a variable which becomes zero when the soil pores are completely filled with water. θ is the volumetric water content [L^3L^{-3}], t is time [T], z is the spatial coordinate positive upward [L], and S is the sink term [$L^3L^{-3}T^{-1}$] and it represents water uptake, usually from root zone of a soil column via transpiration (Section 4.2.4), α is the angle between the flow direction and the vertical axis (i.e., $\alpha = 0^o$ for vertical flow, 90^o for horizontal flow, and $0^o < \alpha < 90^o$ for inclined flow). K, the unsaturated hydraulic conductivity function, is a function of the pressure head, ψ soil water retention parameters, and the saturated hydraulic conductivity, K_s [LT^{-1}].

The above equation describes water flow without accounting for the effect of vapour movement on the total water flux. However, studies have shown that vapour can have significant effect on total water fluxes in unsaturated zone of arid and semiarid regions [Scanlon et al., 2003]. Thus, vapour movement is simulated here along with the water movement and heat transport routines of HYDRUS-1D. Heat flux due to vapour flow is formulated in HYDRUS-1D as advection of sensible heat by water vapor and advection of latent heat by vapour flow [Scanlon et al., 2003; Simunek et al., 2005].

Freezing and thawing is another phenomenon that is particularly important in cold regions. In equation [4-1], soil freezing can be accounted for by using a simple snow module at the surface boundary. This module is implemented in the public domain version of HYDRUS-1D to stop seepage (lowering conductivity) in the subsurface when the soil is frozen. However, a detailed representation of the actual process requires a freezing and thawing module that can account for frozen water and ice blocking effect of pores in frozen soils. Such a freezing and thawing module was developed and coupled with equation [4-1] by Hansson et al. [2004]. An additional term that accounts for the energy stored in the frozen water was also developed and coupled with the heat transport equation of HYDRUS-1D by the same authors [Hansson et al., 2004]. The modified HYDRUS-1D code with the capability to simulate freezing and thawing processes is used here. It is hypothesised here that the detailed freezing and thawing routine of HYDRUS will not change water and heat movement simulation results in the semi-arid study area, and this is verified by comparing estimates from the two versions of HYDRUS-1D with observed soil moisture and soil temperature data.

4.2 Numerical Solution

Using HYDRUS to numerically solve the governing equations requires not only the input data set discussed in chapter 2, but also a good understanding of the following: spatial and temporal discretization, soil water retentivity and hydraulic conductivity functions, boundary conditions, and sink term estimation procedures. Given below is a brief description of each item as used in this modelling exercise.

4.2.1 Space and Time Discretization

Temporal and spatial discretization is the basis of any numerical modelling. Spatial discretization of a soil column is done vertically along soil profiles at all points of interest in the watershed. For example, Figure 4-1 shows a typical heterogeneous soil profile, about 1 meter long, along the valley bottom. The basic soil texture data for each of the five zones are obtained from the Okanagan Plus Project of Agriculture and Agri-Food Canada [Kenney and Frank, 2010]. Please see soil code 'BDV' of Table 3-3 for details on the soil textural values of each of the five zones. The required soil hydraulic parameters for each zone are determined by making use of a computer program called ROSETTA [Section 4.2.2]. The soil column is first discretized into equidistant point distributions (1 cm) by using the finite element module of HYDRUS [Simunek et al., 2005]. Further to this,

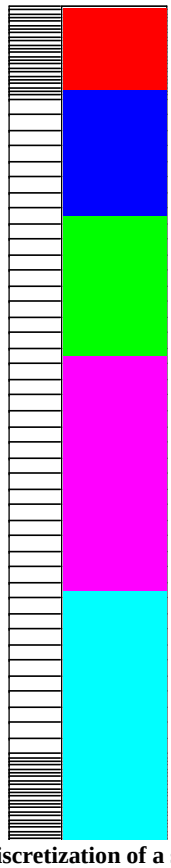

Figure 4-1 Discretization of a soil column

(Not to Scale)

finer spatial discretization (0.25 cm) is manually made in the root zone and near lower boundaries where highly variable fluxes are expected.

The temporal discretization is designed in HYDRUS to automatically vary between preselected minimum and maximum time steps. The minimum and maximum time steps selected for this study are 1×10^{-5} and 0.5 days, respectively. Details on the assumed relationship between time increments and number of iterations for convergence can be found in Simunek et al. [2005].

4.2.2 Hydraulic Retentivity and Conductivity Functions

Actual measurements of soil hydraulic properties are often prohibitally costly and time consuming to obtain. As a result, several indirect methods ranging from simple look up tables to methods with more physical foundations have been developed [Valiantzas and Londra, 2008; Kosugi, 1994; Durner, 1994]. Retentivity and conductivity functions can be formulated indirectly from empirical non-linear regression equations and/or methods with more physical foundations [Van Genuchten, 1980; Mualem, 1976]. The Van Genuchten – Mualem [VGM] model consists of five parameters: residual soil water content (θ_r), saturated soil water content (θ_s), shape parameters [α and n] and saturated hydraulic conductivity [K_S]. These parameters can be determined by making use of a computer program called ROSETTA [Schaap et al., 2001]. The ROSETTA program consists of five hierarchical pedotransfer functions [PTFs] with varying degrees of input data requirement. The PTF known as H2-C2 [Schaap et al., 2001] is used here to determine the above five parameters from measured sand, silt and clay percentages

[Kenney and Frank, 2010]. Tables 4-1 and Table 4-2 show the mean VGM parameters estimated at our experimental sites where HOBO^{TM} station #1 and station #2 are located [Figure 3-4]. It is however important to note that the H2-C2 PTF is a combination of several Artificial Neural Network (ANN) models that were each standardised to different soil types. Each ANN thus produces slightly different estimates of soil hydraulic parameters, and the resulting uncertainty is included in ROSETTA outputs. The parameters in parentheses [Table 4-1] are obtained by constrained calibration based on ROSETTA outputs (details are discussed in Section 4.3.2).

Table 4-1 Soil texture data [%] and VGM parameters at valley bottom (EBY)

Soil code/ Soil layer	Units of VGM parameters: $Q_{r,s}$ [cm^3cm^{-3}], Alpha[cm^{-1}], n[-],K_s [$cmday^{-1}$]									
	Depth[cm]	Sand	Silt	Clay	Q_r	Q_s	Alpha	n	K_s	l
1	0-15	12	68	20	0.073	0.45	0.005	1.6	15	0.5
2	15-24	12	70	18	0.071	0.45	0.005	1.6	16	0.5
3	24-39	10	70	20	0.074	0.46[0.5]	.005[.002]	1.5[1.65]	14	0.5
4	39-64	7	70	23	0.079	0.46[0.55]	.006[.004]	1.5[1.7]	12	0.5

Parameters [in parentheses] are obtained from calibration

Table 4-2 Soil texture data [%] and VGM parameters at Silver Star Mountain (CNN)

Soil code/ Soil layer	Units of VGM parameters: $Q_{r,s}$ [cm^3cm^{-3}], Alpha[cm^{-1}], n[-],K_s [$cmday^{-1}$]									
	Depth[cm]	Sand	Silt	Clay	Q_r	Q_s	Alpha	n	K_s	l
1	0-10	64	31	5	0.0319	0.3944	0.0312	1.4151	59.01	0.5
2	10 24	59	33	8	0.0374	0.3903	0.0233	1.4151	41.92	0.5
3	24-38	59	33	8	0.0374	0.3903	0.0233	1.4151	41.92	0.5
4	38-68	65	28	7	0.0357	0.3896	0.0316	1.4126	50.04	0.5

The reliability of ROSETTA has been assessed in various studies [Scott et al., 2000; Abbasi et al., 2004] which compared soil parameters derived from pedotransfer functions with those determined from model calibration. The aforementioned studies concluded that ROSETTA is a reliable and efficient method for estimating soil hydraulic properties.

On the other hand, the heat transport parameters are derived from the HYDRUS-1D database based on soil textural classes. These parameters are used to estimate thermal conductivity according to the Chung and Horton [1987] equation which is integrated into the HYDRUS-1D code. Other required inputs such as the volumetric heat capacity of the porous media were determined from the default values of HYDRUS-1D based on soil textural classes [Simunek et al., 2005].

4.2.3 Boundary Conditions

Boundary conditions (BCs) can be either system independent, such as constant flux, or system dependent. The latter refers to those conditions that depend on the external situation and the prevailing soil moisture conditions. Upper boundary conditions in HYDRUS-1D can be defined by applying either prescribed flux or prescribed pressure head boundary conditions [Simunek et al., 2005]:

$$\left|-\mathbf{K}\frac{\partial \boldsymbol{\psi}}{\partial \mathbf{x}}-\mathbf{K}\right| \leq \mathbf{E} \quad \text{at } \mathbf{x}=\mathbf{L} \tag{4-2}$$

and,

$$\boldsymbol{\psi}_{\mathbf{A}} \leq \boldsymbol{\psi} \leq \boldsymbol{\psi}_{\mathbf{s}} \quad \text{at } \mathbf{x}=\mathbf{L} \tag{4-3}$$

where E is the maximum potential rate of infiltration or evaporation under the current atmospheric conditions[LT^{-1}], and ψ_A and ψ_s are minimum and maximum pressure head at the soil surface, respectively [L]. However, it is possible that either of the conditions can be violated in the process of computation. For instance, when one of the end points of equation [4-3] is reached, the actual surface flux will be calculated using a prescribed head boundary. If at any point in time the calculated flux exceeds the specified potential flux indicated in equation [4-2], the potential value will be used as a prescribed flux boundary which results in saturation excess surface runoff on top of the soil surface. Runoff can also be simulated in HYDRUS-1D when the precipitation rate exceeds the infiltration capacity of the soil. This time-variable atmospheric boundary condition, coupled with a snow module, is implemented in the current study. The snow routine in the public domain version of HYDRUS-1D assumes that precipitation is in the form of liquid only when the air temperature is above +2 ^{o}C. When it is below -2^{o}C, precipitation is not applied as a flux boundary condition until temperatures rise above zero and snow melts [Simunek et al., 2005]. The proportion of snow water equivalent which joins the groundwater table largely depends on the antecedent soil moisture. Note also that the snow water equivalent in excess of maximum pressure head at the soil surface is simulated as runoff [Section 4.3.2].

The lower boundary condition for most of the cases in this study is taken to be "free draining" which is appropriate for the situation where the water table is far below the bottom node of the soil column. In such cases, the specific discharge rate, q, assigned to bottom nodes, is considered to be 'potential' recharge. In areas where groundwater tables

are expected to be near surface however, recharge can cause local seepage discharge due to a possible rise of the water table. Therefore, a different system dependent lower boundary which has the capability to handle "saturation excess" conditions is specified. This type of BC assumes no flux when the pressure head is negative. However, when the pressure head is zero at saturation of the lower boundary, the corresponding outflow is calculated. Hence, part of the potential recharge that disappears from the soil zone through local seepage is simulated giving a more reliable estimate of actual recharge. Details on the influence of water table depth on groundwater recharge can be found in Smerdon, et al. [2008]. On the other hand, the boundary conditions for temperature at the upper and bottom of the soil columns of all the representative points in the Deep Creek Watershed are defined as Dirichlet and Cauchy type (heat flux) respectively [Simunek et al., 2005].

4.2.4 Sink Term

A good estimate of this term is particularly important in shallow water level aquifers where water may initially contribute to groundwater storage but might later be extracted by transpiration. To better estimate this flux, a fine discretization of soil profile is implemented specifically in the root zone and lower boundaries where highly variable fluxes are expected. The advantage with variable discretization in terms of accuracy and simulation time was justified in a previous study by Carrera-Hernandez et al. [2012]. The sink term is calculated as a function of potential transpiration and the pressure head with a Feddes type uptake function [Feddes et al., 1978]. Note that, HYDRUS-1D, being a Richards equation based finite element code, allows water to move up or down depending

on the pressure head gradient. Potential transpiration flux is estimated in HYDRUS-1D from potential evapotranspiration and leaf area index. Average values of root water uptake parameters for various vegetation cover are integrated to HYDRUS-1D, and this might affect seasonal distribution of soil moisture simulation results (Section 4.3.2). The land use information discussed in Section 3.1.2 is used to derive these parameters as well as root depths at each of the various representative areas in the Deep Creek Watershed. Monthly variable leaf area index are supplied as input to the model [Table 3-2] to account for the vegetation dynamics.

4.2.5 Initial Conditions

There are two options in HYDRUS for supplying initial conditions: pressure head or moisture content. In this study, pressure head is used as initial condition for all soil materials in the flow system as it is known to exhibit lesser spatial variability than that of moisture content. The initial condition is estimated by setting the initial pressure head in Fall of 1960 and running the model for 21 years. A preliminary sensitivity analysis is conducted to test various model spin up times and their effect on pressure head at the end of each spin up period. The reason why the model spinning is initialised in Fall and run for 21 years is because soil moisture content in Fall is generally believed to be at the wilting point and soil moisture conditions and groundwater recharge are considered to stabilize after a 21 year model spin-up.

4.3 Results: Groundwater Recharge Modelling

4.3.1 Model Evaluation Using Field Data

The public version of HYDUS-1D with an empirical snow routine [Simunek et al., 2005] as well as another version of HYDRUS-1D with a detailed freezing and thawing module [Hansson et al., 2004] are first used to simulate soil temperature, snow pack and soil moisture over a one year (Dec 2010 to Dec 2011) experimental period. The recorded climate data as well as soil moisture and soil temperature data are of paramount importance in evaluating the performance of HYDRUS, with and without the freezing and thawing module. An atmospheric boundary condition and free drainage condition are imposed at the soil surface and bottom boundary of the flow domain, respectively. Model results in both cases (HYDRUS-1D with and without freezing and thawing module) are evaluated by making use of the following statistical measures: mean bias error (MBE), root mean square error (RMSE), and correlation coefficient (r).

$$MBE = \frac{\sum_{i=1}^{n}(S_i - O_i)}{n}$$

$$RMSE = \sqrt{\frac{\sum_{i=1}^{n}(S_i - O_i)^2}{n}} \qquad 4\text{-}4$$

$$r = \frac{\sum_{i=1}^{n}(O_i - \bar{O})(S_i - \bar{S})}{\sqrt{\sum_{i=1}^{n}(O_i - \bar{O})^2 (S_i - \bar{S})^2}}$$

where S_i is the simulated value, O_i is the observed value, $\bar{S}$ and $\bar{O}$ are the mean of simulated and observed values respectively, and n is the number of data point.

4.3.2 Snow Depth, Soil Moisture and Soil Temperature

Figure 4-2 and Figure 4-3 show comparative plot between the observed and simulated soil temperatures at two depths at the location of HOBO™ station # 1 (10 cm and 50 cm). A strong correlation (r = 0.97) is found between the simulated and observed soil temperature records [Table 4-3]. While the observed soil temperature records over a year study (Dec 2010 to Dec 2011) are all above zero degrees centigrade, it can be seen from Figure 4-2 that the simulated values near the surface are slightly underestimated between mid-November and the end of February. Snow depth simulations showed that the site was likely covered with snow during this period when the air temperature drop below zero [Figure 4-4]. This insulation phenomenon is known to cause bias [Hejazi and Woodbury, 2011] towards underestimation of soil temperature as indicated by the negative mass

balance error values [Table 4-3]. However, the error values obtained here are relatively closer to zero than values reported in similar studies [Hejazi and Woodbury, 2011], showing a promising performance of the model in our study area. Details on the impacts of a snow pack on soil temperature can be found in Hejazi and Woodbury [2011].

Not surprisingly, the HYDUS-1D model with the freezing and thawing module reproduced the same results as that without the freezing and thawing module. As a matter of fact, no freezing of soil profile can be expected when all the soil temperature records are above zero. Note that the snow routine of the public version of HYDRUS-1D has the capability to halt seepage (lowering conductivity) in the subsurface when the soil is frozen [Figure 4-2]. As can be seen in Figure 4-3 however, no freezing was simulated at the 50cm depth. Additional analysis conducted at a different location in the Deep Creek Watershed also showed no freezing of soil at 20 cm depth – all the simulated and observed soil temperature values were above zero.

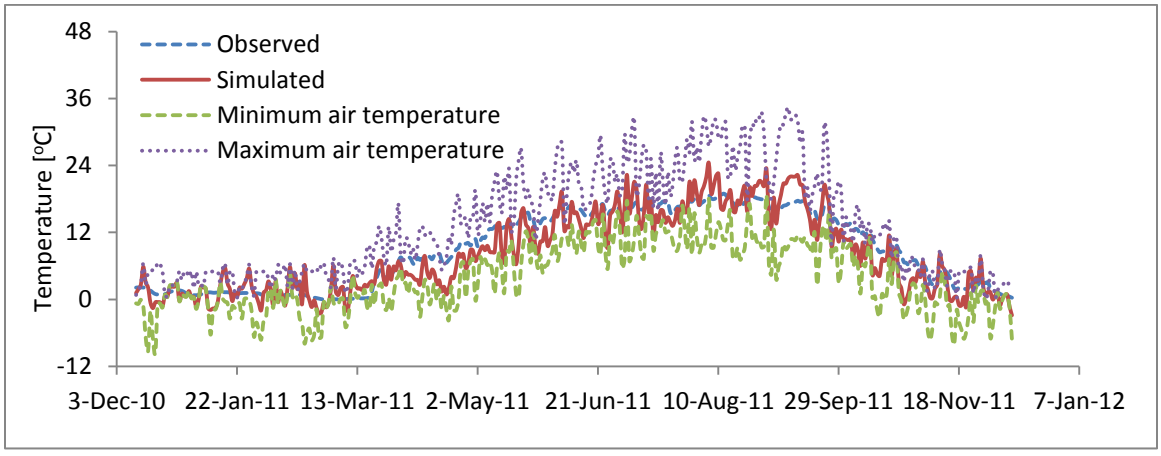

Figure 4-2 Simulated versus observed daily soil temperature at 10 cm depth, valley bottom

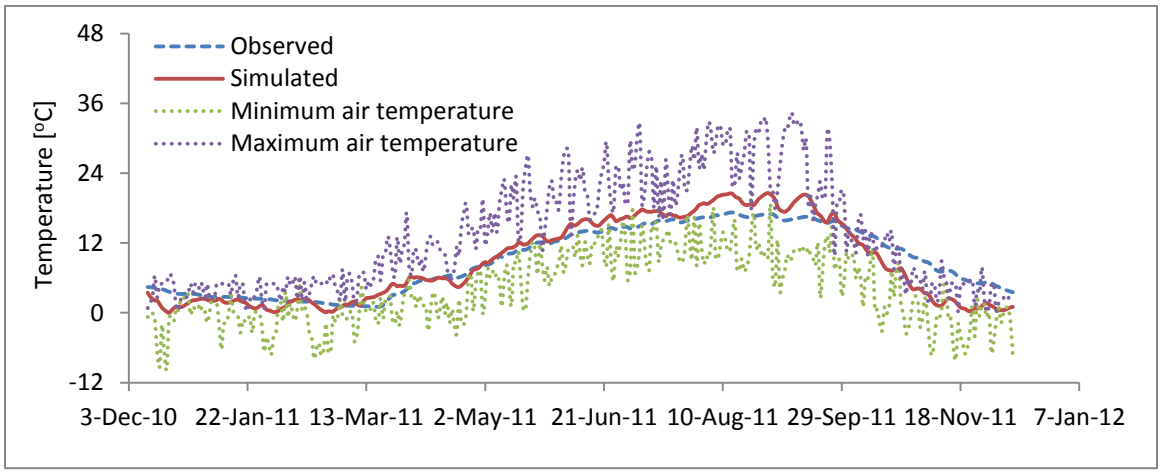

Figure 4-3 Simulated versus observed daily soil temperature at 50 cm depth, valley bottom

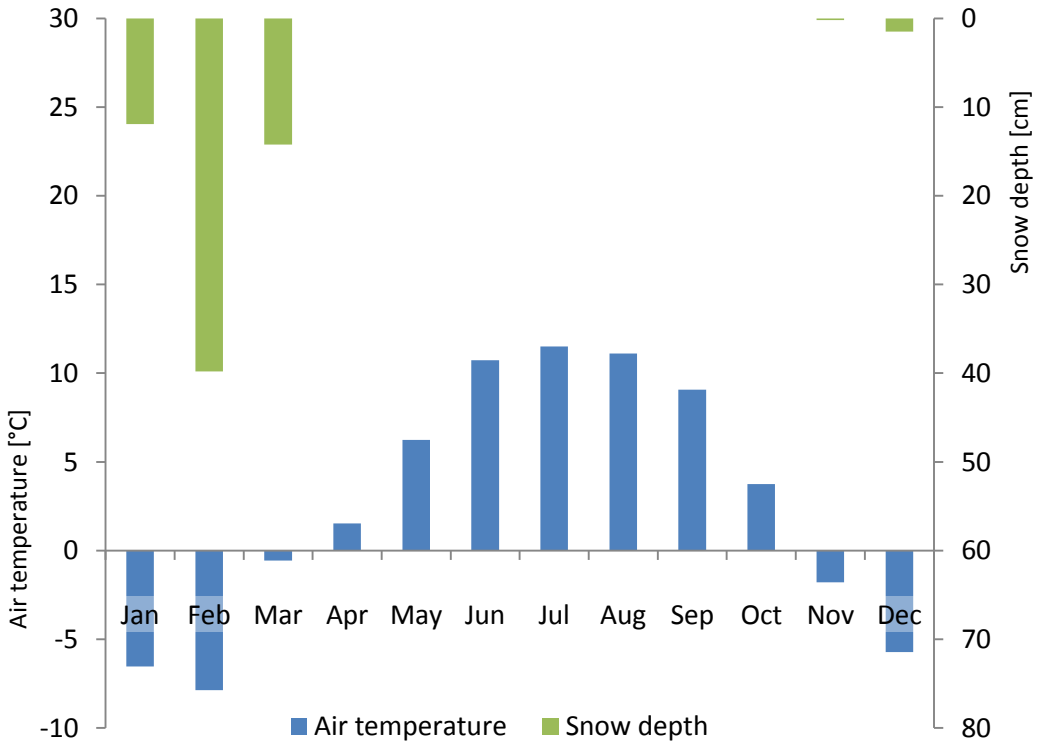

Figure 4-4 Air temperature and simulated snow depth at the valley bottom for the year 2011

Figure 4-5 and Figure 4-6 compare the distribution of the simulated and measured water content at two depths in the soil profile at station # 1. Soil moisture correlations are generally found to be good especially in the top layer (0.84). As indicated by relatively

small MBE values [Table 4-3], model biases in predicting soil moisture from mean VGM parameters at depths of 10 cm and 50 cm are also generally small (0.009 and -0.04 cm^3cm^{-3} respectively). However, a significant mismatch was noted at the 50 cm depth between measured and observed moisture content [Figure 4-6]. This can possibly be attributed to the significant spatial variabity of soil moisture and/or the degree to which the sensors are in contact with the soil material. As mentioned in section 4.2.4, average values of root depths were assumed for seasonal crops. The bias in soil moisture simulation results may also be attributed to the assumption of constant root depth throughout the growing period. Note that the correlation coefficient estimated at the 50 cm depth (r = 0.57) is higher than values reported in previous soil moisture modelling studies such as Hejazi and Woodbury [2011]. However, additional effort is expended here to see if results can be improved by inverse estimation of soil hydraulic parameters from measured transient soil moisture data. To this end, the relatively simple local optimization approach, which is implemented into the HYDRUS 1D code is used. The required upper and lower bounds of the VGM parameters are defined from ROSETTA outputs as $\mu \pm 4 \times \sigma$ where μ and σ are average and standard deviation respectively. The upper and lower bounds are defined based on a previous Bayesian inverse modelling study by Scharnagl et al. [2011]. The calibrated VGM parameters, for the lower two layers, as well as the improvement on soil moisture simulation results (r = 0.79) are shown within Table 4-1 and Table 4-3 respectively. It is however important to note that the gradient-based optimization method of HYDRUS-1D is highly sensitive to the initial values of the VGM parameters, and thus the calibrated parameters indicated in Table 4-1 are not likely the global minimums.

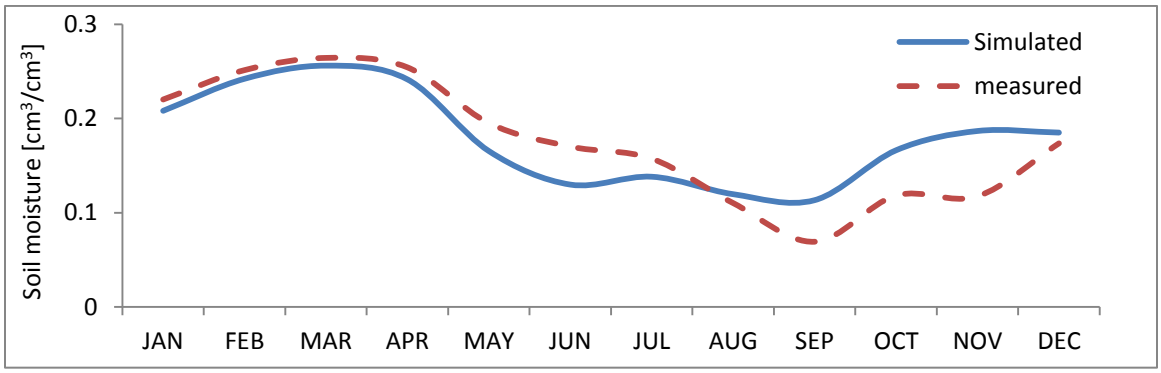

Figure 4-5 Simulated versus observed soil moisture at 10 cm depth, valley bottom for the year 2011

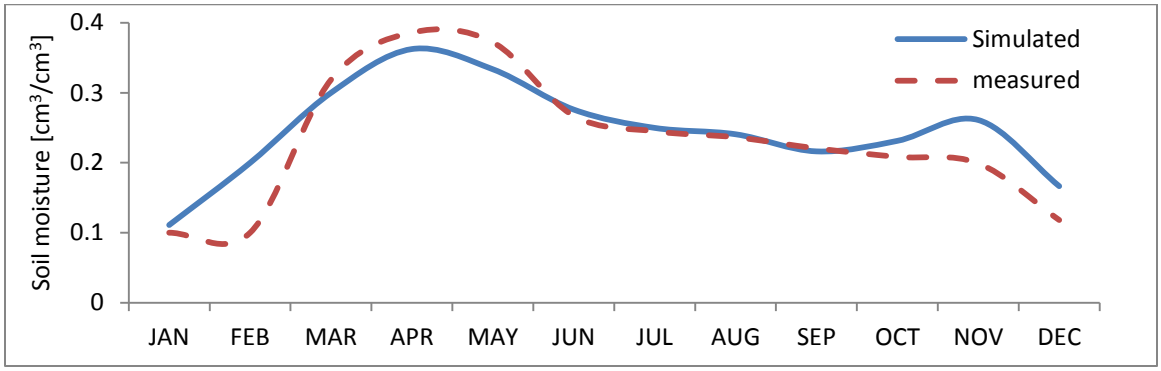

Figure 4-6 Simulated versus observed soil moisture at 50 cm depth, valley bottom for the year 2011

This algorithm is used here to improve soil moisture simulation results at the 50 cm depth. Details on this and other more robust global optimization techniques can be found in Simunek et al. [2012]. The attempt of improving soil moisture simulation results by calibration has motivated the need to evaluate the potential uncertainty in groundwater recharge due to random changes in VGM parameters. To this end, a Monte-Carlo simulation technique is implemented at the same location - HOBO^{TM} station # 1 - by using the ROSETTA outputs as the bases for random number generation. Determining a statistical distribution function for the input parameters requires a fairly large amount of sample data [Hayse, 2000]. In the absence of such data, a normal distribution is typically

assumed. The ROSETTA outputs (μ and σ) are used here to construct a normal distribution for the VGM parameters - parameters are assumed to be uncorrelated. Model results are calculated by randomly sampling a new value from each normal distribution. The outputs from each run of the model (mean value of annual recharge) are saved and a histogram for the output is generated [Figure 4-7] – the ensemble is estimated at 63 ± 9 mm /year.

Note that the temporally averaged annual recharge estimated using the ROSETTA derived mean VGM parameters, at this same location of HOBO^{TM} station #1, is about 54 ± 37 mm/year [Section 4.3.4]. The variability in recharge is likely caused by variations in antecedent soil moisture condition and climate conditions throughout the simulation period (1982-2006) [Section 4.3.4]. Note here that the potential uncertainty due to model parameters (63 ± 9 mm /year) is minimal as compared to the significant temporal variability in direct diffused recharge values (54 ± 37 mm/year).

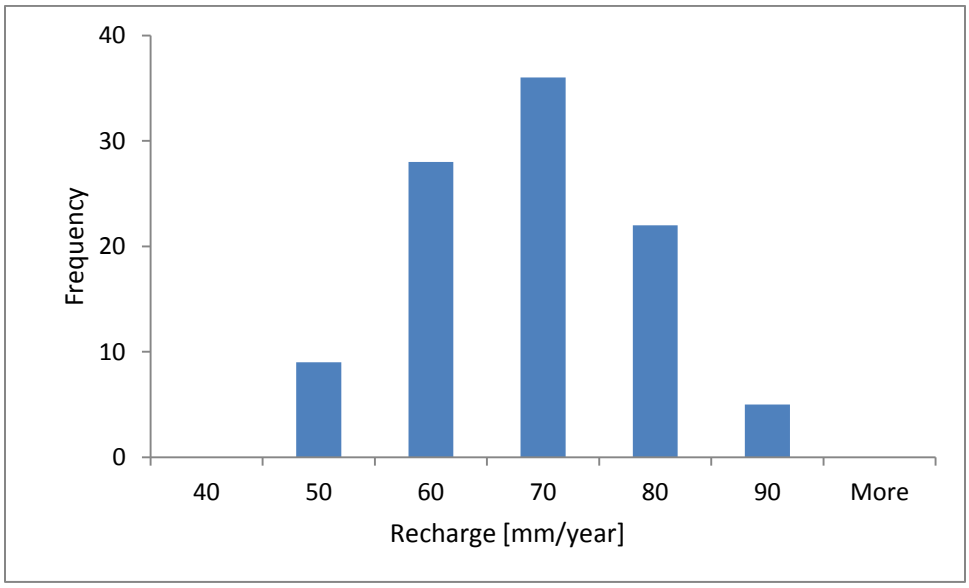

Figure 4-7 Uncertainty due to model parameters using normally distributed parameters (average annual recharge versus frequency)

In addition to the comparative analyses made at HOBO^{TM} station # 1, a HYDRUS 1D run is completed at the location of station # 2 in order to assess the degree to which the field site results can be extrapolated to the other areas of the basin. The contrasts in land cover and soil type at the location of the two weather stations can be seen in Figure 3-4, Tables 4-1 and 4-2. Figures 4-8 and 4-9 compare the distribution of the simulated versus measured water content and soil temperature respectively, at 20 cm depth over a one year experimental period (July 2011 to July 2012). Statistical analyses show very good performance of the model in this area of the basin as well (Table 4-4) highlighting the robustness of the methodology developed in this study. Note that the VGM parameters used in the model are estimated using pedotransfer functions; indicating that ROSETTA can be taken as a reliable method for estimating soil hydraulic properties on a larger scale.

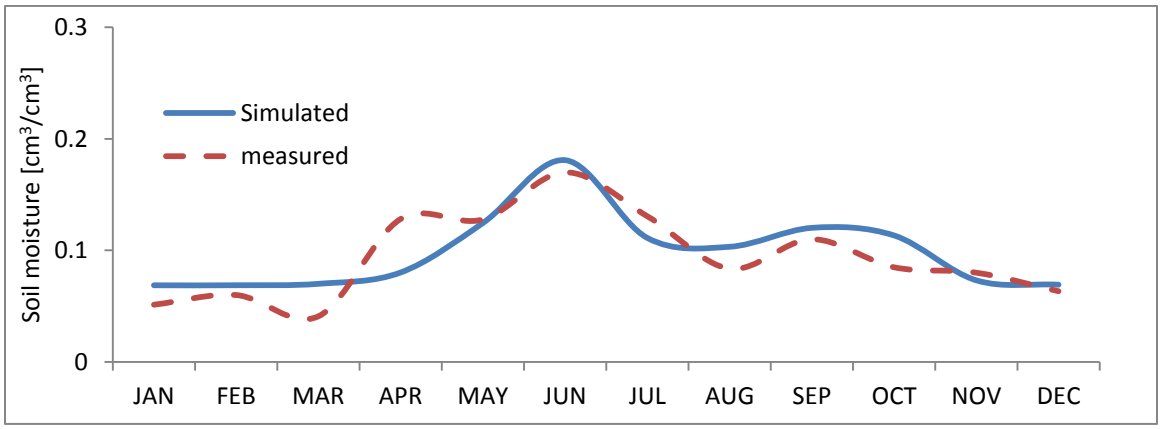

Figure 4-8 Simulated versus observed soil moisture at the Silver Star Mountain at 20 cm depth (July 2011- July 2012)

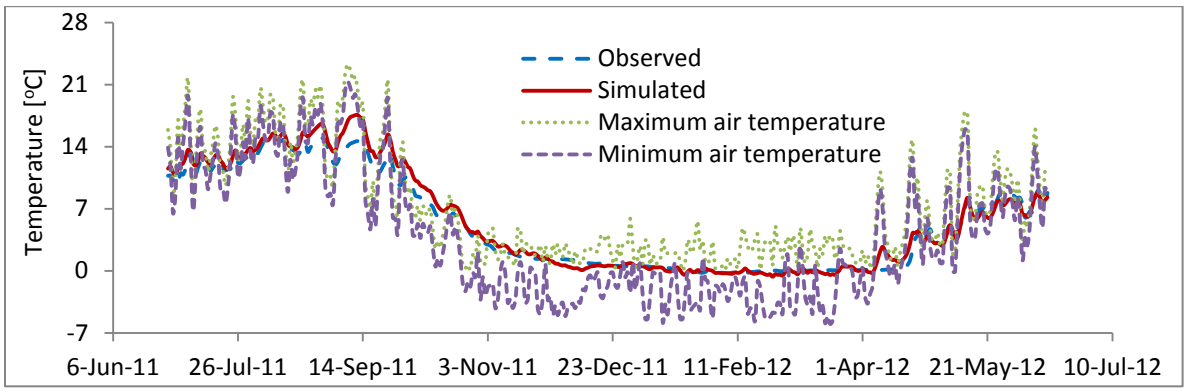

Figure 4-9 Simulated versus observed soil temperature at the Silver Star Mountain at 20 cm depth (July 2011 to July 2012)

Table 4-3 Measured versus simulated variables at valley bottom

Depth [cm]	MBE		RMSE		Correlation	
	Soil temperature [°C]	Soil moisture [cm^3cm^{-3}]	Soil temperature [°C]	Soil moisture [cm^3cm^{-3}]	Soil temperature [-]	Soil moisture [-]
10	-1.08	0.009	2.5	0.036	0.97	0.84
50	-0.25	-0.04[0.03]	2.3	0.11[0.08]	0.96	0.57[0.79]

Table 4-4 Measured versus simulated variables at Silver Star Mountain

Depth [cm]	MBE		RMSE		Correlation	
20	Soil temperature [°C]	Soil moisture [cm^3cm^{-3}]	Soil temperature [°C]	Soil moisture [cm^3cm^{-3}]	Soil temperature [-]	Soil moisture [-]
	0.18	-0.02	1.2	0.002	0.98	0.6

4.3.3 Runoff and Snow Depth Simulation

Figures 4-10 and 4-11 show monthly averaged snow depth and runoff variation throughout a year in the valley bottom. The snow pack plays a significant role on the groundwater recharge pattern. The peak months for snow depth were simulated in December, January and February. The snow started to melt in March, as evapotranspiration /temperature started rising, and it progressively decreases to zero in spring and summer until the next year's snow starts to accumulate in November. The recharge simulated in spring and summer can thus be attributed to snow melt. Note that the proportion of snow water equivalent which joins the groundwater table largely depends on the antecedent soil moisture. In the cases when snowmelt has to satisfy the soil moisture requirements, the spring rain events will be responsible for the simulated recharge. These hydrologic processes at and near the soil surface are controlled by the variable system-dependent boundary condition discussed in Section 4.2.3.

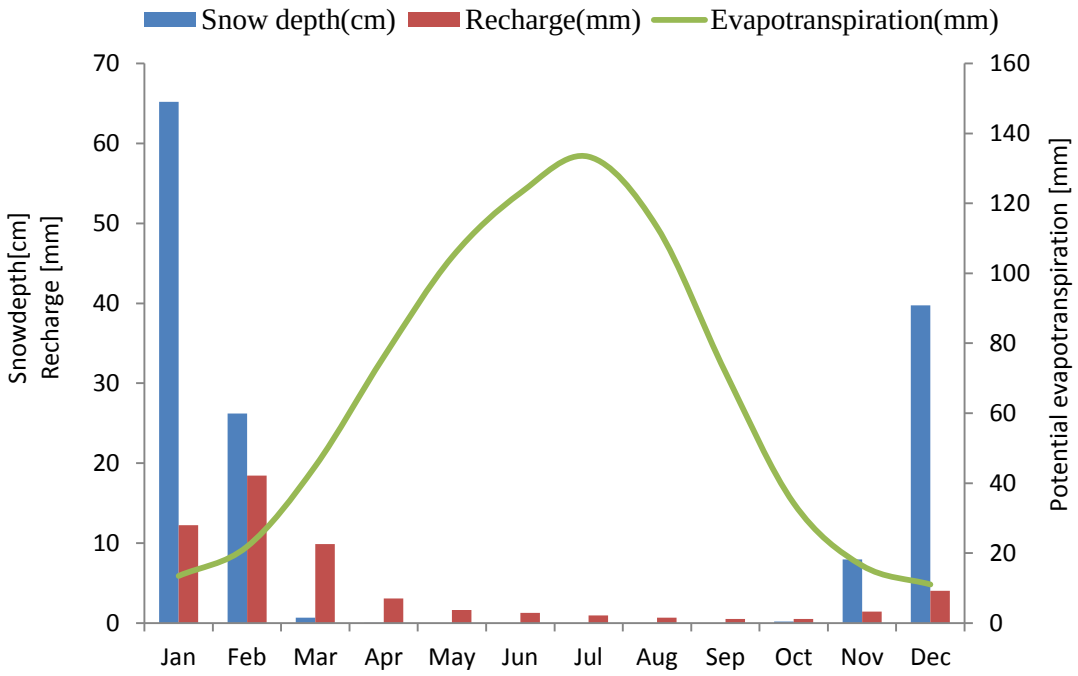

Figure 4-10 Average monthly variations in snow depth, recharge and potential evapotranspiration (1982-2006)

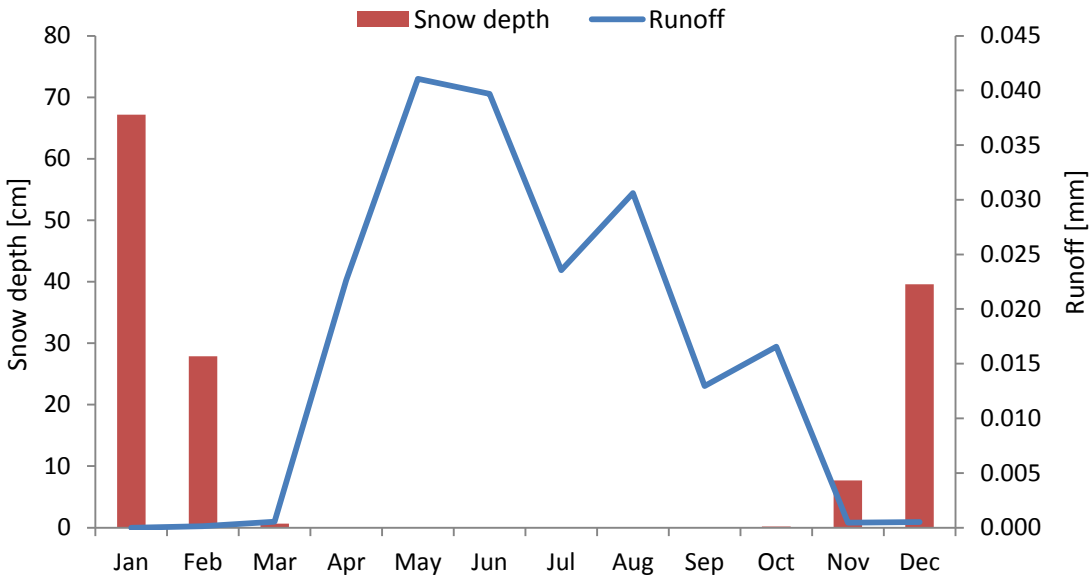

Figure 4-11 Average monthly variations in runoff and snow depth (1982-2006)

4.3.4 Temporally and Spatially Varying Recharge

After evaluating the performance of HYDRUS-1D using field data and ROSETTA derived VGM parameters, groundwater recharge is simulated at various locations in the Deep Creek watershed by making use of the long term gridded climate data and ROSETTA derived VGM parameters. The various locations termed here as representative points, were determined after discretizing and combining the HYDRUS-1D input variables into 500 m × 500 m cells in ArcGIS™. For each of the fourteen HYDRUS columns shown in [Table 4-5], a total of 46 years and four months are simulated. The recharge results from each of the fourteen unique HYDRUS columns are then assigned to all areas in the watershed that have similar input data. This approach, which is similar to that of Liggett and Allen [2010] and Jyrkama et al. [2002], is used here to produce the raster map of recharge shown in Figure 4-14 [Section 4.3.6].

Table 4-5 Representative locations and IDs for model inputs

Representative area [#]	UTM_EAST [m]	UTM_NORTH [m]	Climate ID	Soil code	Land use	Area coverage % of total area
1	343587	5592330	440142	EBY	Agriculture	45.4
2	343096	5593010	430141	BDV	Agriculture	
3	342022	5595031	520137	BDV	Agriculture	
4	342274	5595604	380139	AMG	Agriculture	
5	341877	5585964	570140	BDV	Agriculture	
6	340848	5605693	180133	CYV	Forest	42.6
7	341146	5608663	120133	HOS	Forest	
8	338150	5589981	500132	TUN	Forest	
9	345159	5584603	590147	CLP	Forest	
10	338718	5588885	520.133	HST	Forest	
11	346739	5584908	580150	CNN	Forest	
12	346312	5581980	640150	SNW	Barren	0.1
13	338305	5580400	690134	AMG	Rangeland	3.5
14	335199	5584724	610127	GGI	Rangeland	

4.3.5 Temporal Variability

The daily recharge results are aggregated into monthly and annual time series. Long-term average monthly recharge results are analysed to study seasonal variation at various parts of the watershed [Table 4-6].

Table 4-6 Average monthly and annual recharge [mm] at various parts of the watershed

	Valley bottom	Western DC	South DC	Eastern DC	North DC
	Recharge [mm]				
Annual	35	90	19	152	66
% Precipitation	8	14	5	21	11
January	3	4	1	7	4
February	12	7	1	9	12
March	11	38	4	73	33
April	3	27	5	41	13
May	2	7	3	9	2
June	1	2	2	4	1
July	1	1	1	2	0
August	0	0	1	1	0
September	0	0	1	1	0
October	0	0	0	0	0
November	0	1	0	2	0
December	2	3	0	4	2

The monthly data are further analysed by plotting the three major water balance components as shown in Figure 4-12. High recharge values are generally estimated in February, March and April, because of the lagged response to higher precipitation combined with spring snow thaw. The low recharge values over the summer months can be accounted for the increased summer evapotranspiration [Figure 4-12]. This pattern is further explained by simulating snow depth and runoff in the different representative areas within the study area.

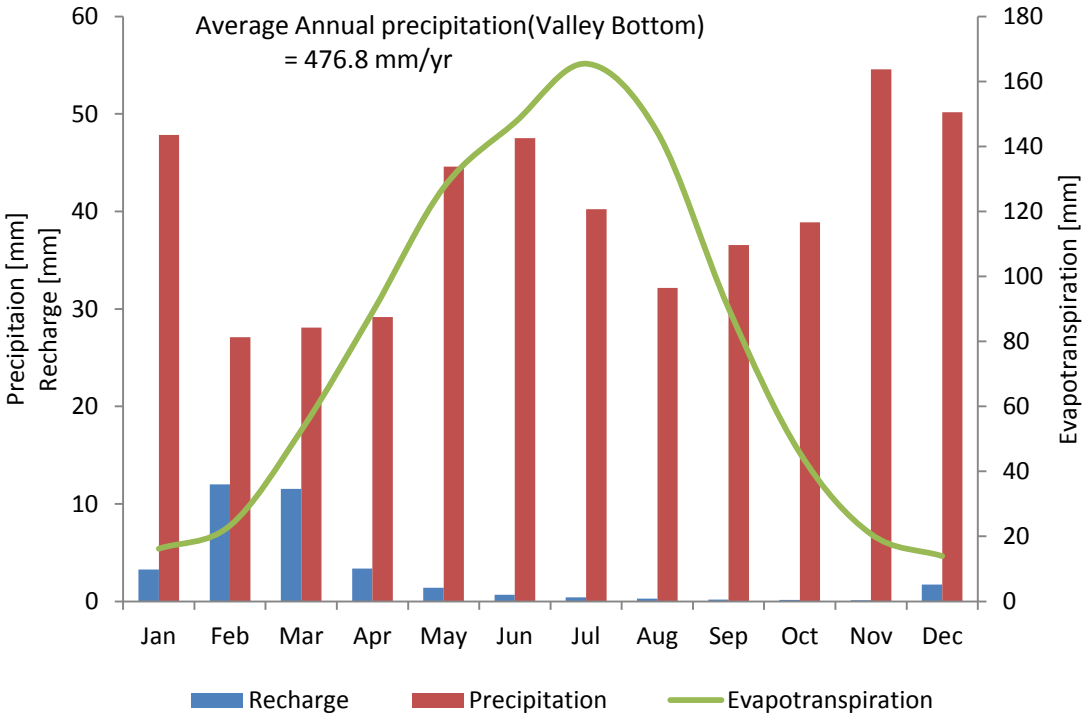

Figure 4-12 Average monthly variations in recharge, precipitation and evapotranspiration (1982-2006)

Temporal recharge analysis is further conducted by using annual recharge results. Any informative recharge estimate should give an indication of how recharge varies over time. Figure 4-13 shows the annual variation of recharge, along with precipitation and evapotranspiration, at the valley bottom. Note in Figure 4-13 that recharge is near zero during the years when evapotranspiration is high and precipitation is low (e.g., 1987). Such dry years can also affect the magnitude of recharge the following year (e.g., 1988). This is because the precipitation received following a dry year has to satisfy the soil moisture requirement before it drains out of the soil column as recharge. On the other hand, high recharge is estimated during the period when high precipitation and low evapotranspiration is observed (e.g., 1996). Such climatic condition generally results in high soil moisture condition. As a result, the precipitation that falls the following year can

easily result in higher recharge values (e.g., 1997). Analysis of the result shows a wide variation, ranging from 0.2% to 17% of annual precipitation over the 25 years simulation period. This is a significant variation over the years, caused by antecedent soil moisture condition and climatic conditions. It illustrates the common flaw of assigning a constant percentage of precipitation throughout the simulation period. For instance, the recent work in the Deep Creek watershed by Ping et al. [2010] used a groundwater model to estimate recharge as a fitting parameter. They assumed initial value of recharge (5%) from similar works in North America which has the same climate as the Okanagan basin, and calibrated this value to 5.5%. However, similarity in climate is not a sufficient condition for similarity in recharge estimates. To this end, a relatively simple sensitivity analysis is conducted at the location of the HOBO weather station in the valley bottom by varying land use, soil type and water table depth, while keeping the climate data the same. The actual land use, dominant soil type and lower boundary conditions at this particular location are pasture land, silty clay loam and free draining respectively. Whereas synthetic situations of clay soil, alfalfa crop and seepage lower boundary conditions were assumed to study the magnitude of change in the recharge results. The simulation results show that average annual recharge, in the latter case, would be about 75% less than that estimated using the actual condition (53.3 mm/year). This significant difference in recharge clearly shows the fact that the two study areas need to have similar soil profiles and land uses as well as other model input data in order to transpose parameters/model results from one area to the other, if possible at all. Besides, recharge also exhibits significant spatial variation across the Deep Creek watershed.

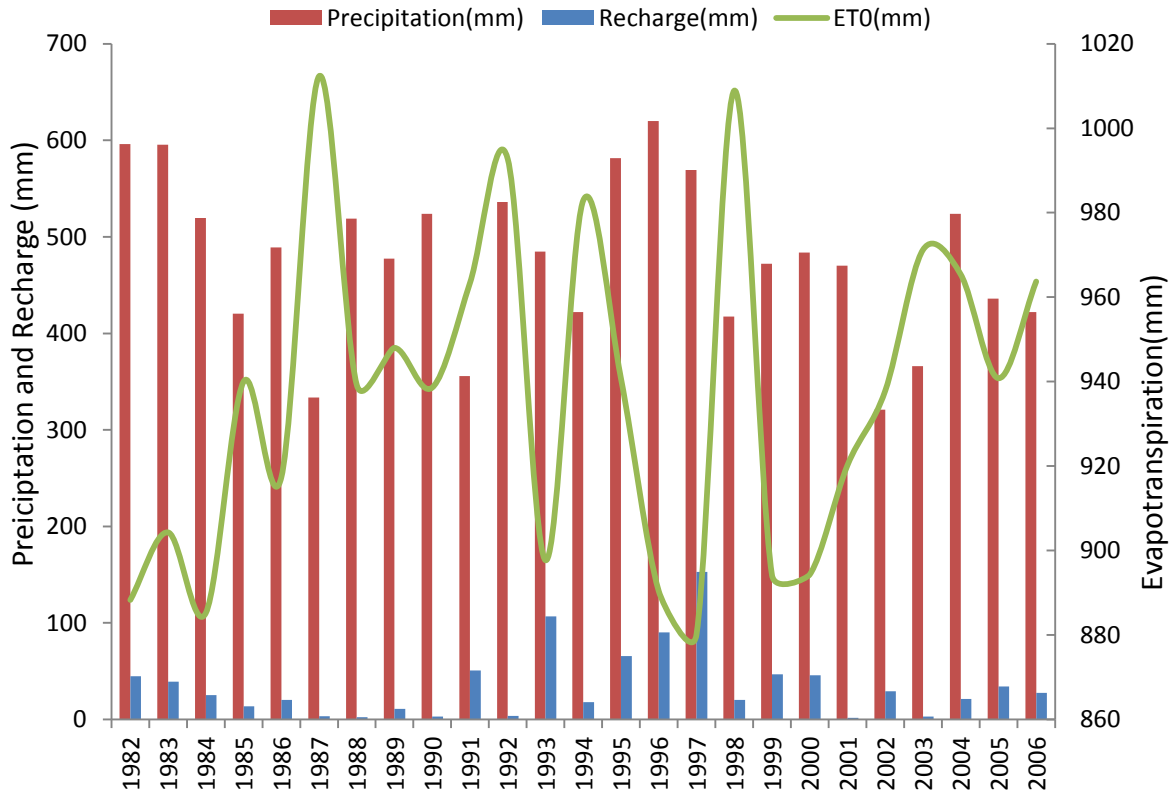

Figure 4-13 Temporal variation of annual recharge at the valley bottom (1982-2006)

4.3.6 Spatial Distribution of Recharge

Similar to the temporal variation, recharge also exhibit significant spatial variation over the Deep Creek watershed. Figure 4-14 shows a map of long term average annual recharge throughout the Deep Creek watershed. Long term average annual recharge values estimated at different parts of the watershed are shown in Table 4-6. The results indicate significant spatial variation across the watershed. For instance, the mean recharge at the valley bottom is estimated to be 35.2 ± 30.5 mm /year. Whereas a higher recharge amount estimated at 152.1 mm/year ± 61.5 mm/year is simulated in the mountains. The large differences in recharge can be accounted for by temporal and

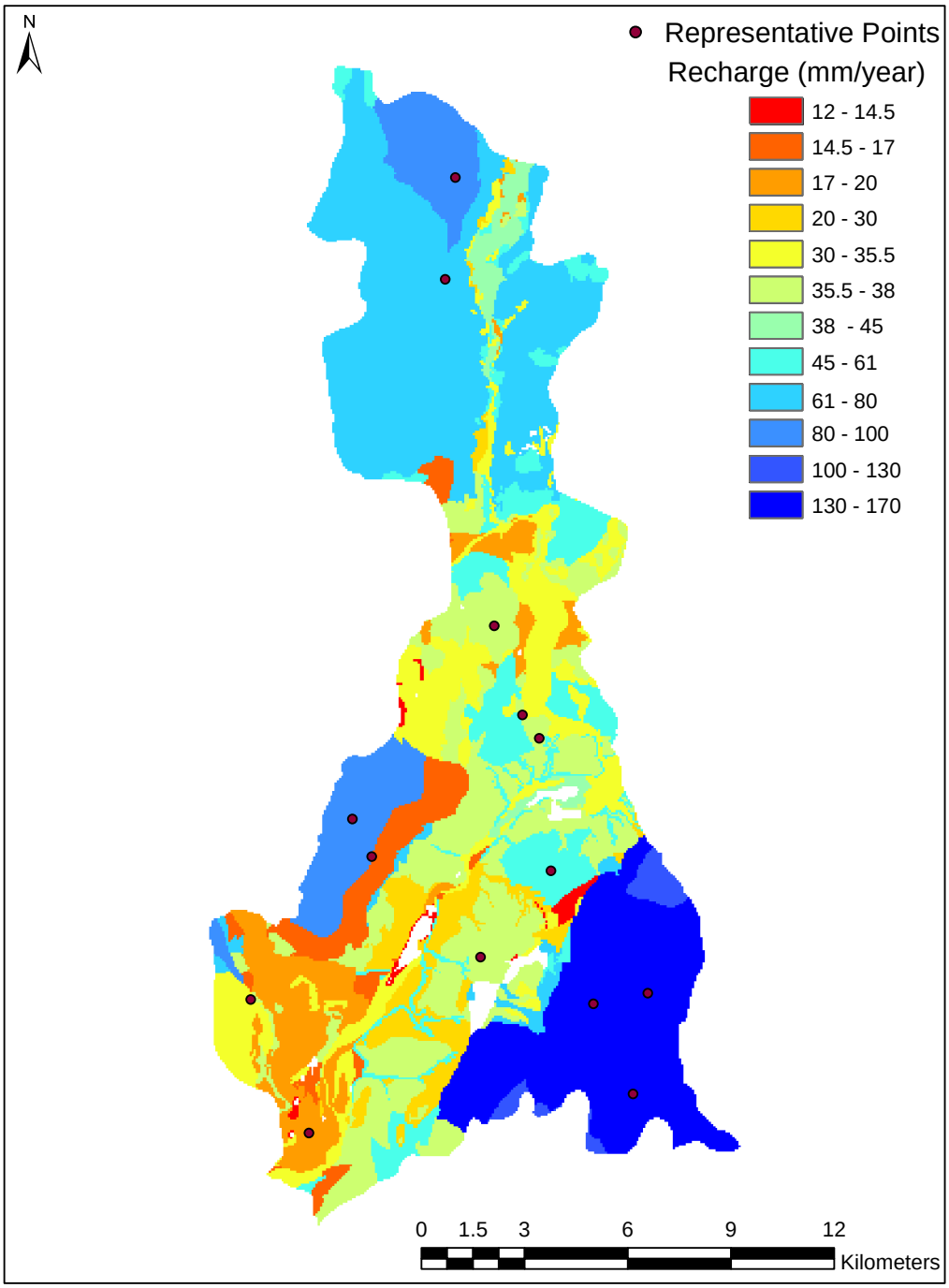

Figure 4-14 Spatial map of average annual recharge

spatial variations in antecedent soil moisture and climatic conditions, as well as for the contrasts in soil hydraulic parameters.

4.4 Transient, Spatially Varying Recharge for Groundwater Modelling

This section is aimed at demonstrating the significance of the recharge estimation method in transient groundwater modelling. This demonstration is done by applying the spatially and temporally varying recharge values as upper boundary condition to a saturated zone transient groundwater model, MIKESHE [Abbott et al., 1986].

The major aquifer within the valley center of the Deep Creek watershed consists of alluvial sediments termed as "Spallumcheen A" by Monahan [2006] and Fulton [2006]. The sapllumcheen A aquifer extends laterally into similar other confined aquifers designated as Hullcar, Sleepy Hollow, and Okeef [Monaha, 2006; Ping et al., 2011]. Figure 4-15 shows the confined aquifer layer with thickness varying between 139 to 420 meters, and the location of pumping wells [Table 7-3]. The top of the aforementioned aquifers is overlain by aquitards which vary in thickness from 0.5 to 208 meters [DHI Cambridge, 2011]. The overlaying alluvial deposits and the laterally extended local unconfined aquifers (Hullcar, Sleepy Hollow, and Okeef) are shown in Figure 4-16. Note that Hullcar, Sleepy Hollow and Okeef are names given for both the confined and unconfined aquifers at the locations indicated in Figure 4-15 and Figure 4-16, respectively. The thicknesses of the unconfined aquifers are reported to vary between 0.5

to 131 meters [DHI Cambridge, 2011]. Detailed description of the complex aquifers of the study area can be found in Ping et al. [2011]. The aquifer system and its interaction with the surface water and pumping wells has been previously studied by DHI Cambridge [2011] and improved by Assefa et al. [2011] using the MIKESHE model [Abbott et al., 1986]. The spatial boundary of the model was set to match the boundary of the Deep Creek watershed covering a total of 245.4 km^2. Lateral transfer of water from adjacent aquifers is represented in MIKESHE as outer boundary condition based on previous geochemistry study by Nichol et al. [2011] [Assefa et al., 2011]. The saturated zone groundwater model of MIKESHE is adapted here to demonstrate the importance of the developed recharge modelling methodology in transient groundwater modelling.

To this end, two scenarios of the groundwater model are prepared. While the first scenario uses the spatially and temporally varying recharge as upper boundary condition, the second scenario uses the traditional method of applying uniform recharge boundary condition across the watershed. For each scenario, the groundwater level is simulated and extracted at the location of observation well number 122 [Figure 3-4]. Note that observation well numbers are series of numbers assigned to each provincial observation well for identification purposes. Well 122, with static level and depth of about 1.5 meter and 318 meter respectively, was established in the spallumcheen aquifer for a groundwater research project (Federal-Provincial Okanagan River Basin Study). Water levels were taken monthly off a recorder chart by the BC Ministry of Environment and are available from GeoBC [http://geobc.gov.bc.ca/].

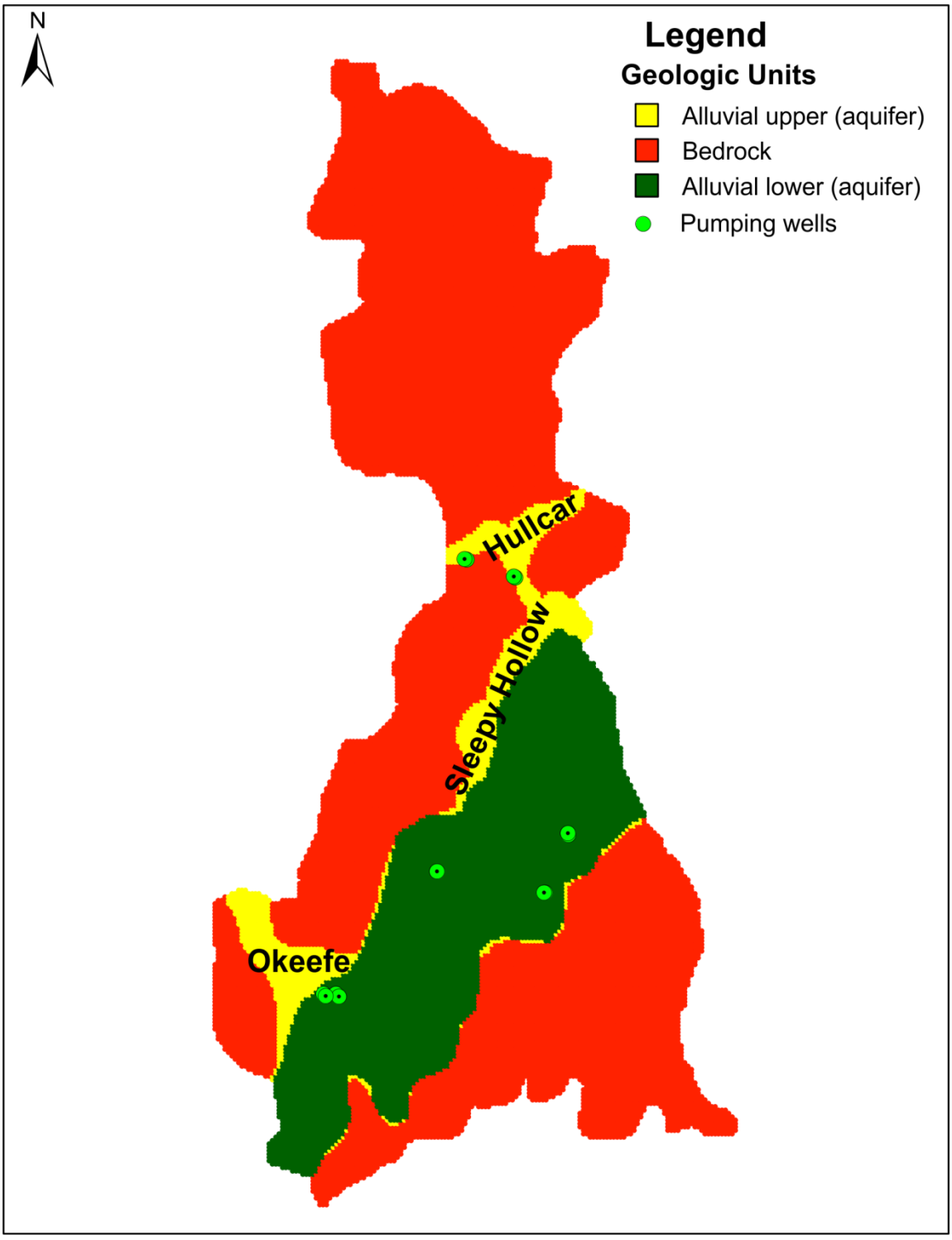

Figure 4-15 Geologic Units of Confined Aquifer Layer

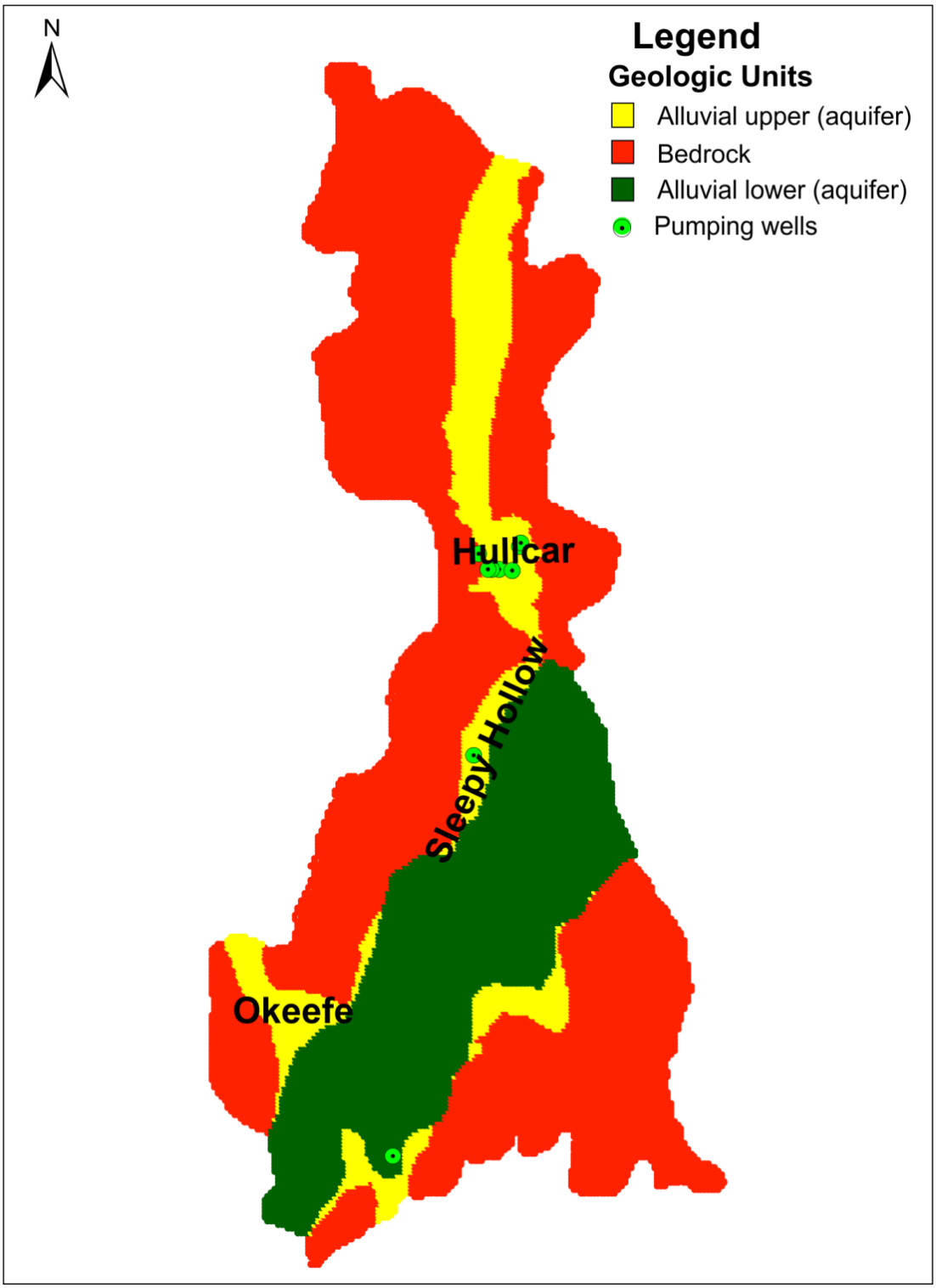

Figure 4-16 Geological units of unconfined Aquifer Layer

Figure 4-17 and Figure 4-18 show a comparison of observed versus simulated groundwater levels, which are simulated using the spatially and temporally varying recharge boundary condition and the uniform recharge boundary condition, respectively. As discussed above, the observation well is installed in the confined spallumcheen aquifer. Water level increases over time following the climate (and recharge) pattern over the simulation period (e.g., Figure 4-13). Analyses of the groundwater level results show that the water table simulated using the variable recharge condition to be within 0.6 m of the observed values, whereas the water levels estimated using uniform recharge boundary condition can fluctuate by as much as 1.6 m. Root mean square errors are estimated at 0.3 m and 0.94m, respectively.

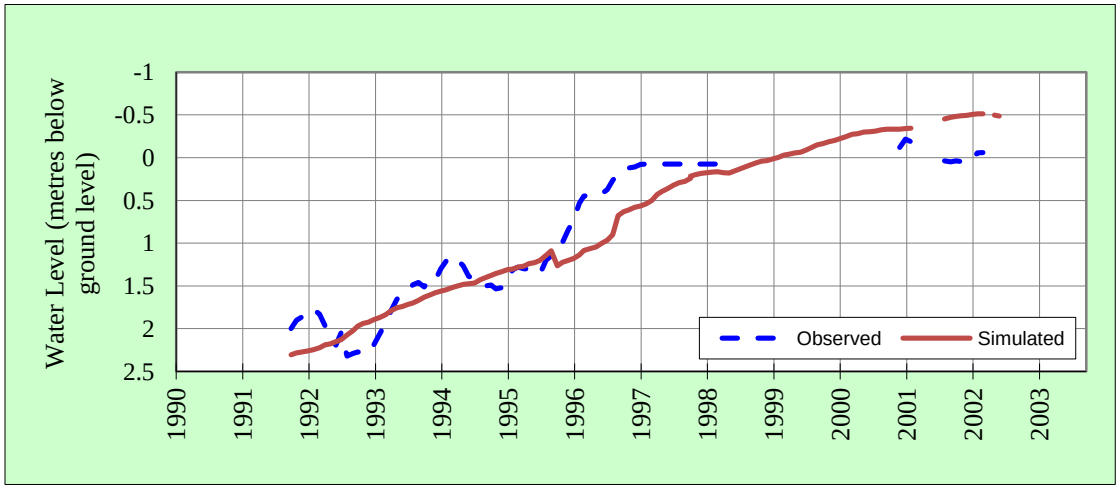

Figure 4-17 Hydrograph of groundwater levels- variable recharge boundary condition

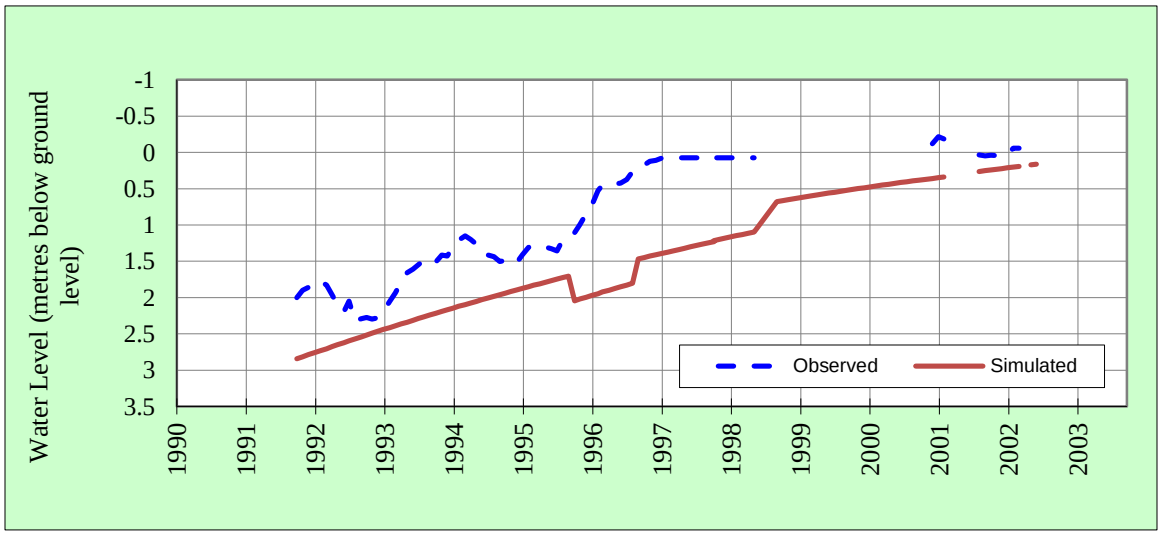

Figure 4-18 Hydrograph of groundwater levels- uniform recharge boundary condition

In summary, this chapter has presented a new methodology for groundwater recharge estimation by taking advantage of field data and various modelling tools. The detailed calculation of groundwater recharge here has clearly shown that previous estimates [Jyrkama et al., 2002; Liggett and Allen, 2010; Toews and Allen, 2009; Jyrkama and Sykes, 2007] using water balance models such as HELP are sub-optimal. While this is generally known, it is not clearly documented in the literature or recognized by regulatory agencies (e.g., EPA). Unfortunately, HELP has not been used in the Deep Creek watershed to quantitatively compare results although it has been used in Vernon area (south of the Deep Creek Watershed) where average annual recharge was estimated at 109 mm/year [Liggett and Allen, 2010]. To their credit, Liggett and Allen [2010] acknowledged the fact the HELP over predicts recharge. Note that Liggett and Allen [2010] used the most recent version of HELP (Version 3.80D). Their result is significantly higher than the mean annual recharge estimated at the southern part of the Deep Creek watershed (19 mm/year) as well as the watershed average (77.8 mm/year).

The following chapter focuses on further evaluating the reliability of the government soil data [Kenney and Frank, 2010] for plot scale soil moisture and recharge modelling under changing climate.

Chapter 5

Model Parameterization and Recharge under Changing Climate

Soil is one of the key inputs in hydrologic modelling, and is known to exhibit significant heterogeneity within a watershed [Hollaender et al., 2009a]. It has been discussed in Section 4.2 that the catchment scale groundwater recharge modelling procedure made use of a government soil texture data in a 500 m x 500 m pixel size [Assefa and Woodbury, 2013]. This part of my research is focused at evaluating the reliability of the recharge estimation method and the ROSETTA derived soil hydraulic parameters for a plot scale vadose zone hydrologic modelling. To this end, model parameterization and their impact on vadose zone water movement processes are investigated at the experimental site in the valley bottom (station # 1). The site is characterised by cohesive soil profile and pasture land use.

5.1 Model Parameterization

The Van-Genuchten soil hydraulic parameters are estimated in two different ways. The first method is based on direct estimation from the ROSETTA code [Table 4-1] whereas the second set of parameters, shown in Table 5-1, is estimated by calibration. The calibration is performed at the experimental site in the valley bottom by using the observed transient soil moisture data (Dec 2010 to Dec 2011). Both set of VGM parameters are used to develop the retentivity and conductivity functions shown in Figure 5-1 and Figure 5-2. Retentively function can be obtained by plotting PF values (logarithm of soil suction pressure) against moisture content values [Hendriks, 2010]. In order to evaluate the predictive power of the retentively functions, moisture content that correspond to a pF value of 2 (field capacity) and pF 4.2 (wilting point) [Hendriks, 2010] are estimated. The corresponding moisture content values are shown in Table 5-2.

Table 5-1 Soil texture [%] and calibrated parameters at valley bottom

Soil code/	Units of VGM parameters: $Q_{r,s}$ [cm^3cm^{-3}], Alpha[cm^{-1}], n[-],K_s [cm day^{-1}]								
Soil layer	Depth[cm]	Sand	Silt	Clay	Q_r	Q_s	Alpha	n	K_s
1	0-15	12	68	20	0.03	0.45	0.008	1.8	15
2	15-24	12	70	18	0.03	0.39	0.003	1.8	16
3	24-39	10	70	20	0.03	0.45	0.002	1.8	14
4	39-64	7	70	23	0.03	0.45	0.004	1.6	12

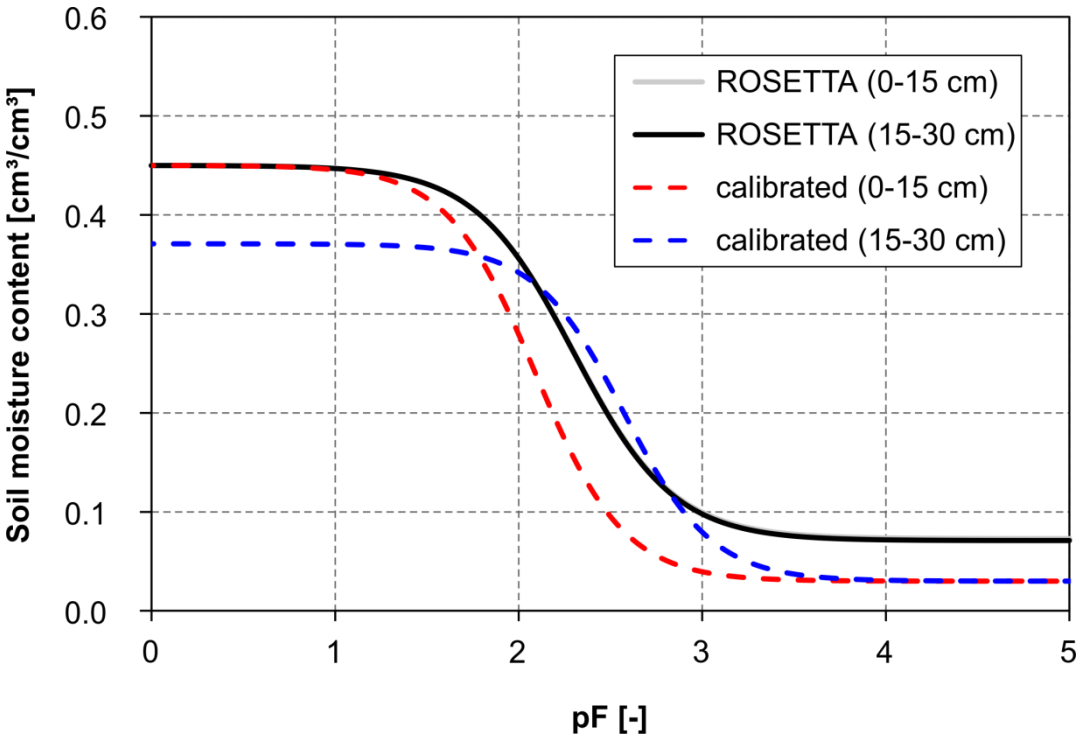

Figure 5-1 Retention curves based on van Genuchten Model at the location of HOBO station # 1

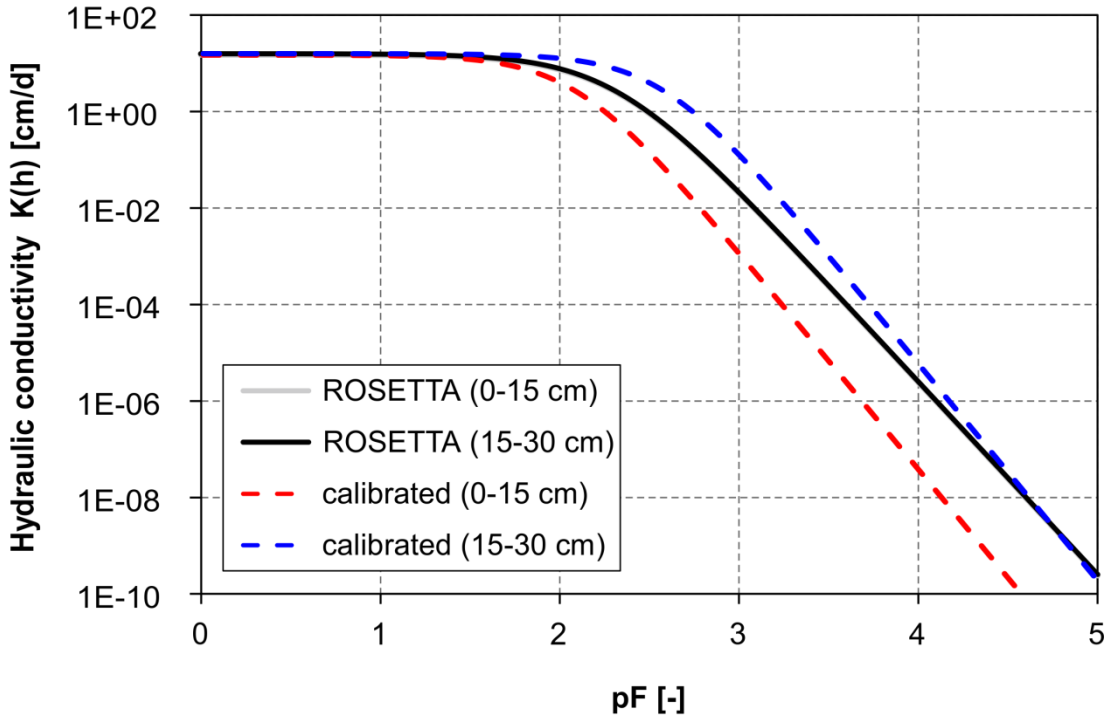

Figure 5-2 Soil hydraulic models based on van Genuchten-Mualem Model at the location of HOBO station # 1

Table 5-2 Soil moisture values at field capacity and wilting point

Soil moisture [cm^3cm^{-3}]	Sample 0 – 15 cm		Sample 15 – 24 cm	
	ROSETTA	Calibration	ROSETTA	Calibration
Field capacity [pF 2]	0.35	0.28	0.35	0.34
Wilting point [pF 4.2]	0.07	0.03	0.02	0.03

As can be seen in Table 5-2, the error in moisture content due to the two different set of parameters may range between 0.01 and 0.07 cm^3cm^{-3}, which is equivalent to 1 – 7%. Note here that ROSETTA program consists of five hierarchical pedotransfer functions (PTFs) with varying degrees of input data requirement (Section 4-2-2). The PTF known as H2-C2 [Schaap et al., 2001] is used here to determine the soil hydraulic parameters from sand, silt and clay percentages [Kenney and Frank, 2010]. Schaap et al. 2001 have estimated the error in the H2-C2 PTF at about 8%, which is greater than the maximum error estimated here due to the two different set of parameters (7%). Note that soil moisture and matric potential are generally known to exhibit significant spatial and temporal variability as the soil goes to saturation by precipitation, drained by gravity and dried by evapotranspiration and root extraction [Hillel, 2004] - the error due to soil moisture measurement alone is estimated at about 3.1% [Table 3-4]. The impact of the two set of parameters, ROSETTA derived [Table 4-1] and calibration parameters [Table 5-1], on water movement is further evaluated by simulating soil moisture at the experimental site in the valley bottom. The simulation results shown in Figure 5-3 and Figure 5-4 are statistically analysed (correlation coefficient and RMSE) to estimate degree of fit between model outputs and observed values [Table 5-3]. The results suggest

promising performance of the ROSETTA derived parameters for plot scale modelling, with correlation coefficient and RMSE estimated at 0.84 and 0.036 cm^3cm^{-3}, respectively. In fact, calibration can always improve simulation results as demonstrated by the higher correlation coefficient (0.94) and lower RMSE values (0.025 cm^3cm^{-3}).

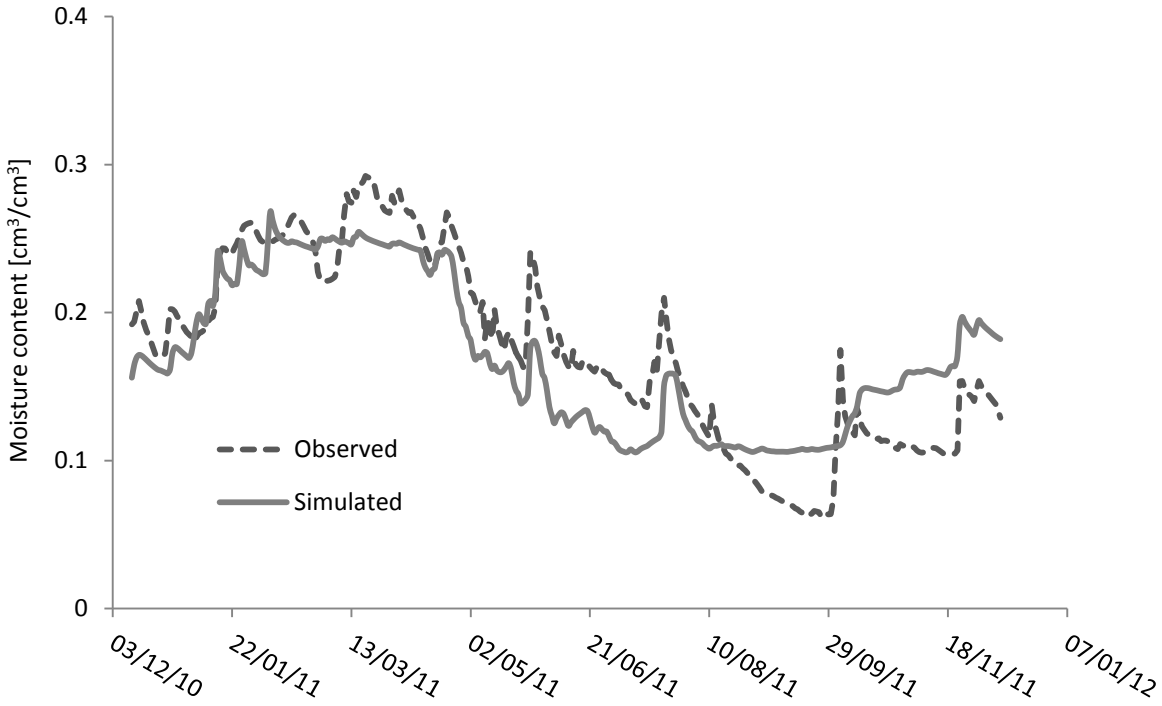

Figure 5-3 Soil moisture simulated at the location of HOBO station # 1 using ROSETTA derived soil parameters

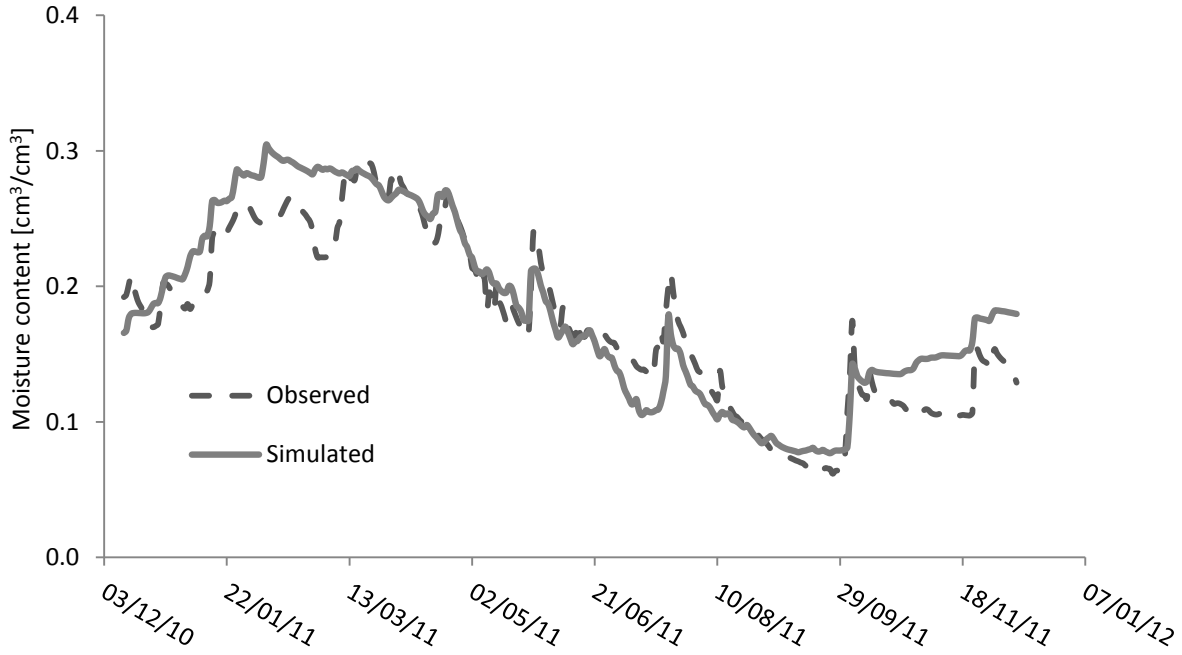

Figure 5-4 Soil moisture simulated at the location of HOBO station # 1 using calibrated soil parameters

Table 5-3 Measured versus simulated soil moisture at HOBO™ station #1

Depth [cm]	RMSE [cm^3cm^{-3}]		Correlation [-]	
	ROSETTA	Calibration	ROSETTA	Calibration
10	0.036	0.025	0.84	0.94

The reliability of the ROSETTA derived soil hydraulic parameters is further evaluated by simulating groundwater recharge under changing climate [Section 5.3].

5.2 Downscaling – Synthesis of Climate Data

As discussed in Chapter 2, downscaling is the means of relating the large scale atmospheric predictor variables to local or station-scale meteorological records. The most common regression based technique used to map global climate models to ground station is the Statistical Downscaling Model [SDSM, Wilby et al., 2002]. SDSM uses large scale circulation patterns and atmospheric variables to linearly condition (equation 5-1) local scale weather parameters (e.g., temperature).

$$\hat{y} = \alpha_0 + \alpha_1 x_1 + \ldots + \alpha_p x_p \qquad 5\text{-}1$$

Where: $\hat{y}$ = predictand [estimation of dependent variables]

x_i = i-th predictor

p = number of predictors

α_i = i-th coefficient

SDSM is used here to synthesise future climate scenarios of daily precipitation, daily minimum temperature, and daily maximum temperature by using predictor variables derived from the HadCM3 A2 experiment. The HadCM3 is a third generation coupled atmosphere-ocean general circulation model, with a horizontal resolution of about 2.5° latitude by 3.75° longitude, developed by the U.K. Meteorological office, Hadley center [Gordon et al., 2000]. The set of predictor variables for the baseline period (1969 – 2000)

are derived from National Centre for Environmental Prediction (NCEP) reanalysis data, obtained from the Canadian Institute for Climate Studies [http://www.cics.uvic.ca/].

The selection of predictor variables is usually limited by data availability in both the NCEP and GCM data archives as well as by the degree to which the predictor variables influence climate of the study area. In this study, twenty six daily NCEP predictor variables are first identified based on data availability and relevant studies in the Okanagan Basin [Cannon et al., 2002]. Next, monthly relationship between each predictor and the predictand of interest (e.g., maximum temperature, Table 5-5) is investigated in SDSM [Wilby et al., 2002]. The procedure requires defining the process type and significance level. The latter is required to test the significance of predictor-predictand relationship (e.g., percentage of variance explained at 5% significance level, which is the default value in SDSM: Tables 5-4, 5-5, and 5-6). SDSM reports statistically significant predictor–predictand relationships [Wilby et al., 2002]. Note here that the regression technique used in SDSM makes the assumption that the input data are normally distributed. As this is not the case for precipitation, it is necessary to apply a particular transformation to the data set so that its distribution becomes more normal. The data transformation options in SDSM include logarithm, power, squares, cubes, fourth powers, fourth root, etc. The fourth root transformation, the default method in SDSM, is used here as it resulted in strongest predictor-predictand relationships at the selected significance level (Table 5-6).

The process type can be defined as conditional or unconditional depending on the type of the predictand variable. Conditional is selected when the predictor-predictand

relationship is controlled by an intermediate process (as with precipitation where amounts depend on the occurrence of wet day); otherwise, unconditional process is selected (as in the case of minimum temperature and maximum temperature).

Once the above have been defined, each of the predetermined 26 predictor variables is analysed, in SDSM, with respect to each of the three predictands (precipitation, minimum temperature and maximum temperature). The percentage of variance explained by each predictand–predictor pairs is examined, and the variables which have higher percentage of variance explained are selected. Tables 5-4, 5-5, and 5-6 show the selected predictors and the corresponding results (percentage of variance explained) for minimum temperature, maximum temperature and precipitation, respectively. Scatterplots of each predictor-predictand pair were also used to assist the procedure of screening predictor variables. For instance, the predictor - predictand scatterplots shown in Figures 5-5 and 5-6 suggest that maximum temperature and minimum temperature are associated with near surface specific humidity (shumna) and mean temperature at 2m (tempna), respectively.

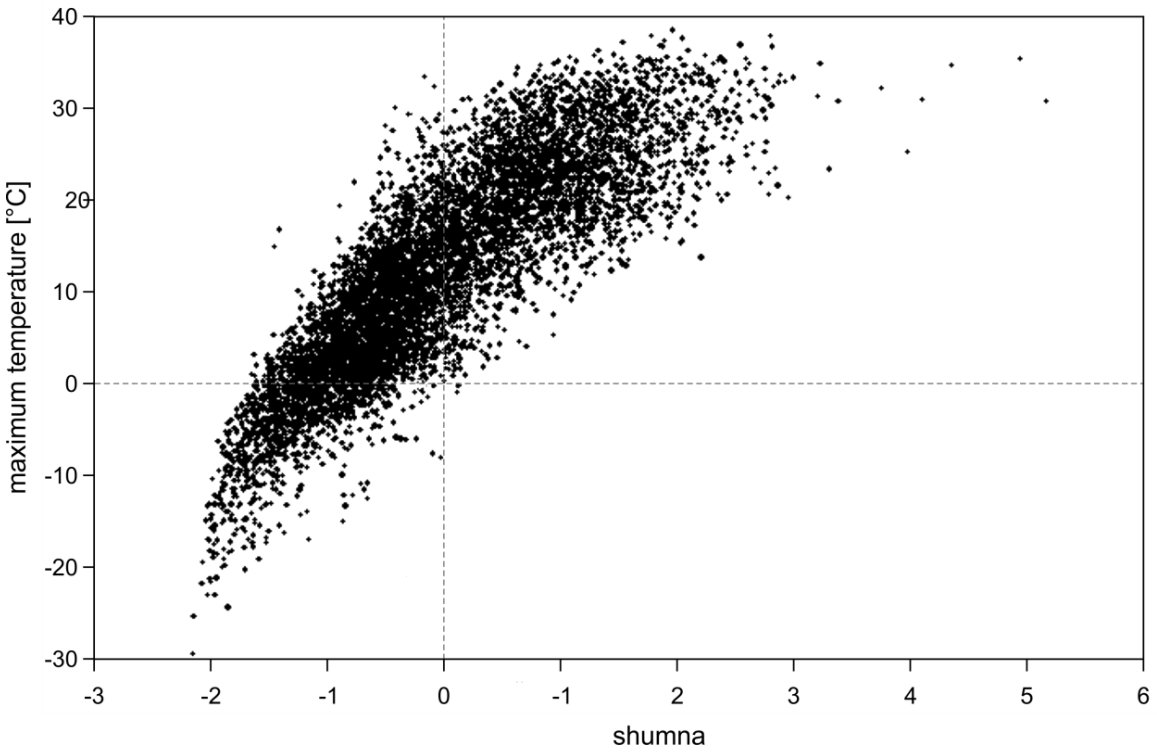

Figure 5-5 Scatterplot, showing the association between maximum temperature and shumna.

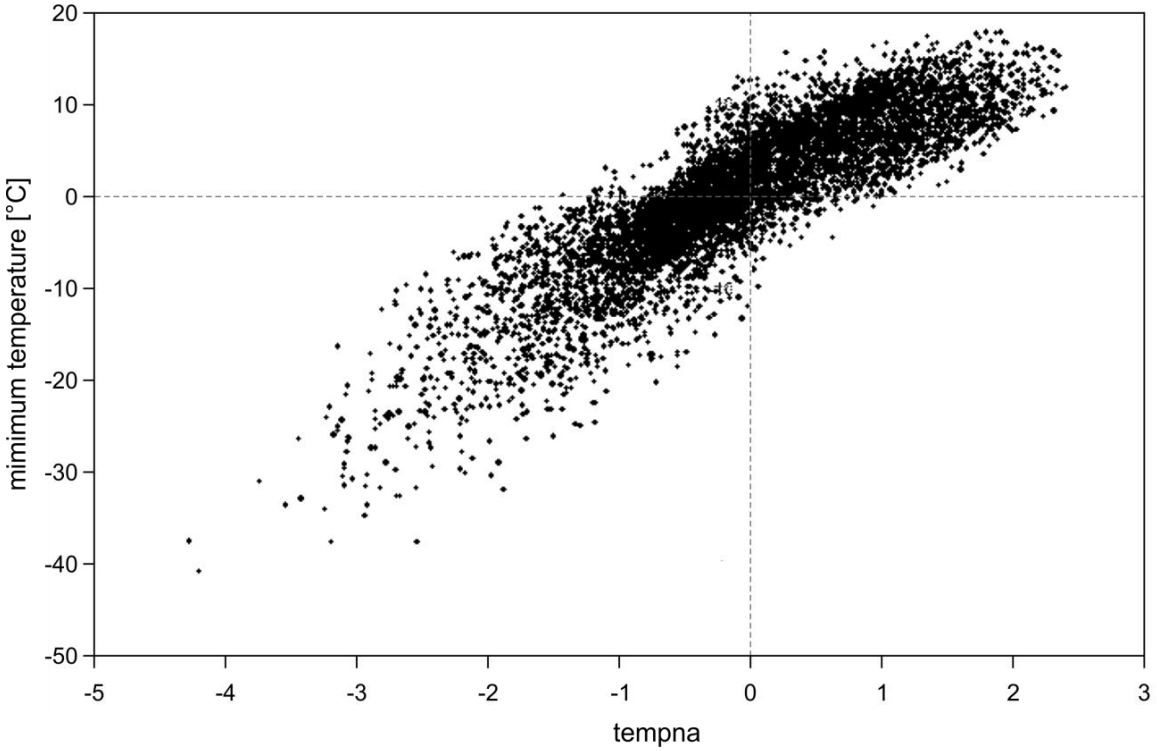

Figure 5-6 Scatterplot, showing the association between minimum temperature and tempna

Next, all of the selected predictor variables, shown in Tables 5-4, 5-5, and 5-6 are used in SDSM to formulate the statistical relationships necessary for downscaling minimum temperature, maximum temperature and precipitation, respectively. These analyses are done by using daily climate data for the base period (1969 – 2000). A period of about 30 years is often suggested as it is likely to contain wet, dry, warm, and cold periods [Carter et al., 1994]. The degree of fit of the downscaled climate data and the observed variables (calibration results), for minimum temperature, maximum temperature, and precipitation are shown in in the last columns of Tables 5-4, 5-5, and 5.6, respectively. Model results are further summarised to long term monthly average data [Figures 5-7 and 5-8]. As can be seen in the figures, the downscaled climate variables were able to replicate seasonal variation of the observed variables very well.

Table 5-4 Percentage of variance explained at 5% significance level (predictor vs. minimum temperature)

	mslpna	p_una	p5_vna	p5zhna	shumna	tempna	calibration result
Jan	10.5	37.8	10.1	9.9	52.9	58.8	51.3
Feb	14.4	22.9	16.2	16.4	51.8	56.4	49.5
Mar	10.7	22.0	18.3	16.6	51.6	56.2	50.2
Apr	14.0	7.6	17.2	17.5	42.8	43.4	42.3
May	12.6	0.9	10.4	10.1	24.0	21.0	34.3
Jun	11.4		3.5	3.8	18.1	15.8	34.1
Jul	9.6	1.0	3.4	4.0	26.5	15.3	30.9
Aug	7.0	2.3	6.3	6.9	37.3	13.8	23.1
Sep	28.7	15.1	23.6	22.3	48.1	22.0	41.1
Oct	23.9	21.7	22.7	23.0	52.6	44.3	40.5
Nov	16.3	27.7	16.5	16.5	51.4	61.5	44.2
Dec	11.0	30.5	15.1	15.6	45.5	55.6	43.7

Table 5-5 Percentage of variance explained at 5% significance level (predictor vs. maximum temperature)

	p_una	p500na	p8_una	r850na	shumna	tempna	calibration result
Jan	52.7	12.9	39.8	13.8	55.8	60.9	69.2
Feb	28.4	7.8	22.6	8.6	43.7	50.1	54.1
Mar	2.3	23.1		6.0	19.7	21.3	41.1
Apr	13.2	54.4	9.0	18.5	34.9	31.2	63.4
May	24.6	70.4	12.5	36.8	31.5	31.5	73.0
Jun	39.3	66.1	20.7	44.4	22.8	28.5	70.0
Jul	35.2	71.4	19.8	56.5	9.3	69.3	75.8
Aug	24.6	68.3	12.6	51.9	5.6	66.3	74.3
Sep	6.9	62.5	2.7	43.8	13.8	64.8	75.6
Oct		26.8		7.0	36.6	48.1	53.9
Nov	34.2	10.9	23.4	8.7	48.8	56.8	62.3
Dec	44.7	10.8	38.5	18.8	50.7	59.7	67.3

Table 5-6 Percentage of variance explained at 5% significance level (predictor vs. precipitation)

	pmslpna	p850	r500	r850	rhum	calibration result
Jan	10.6	8.2	12.9	11.3	9.4	19.3
Feb	11.7	10.1	8.7	9.5	7.7	17.9
Mar	9.0	6.7	6.3	9.2	10.4	21.7
Apr	7.7	6.6	7.4	8.3	8.4	18.8
May	8.4	12.8	8.4	13.8	11.6	26.2
Jun	4.4	10.0	8.3	12.0	8.9	22.0
Jul	5.3	11.9	6.6	13.3	12.5	27.8
Aug	4.3	10.5	9.3	15.6	14.1	21.0
Sep	12.1	18.2	12.2	19.5	15.8	39.5
Oct	12.4	14.2	10.8	12.4	8.9	28.2
Nov	8.0	7.2	7.1	7.8	5.7	20.3
Dec	11.9	10.5	12.0	11.1	6.2	19.0

The predictors in the above tables are: mslpna (surface meridional velocity), p_una (1000 hPa U-component), p5_vna (500 hPa V-component), p5zhna (500 hPa Divergence), shumna (near surface specific humidity), tempna (mean temperature at 2m), p850 (850 hPa geopotential height), p500 (500 hPa geopotential height), r500 (500 hpa relative humidity), r850na (relative humidity at 850 hPa pressure levels).

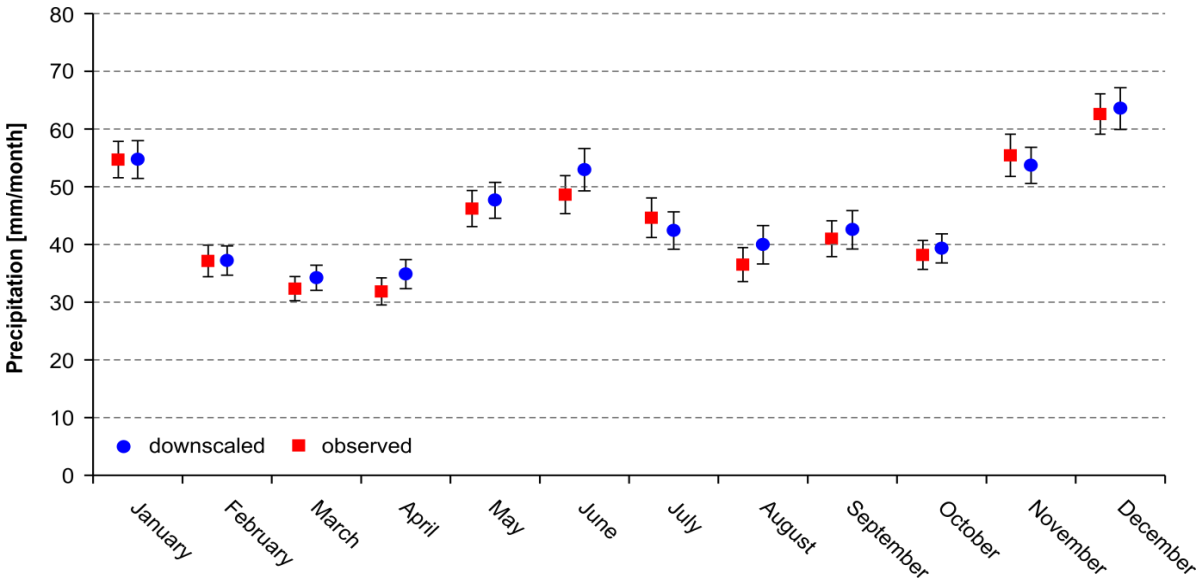

Figure 5-7 Model result: Observed versus downscaled precipitation (1969-2000)

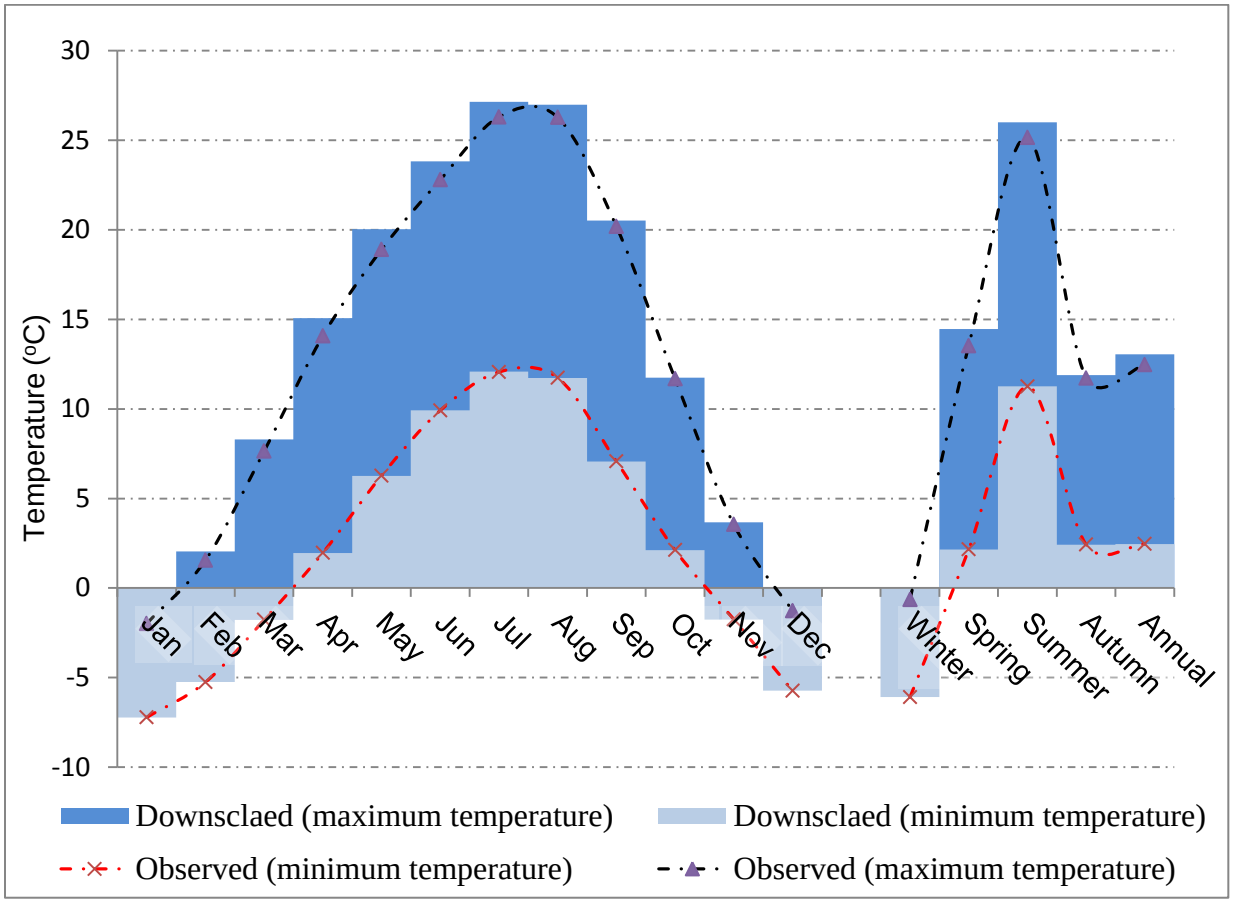

Figure 5-8 Model result: Observed versus downscaled temperature maximum and minimum (1969-2000)

5.3 Application for Future Periods

The impact of parameterization on water movement is evaluated by simulating groundwater recharge under changing climate. To this end, HadCM3 A2 predictor variables are first used for the period of 2001 to 2006 in an attempt to better match observed and synthesised values by adjusting the two stochastic model parameters, i.e. variance inflation and bias correction. Next, future climate scenarios are synthesised using the GCM predictor variables for the periods from 2010 to 2029, and 2030 to 2049. The assumption here is that the statistical relationship formulated under the observed climate conditions would remain valid under the future climate conditions, and this is one of the known limitations in statistical downscaling techniques [Fowler et al., 2007].

The synthesized climate data (daily precipitation and daily temperature minimum and maximum) are then forced into various scenarios of HYDRUS-1D to simulate groundwater recharge. Details on recharge modelling procedures are provided in Chapter 4. The recharge simulated using ROSETTA VGM parameters [Table 4-1] and calibration parameters [Table 5-1] are aggregated into annual values for each of the three periods (historical and two future periods) [Figures 5-9, 5-10, and 5-11].

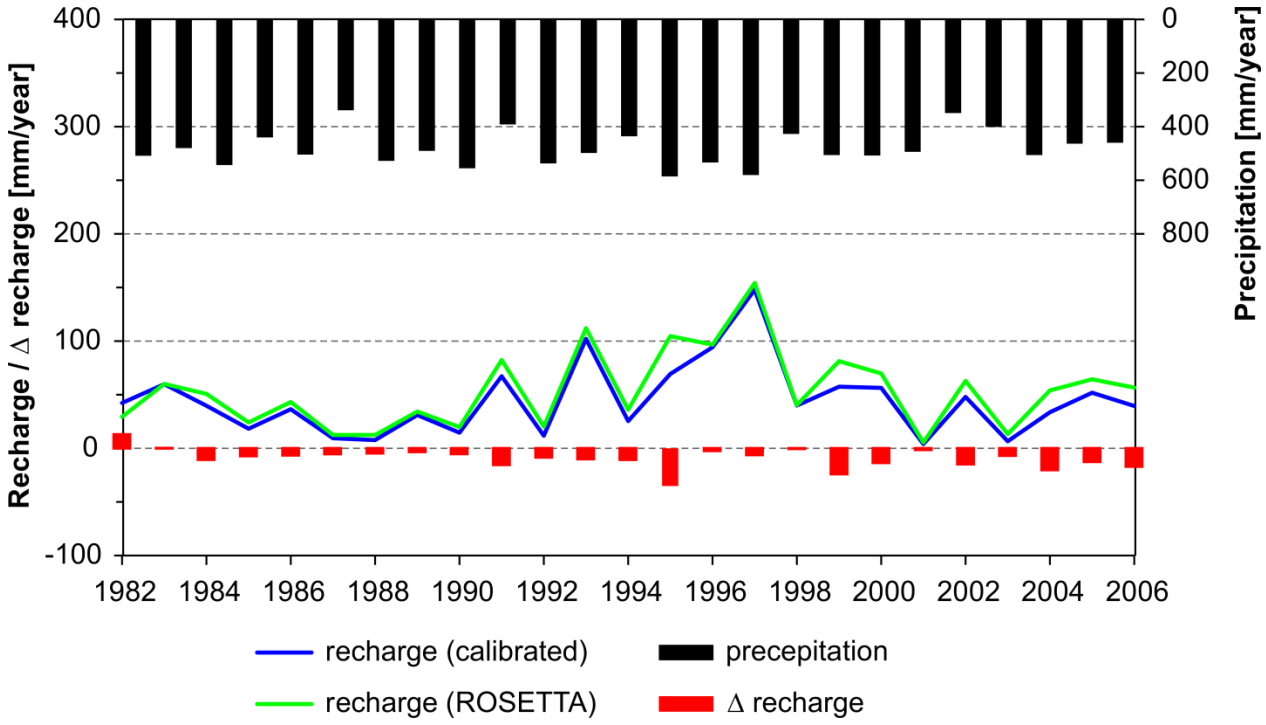

Figure 5-9 Recharge under the historical climate using ROSETTA and calibrated parameters at the location of HOBO station # 1

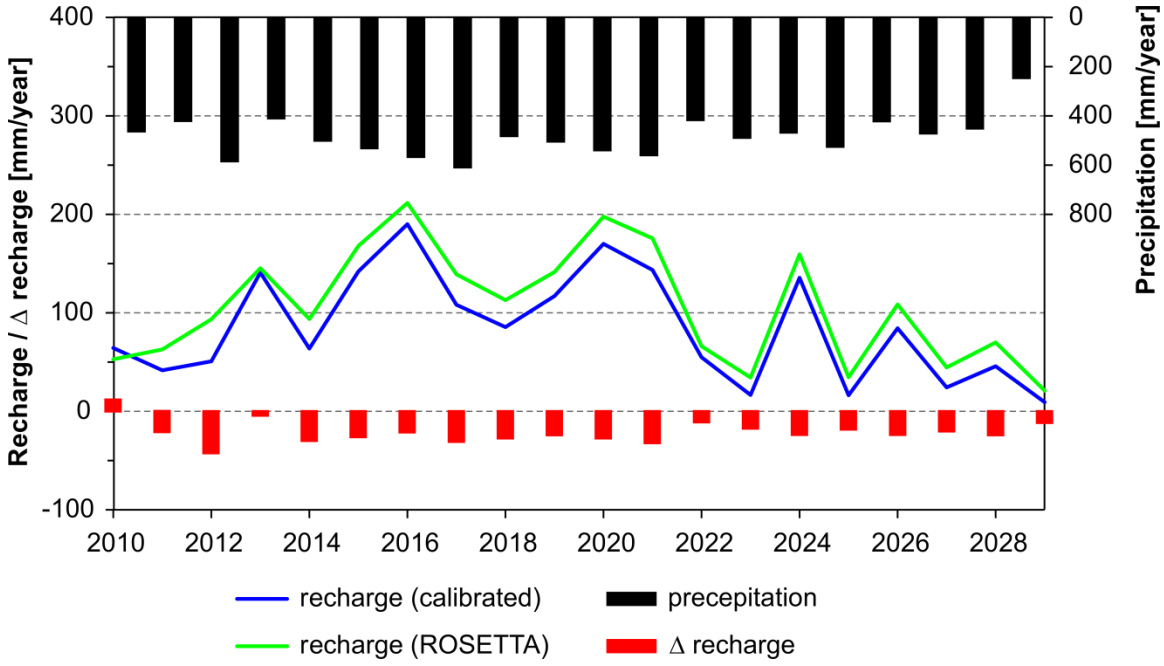

Figure 5-10 Recharge under the future climate (2010-2029) using ROSETTA and calibrated parameters at the location of HOBO station # 1

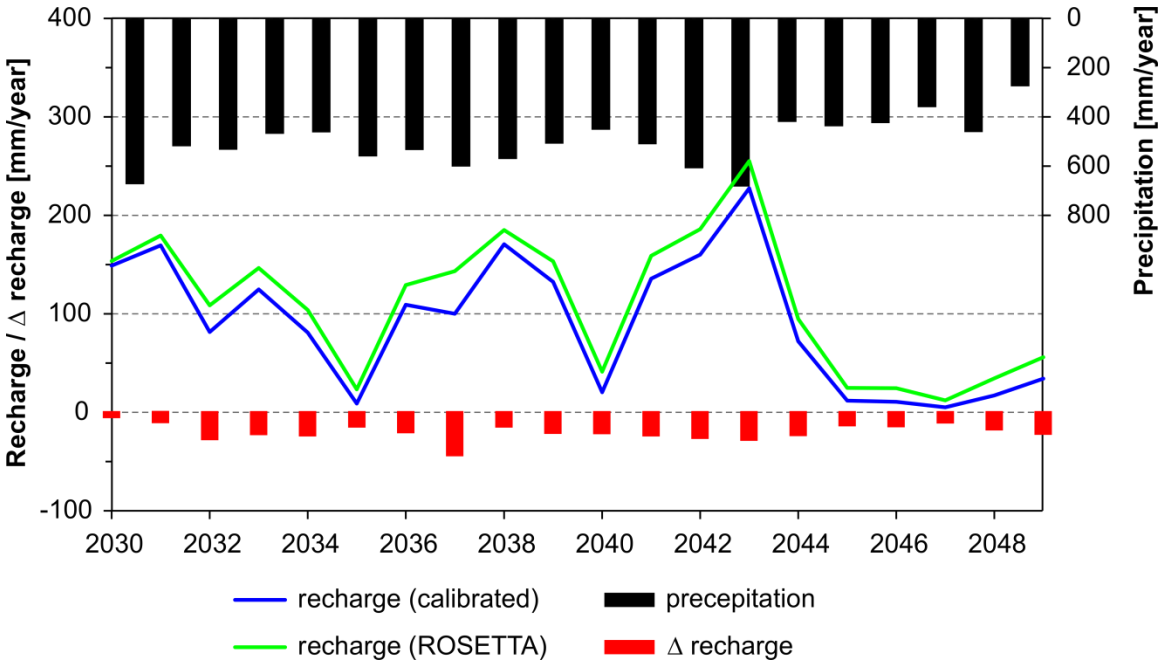

Figure 5-11 Recharge under the future climate (2030-2049) using ROSETTA and calibrated parameters at the location of HOBO station # 1

To evaluate the differences in annual recharge due to model parameters in relation to the natural variability of recharge (temporal variability), the results from all of the above scenarios are further analyzed and summarized - Table 5-7 shows the average annual recharge estimated using the ROSETTA and calibrated model parameters under the historical and future periods. As can be seen in the table, the maximum difference in the annual recharge, due to model parameterization, is about 20 mm/year. This difference is however less than 5% of the total precipitation. On the other hand, the difference in recharge (deviation from the average) due to temporal variability can be as high as 70 mm/year [Table 5-7]. This value is equivalent to 14% of precipitation. It can thus be realized here that the uncertainties in groundwater recharge due to the two different set of

Table 5-7 Average annual groundwater recharge using ROSETTA derived and calibrated parameters

Annual recharge	Historical period				Future 1 (2010-2029)		Future 2 (2030-2049)	
	Observed [1982-2006]		Downscaled (1982-2001)					
	ROSETTA [mm/year]	Calibration [mm/year]	ROSETTA [mm/year]	Calibration [mm/year]	ROSETTA [mm/year]	Calibration [mm/year]	ROSETTA [mm/year]	Calibration [mm/year]
Average	54	45	78	61	107	87	111	91
Standard deviation	36	33	43	39	58	55	70	67
Average precipitation	482		485		488		502	

model parameters are negligible as compared to the significant temporal variability. The results thus reinforce the conclusions made with the preliminary results discussed in section 5.1– that the gridded soil data developed by Kenney and Frank [2010] can be taken as a reliable resource for modelling water movement in the vadose zone.

In an effort to explain why average annual recharge increases significantly when the increase in average annual precipitation is mild [Table 5-7], the daily recharge values hind casted for the past climate (20 years, 1982-2001) and the two future projections are aggregated into monthly average values, and plotted with the seasonal distribution of precipitation and evapotranspiration for the respective three periods (historical and the two future periods) [Figure 5-12]. Potential evapotranspiration is estimated using the Hargreaves method which is built in the HYDRUS-1D code. The Hargreaves method requires daily mean temperature, computed as mean of the minimum and maximum air

temperature [°C]; the temperature range between the mean daily maximum and minimum air temperature [°C] and extraterrestrial radiation [J $m^{-2}s^{-1}$]. The parameters required to

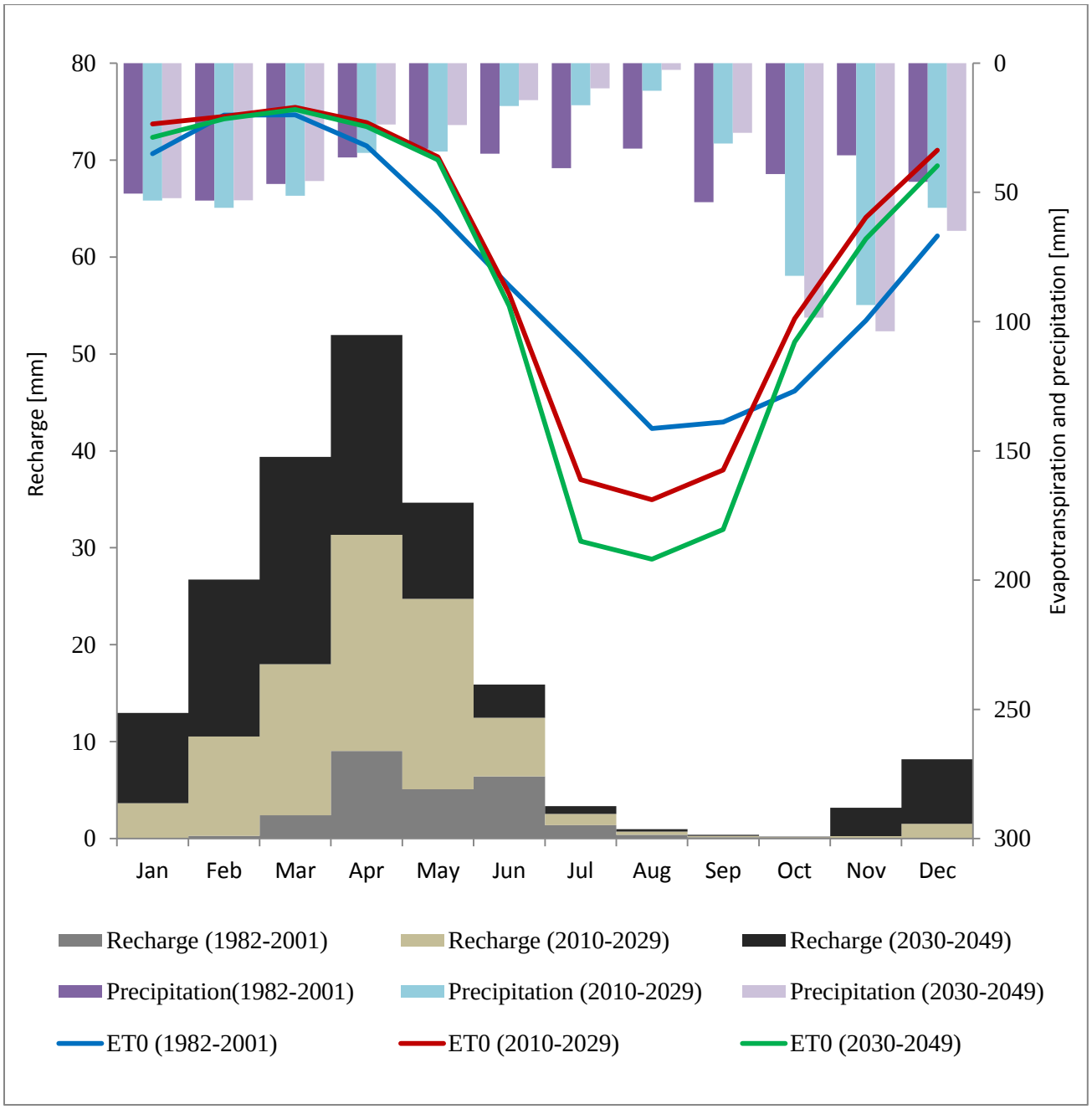

Figure 5-12 Seasonal variation of recharge, precipitation and evapotranspiration for the historical (1982-2001) and two future periods (2010-2029; 2030-2049)

estimate the latter are derived from the HYDRUS-1D database based on geographical location [Hargreaves, 1994; Simunek et al., 2005].

Note in Figure 5-12 that reduction in monthly precipitation and increase in monthly evapotranspiration is expected in the summer months of the future climates. However, the summer months are not generally important in terms of replenishing the ground water aquifer. An increase in precipitation and decrease in evapotranspiration is noted in the rather important seasons (Fall and Winter), with a clear reduction in Spring evapotranspiration. Such climatic condition generally favours recharge. For instance, see the months March and April in Figure 5-12 when high recharge values are estimated in both the historical and future climatic conditions. The high recharge values can be attributed to the lagged response to higher precipitation (e.g., October, December and November) combined with spring snow melt. Therefore, the reason why average annual recharge is so high in the two future periods when the increase in average annual precipitation is mild [Table 5-7] is because of the discussed seasonal variation in the projected evapotranspiration and precipitation values. More results and analyses on the seasonal distribution of recharge, in relation to other water balance components, can be found in Chapter 4 of this thesis [e.g., Section 4.3.3].

Chapter 6

Analysis of Variability and Extremes

Changes in climate variability and extremes are considered crucial feature of climate change studies. To this end, daily climate data, previously downscaled using a statistical downscaling technique and four GCM scenarios [CGCM3A2, CM2.1-B1, ECHAM5-B1, HadCM3-B2] [Stahl et al., 2008; Neilsen et al., 2010] are analysed for variability and extremes. The projected GCM scenarios of daily maximum temperature, daily minimum temperature, and total daily precipitation are grouped into three tri-decades centred on the 2020's [2010-2039], 2050's [2040-2069], and 2080's [2070-2099]. The consistency of the aforementioned Okanagan GCM scenarios in predicting average and extreme events is evaluated. Each downscaled parameter is analysed for variability and extremes with respect to the historical period (1977-2006) using frequency analyses techniques and indices derived from a FORTRAN code known as STARDEX [Stardex, 2004] [Section 6.2].

6.1 Variability in Basic Weather Parameters

Various studies have shown that slight changes in average temperature can cause significant variability in extreme events [Meehl et al., 2000; Katz, 1992; Pancura and Lines, 2005]. Preliminary analyses are conducted here to evaluate if changes in variance and average of temperature can in fact suggest increase in the probability of occurrence of extreme temperature events in the Okanagan Basin. To this end, the downscaled parameters are analysed relative to the historical period (1977-2006). The future climate is analysed using all of the four GCM scenarios each grouped into three tri-decade periods (2020's, 2050's, and 2080's).

6.1.1 Minimum and Maximum Daily Temperature

Changes in average and standard deviation of the historical and projected distributions are analysed for minimum and maximum air temperature of the four GCM scenarios. The results, shown in Appendix A1 and Appendix A3 respectively, are further summarised in Tables 6-1 and 6-2. As can be seen in the tables, an overall increase in minimum and maximum temperature is anticipated in the future periods. While the increase in maximum temperature is estimated to range, on average, between 2.1 and 5.2 ^{o}C by the 2080's, with about 2% to 15% increase in variability; the rise in minimum temperature is estimated to range between 1.4 and 3.9 ^{o}C by the 2080's, with about 0 to 19% increase in variability. These results apparently project a warmer climate in the North Okanagan. However, the question remains, whether these changes in mean and variability actually suggest increases in the probability of occurrence of extreme temperature events?

Table 6-1 Changes in mean and variability of maximum temperature relative to the historical climate (1977-2006)

Maximum temperature [^{o}C]	2020's		2050's		2080's	
	Changes in mean	Changes in variability	Changes in mean	Changes in variability	Changes in mean	Changes in variability
CGCM3-A2	0.7	0.2	1.9	3.5	3.4	6.8
HADCM3-B2	1.5	6.3	0.7	11.1	3.7	14.6
ECHAM5-B1	0.4	0.0	1.1	0.9	2.2	1.9
CM21-B1	1.1	3.5	1.7	3.3	2.1	8.1

Table 6-2 Changes in mean and variability of minimum temperature relative to the historical climate (1977-2006)

Minimum temperature [^{o}C]	2020's		2050's		2080's	
	Changes in mean	Changes in variability	Changes in mean	Change in variability	Changes in mean	Changes in variability
CGCM3-A2	0.7	0.0	1.6	0.0	3.0	0.0
HADCM3-B2	1.0	7.9	1.7	19.0	3.0	18.0
ECHAM5-B1	0.4	0.0	1.1	0.0	2.0	1.0
CM21-B1	0.5	0.9	1.1	0.3	1.4	6.1

In order to answer the aforementioned question, changes in the probability of occurrences of extreme events are analysed by using the historical climate and the projected four GCM scenarios. The probability density function for the three tri-decade periods of each of the four scenarios of daily maximum and minimum temperature are shown in Appendix A2 and Appendix A4, respectively. Analyses of the results do in fact demonstrate significant increases in the probability of occurrence of extreme events. For instance, analysis of the daily maximum temperature show that a 100 year return period event in the current climate (30^{o}C) will likely be about 2 to 6 times more likely in the 2080's, with probability of exceedence estimated between 0.02 to 0.06.. Similarly, the shift towards warmer temperatures is statistically quantified based on the minimum temperature distribution curves [Appendix A4]. The probability of occurrence of a very

cold day (< -15^{o}C) under the current climate is estimated to be 0.046, whereas, the same extreme event is determined to be about 1.2 to 2.6 times less likely in the 2080's, with probability of exceedence estimated between 0.018 to 0.04. The threshold events in all cases are represented by red lines in the appendices [Appendix A2 and Appendix A4]. The probability of exceedences and return periods estimated for the historical period and each of the four GCM scenarios are shown in Table 6-3 and Table 6-4 below. The results in all cases showed that changes in average and standard deviation of downscaled climate data does in fact suggest increases in the probability of occurrence of extreme temperature events in the North Okanagan.

Table 6-3 Maximum temperature (T_{max}) -probability of exceedence and return periods for historical climate and three tri-decade projections of four GCM scenarios

Maximum temperature [^{o}C]	Exceedence Probability [p > 30^{o}C]				Return period[year]			
	1977 to 2006	2020's	2050's	2080's	1977 to 2006	2020's	2050's	2080's
CGCM3-A2	0.010	0.012	0.019	0.031	100	63	55	40
ECHAM5-B1	0.010	0.010	0.014	0.019	100	100	71	53
CM21-B1	0.011	0.016	0.018	0.025	94	63	55	40
HADCM3-B2	0.009	0.020	0.021	0.043	107	50	48	23

Table 6-4 Minimum temperature (T_{min}) - probability of exceedence and return periods for historical climate and three tri-decade projections of four GCM scenarios

Minimum temperature [^{o}C]	Exceedence probability[P<-15^{o}C]				Return period[year]			
	1977 to 2006	2020's	2050's	2080's	1977 to 2006	2020`s	2050's	2080's
CGCM3-A2	0.046	0.035	0.028	0.018	22	28	36	55
ECHAM5-B1	0.051	0.036	0.036	0.027	20	28	28	37
CM21-B1	0.048	0.041	0.034	0.034	21	24	29	29
HADCM3-B2	0.049	0.046	0.045	0.040	20	22	22	25

In addition to the preliminary study of variability in average climate and extreme events, consequences of climate change on the number of cold days are also analysed with respect to three threshold temperatures (-10°C,-15°C,-20°C) [Pancura and Lines, 2005]. Histogram analyses are made using all of the four GCM scenarios, and the results suggest that the number of days with minimum temperature (T_{min}) < -10°C (cold days), T_{min} < -15°C (very cold days), and T_{min} < -20°C (bitterly cold days) will likely be less common in the future climate. The anticipated changes in cold, very cold and bitterly cold days, as projected using one of the GCM scenarios (CGCM3-A2), is shown in Figure 6-1. Results for the remaining three scenarios can be found in Appendix A5.

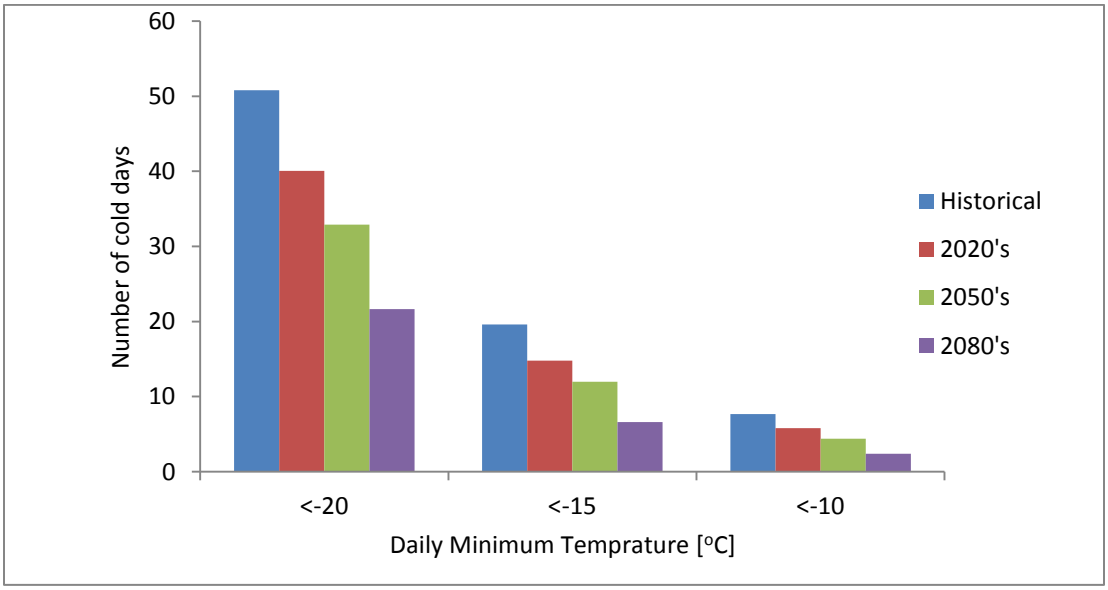

Figure 6-1 Number of cold days per year for historical climate and three tri-decade projections of CGCM3-A2 scenario.

6.1.2 Daily Precipitation

As precipitation does not follow a normal distribution function [IPCC, 2001], the frequency and magnitude of precipitation series are analysed by fitting a simple empirical distribution to the daily precipitation data [Wilby et al., 2002]. The step by step procedures are given below.

Step 1 - Sort annual maximum daily precipitation of the historical and the future climate scenarios in descending order, and plot these according to the return period. The return period is calculated as $(n+1)/m$, where n is the number of maximum precipitation and m is the rank with one assigned to the highest precipitation and n to the lowest.

Step 2 –Fit a trend line to the plot produced in Step 1 (logarithmic function is selected based on the displayed R-squared value of chart). The plot produced for the historical period is shown here for demonstration purpose [Figure 6-2].

Step 3 – Equations developed in Step 2 are used to extrapolate 50 year and 100 year return period events.

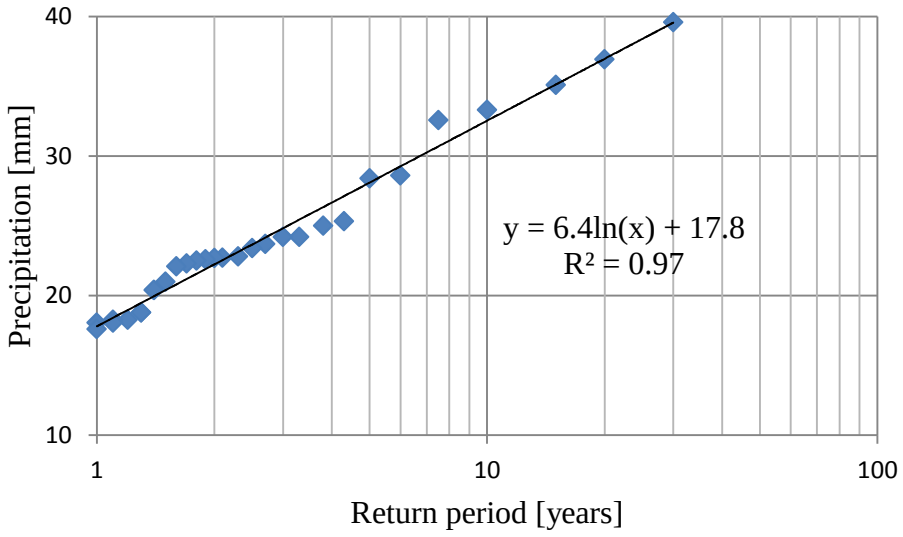

Figure 6-2 Return periods versus annual daily maximum precipitation for historical climate (1977-2006). The dashed line shows the fitted trendline.

Step 4 – Prepare another plot for selected events of 100, 50, 30, 20, 15,10,5,4,3,2 and 1 year return period (e.g., Figure 6-3). The eleven points are selected to present the results in a readable format, and to assist visual comparison of the changes in future precipitation events relative to the historical climate. Figure 6-3 demonstrates the anticipated changes in return periods for one GCM scenario (CM21-B1). The dashed lines represent the logarithmic trendlines fitted to the eleven points. The results for the remaining three scenarios (CGCM3-A2, HADCM3-B2, and ECHAM5-B1) can be found in Appendix A6.

Note that empirical frequency analysis is conducted here as the aim of the frequency analyses in this chapter is limited to evaluating the consistency of the aforementioned Okanagan GCM scenarios in projecting future extremes. To this end, analyses of the results from all the GCM scenarios consistently show an overall increase in annual

maximum precipitation events (Figure 6-4, Appendix A6). Attempt is made to compare changes in return periods of historical and future events by using 100 year return period events and relatively lower events of 2 year return period. The results show that a 100 year event (48.2mm) in the base climate period (1977-2006) may occur every 4 to 10 years in the 2080's, and a relatively lower event of about 2 year return period in the base climate period (23 mm) may occur every year in the 2080's. Although it is difficult to derive quantitative conclusion based on these preliminary empirical analyses, the results are suggestive of the potential increase in future precipitation events. Figure 6-4 shows the anticipated increase extreme events as projected by all of the four GCM scenarios considered in this study. Similar analysis about potential changes in stream flow values and the potential uncertainty in the method is discussed in Section 7.2.4.

6.2 Variability in STARDEX Extremes

This study has also used open source FORTRAN code called STARDEX [Stardex, 2004] in an attempt to evaluate the impact of climate change on annual extreme weather indices. The indices are derived for two climate variables, temperature and precipitation. Four extreme indices are estimated for historical (1977-2006) as well as tri-decade future climate (2010 – 2039; 2040 – 2069; and 2070 –2099). The future climate projected using

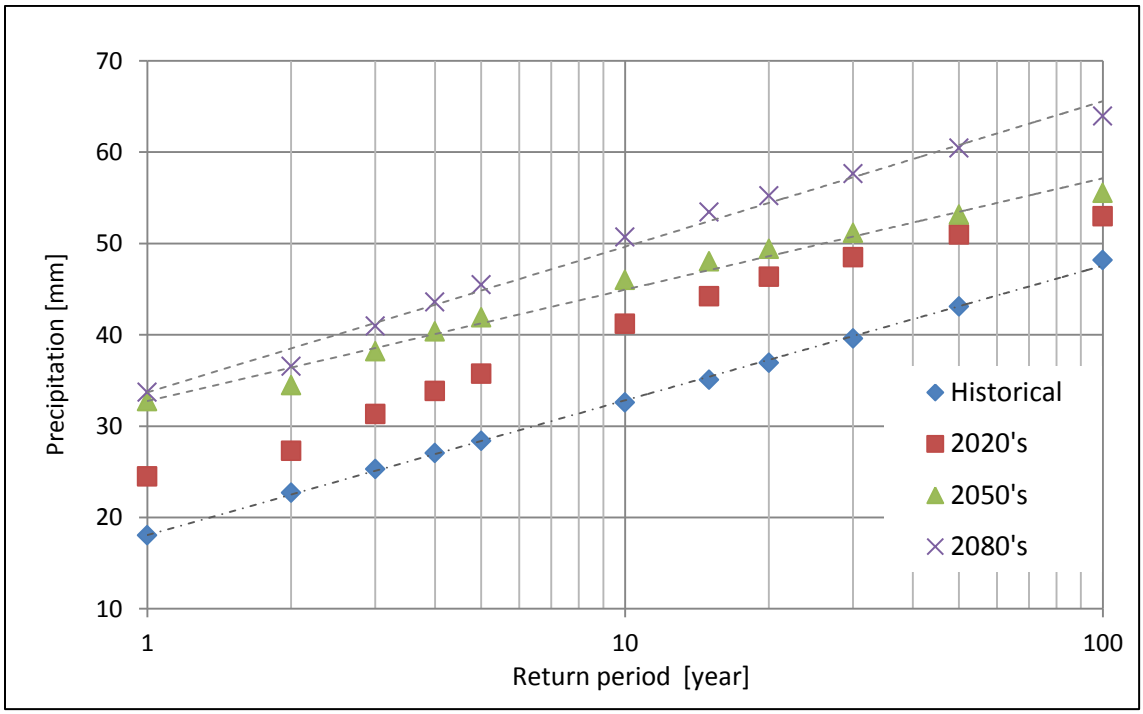

Figure 6-3 Changes in return periods of annual daily maximum precipitation for historical climate and three tri-decade projections of the CM21-B1 GCM scenarios. The dashed lines show the fitted trendlines.

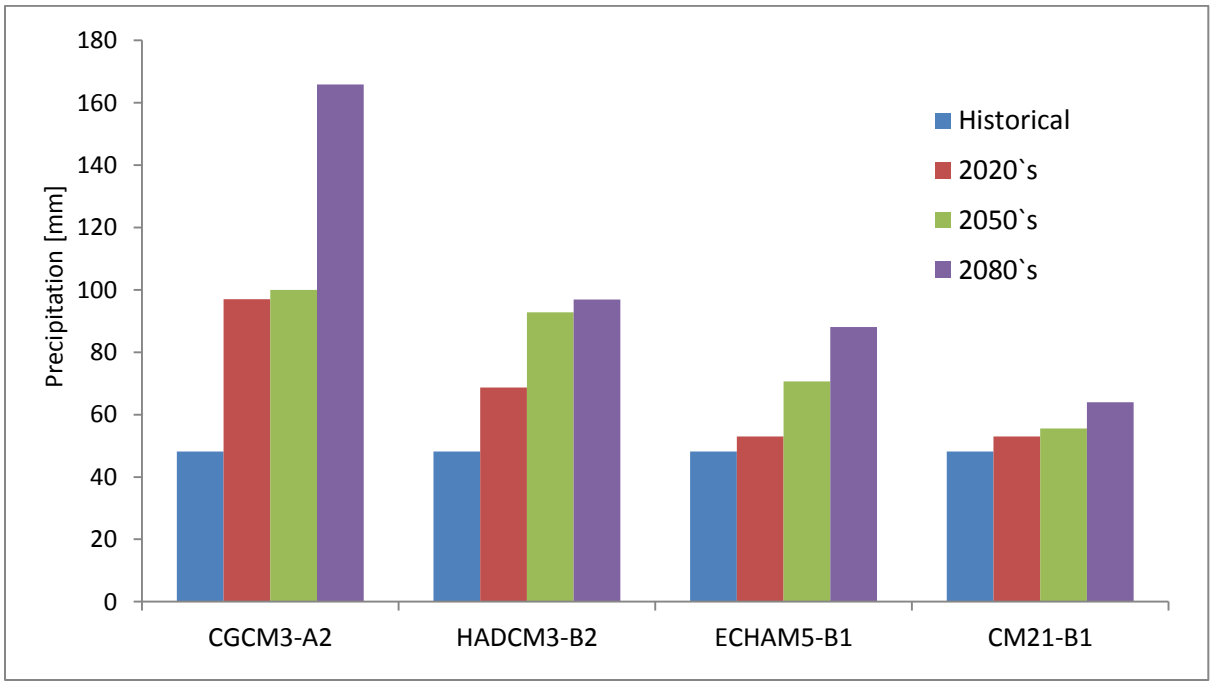

Figure 6-4 Hundred year return period precipitation events for historical climate and three tri- decade projections of four GCM scenarios.

all of the four GCM scenarios are considered here as well. The software requires an ASCII file input containing daily climate data in the following order: year, month, day, minimum temperature, maximum temperature, average temperature, and precipitation. The result files are printed to text files which contain time series of indices. The indices considered here are: threshold value of the 90th percentile of maximum daily temperature (Tmax90p), threshold value of the 10th percentile of the minimum daily temperature (Tmin10p), the number of frost days (125Fd) and threshold value of the 90th percentile of daily precipitation (wettest days) (Prec90p). A brief description of each index and discussion of the anticipated changes under various scenarios of changing climate is given below.

6.2.1 Tmax90p and Tmin10p

Tmax90p and Tmin10p represent the highest temperature within 90^{th} percent of the hottest days and the threshold value of the 10^{th} percentile of the daily minimum temperature respectively. The statistics of these two extreme indices are estimated for the historical period as well as the tri-decades of the four GCM scenarios in [Appendix A7 and Appendix A8]. Summary of these two extreme indices, shown in Figure 6-5 and Figure 6-6, indicate an increase in mean threshold values of all the GCM scenarios. These findings further confirm the conclusions made in Section 6.1.1 that the future will be significantly warmer in Northern Okanagan. For instance, a 100 year event in the current climate may be 2 to 6 times more likely in the 2080's.

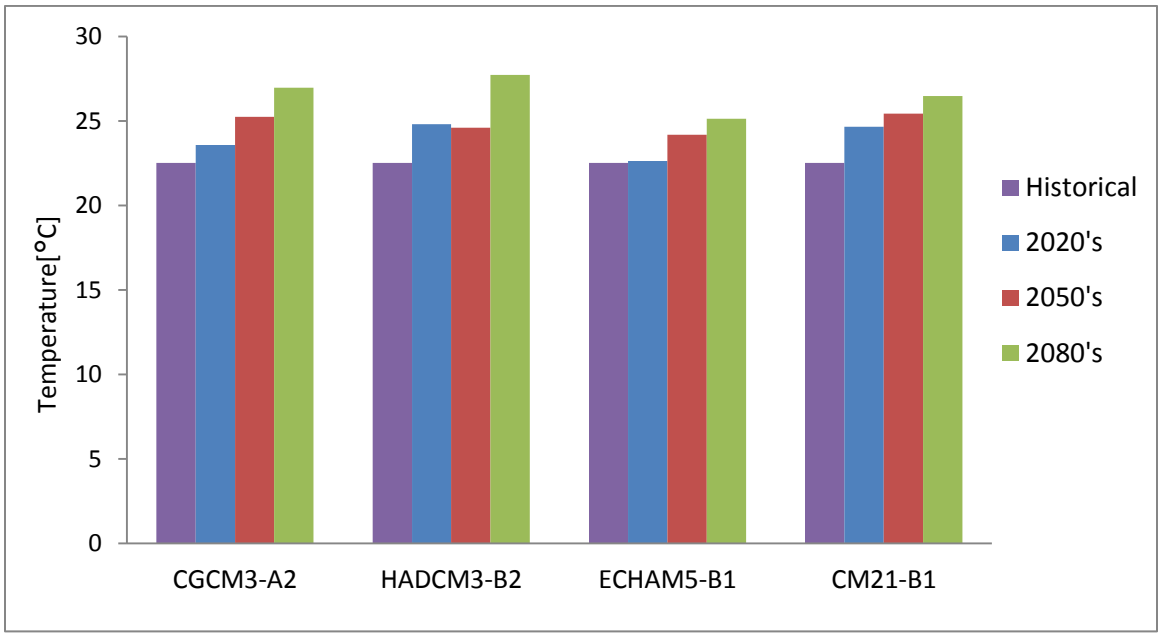

Figure 6-5 Mean threshold values (highest temperature within 90th percent of the hottest days), for historical climate and three tri- decade projections of four GCM scenarios.

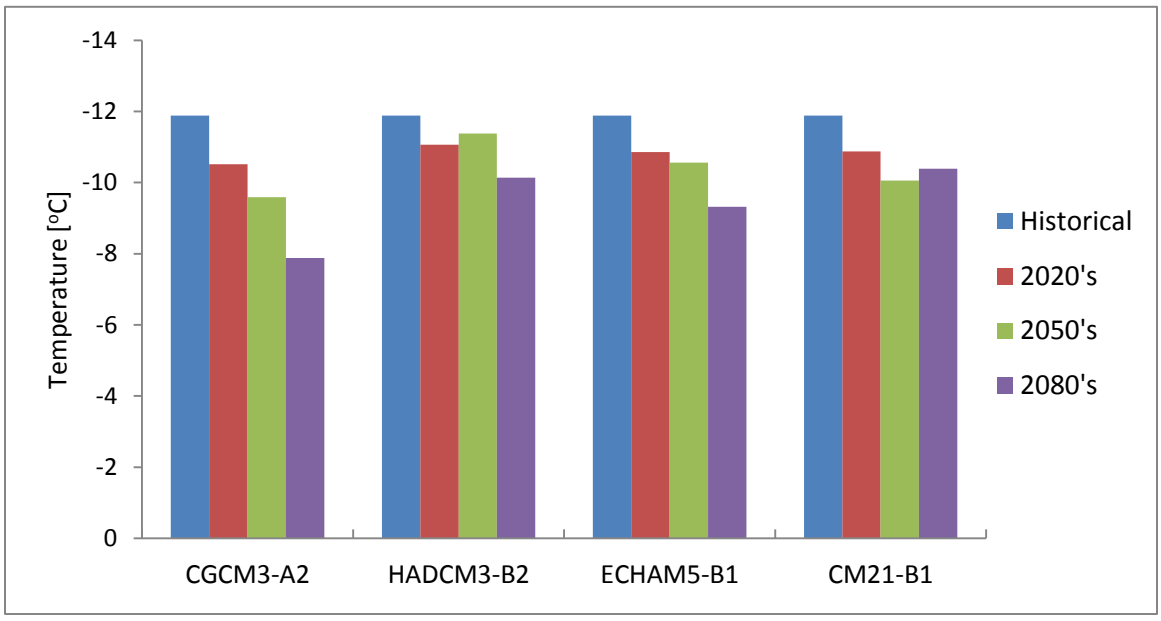

Figure 6-6 Mean threshold values (highest temperature of the 10 percent of the coldest days) for historical cli mate and three tri-decade projections of four GCM scenarios.

6.2.2 Number of Frost Days [125Fd]

The number of frost days (125Fd) is another STARDEX index representing the number of days with negative temperature. The relevant statistics estimated for the historical period are compared with the future tri-decade statistics of all the four GCM scenarios [Appendix A9]. Analyses of the results show a general decreasing tendency in the number of frost days [Figure 6-7], and this is in agreement with the theory of global warming.

6.2.3 Prec90p

In addition to the frequency analysis technique discussed in Section 6.1, variability in precipitation extremes is also analysed using the STARDEX intensity extreme that represents the highest precipitation within 90^{th} percent of the wettest days [Prec90p]. Similar to the other indices, this extreme index is estimated for the historical period as well as for the projected tri-decades of all the GCM scenarios [Appendix A10]. A summary of the results are shown in Figure 6-8. As can be seen in the figure, the future climate is projected to be wetter by all of the GCM scenarios considered in this study.

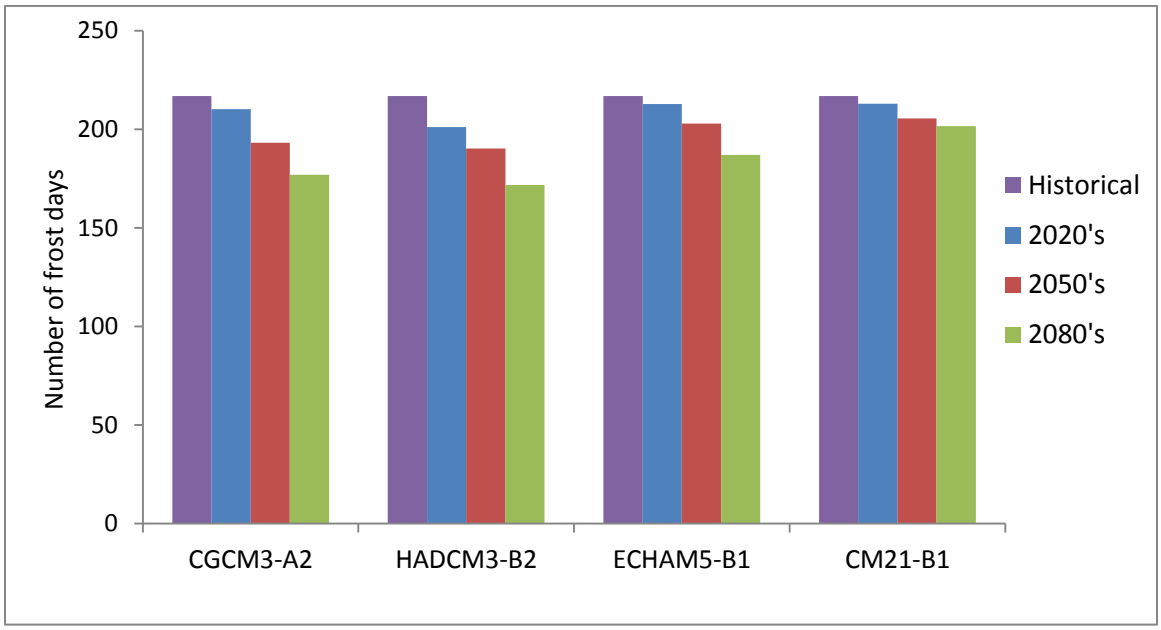

Figure 6-7 Frost days per year for historical climate and the three tri-decade projections of four GCM Scenarios

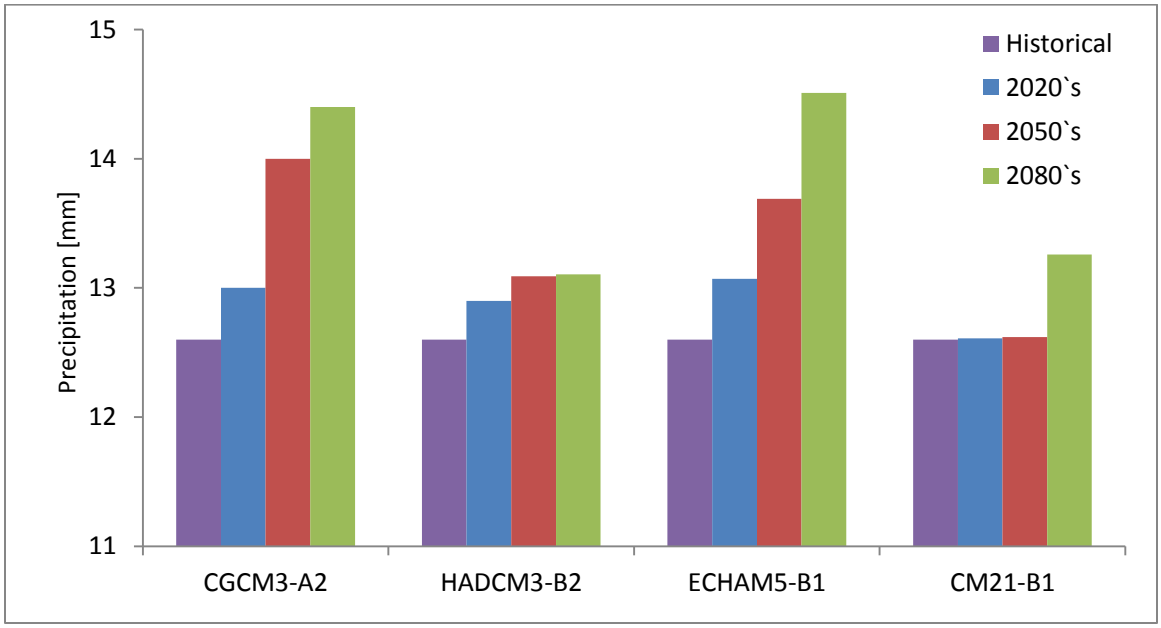

Figure 6-8 Mean threshold values (highest precipitation within 90th percent of the wettest days), historical climate and three tri- decade projections of four GCM scenarios

It is evident from the above analyses that the future will be both warmer and wetter with significant increases in magnitude and probability of occurrence of extreme events.

In the next chapter, the projected climate data from all of the four GCM scenarios are used in a fully integrated hydrological model to further evaluate the resulting changes in magnitude and frequency of occurrence of extreme events, as well as the implication of policy in water resource sustainability in the changing world.

Chapter 7

Water Resource Management and Policy

7.1 General

Sustainable use of water resources requires a water management policy that takes all water sources of a watershed into consideration. However, the provincial B.C. water act has conservatively focused on surface water resources only [B.C. Reg. 204/88 O.C. 889/88]. Part 2 of the water act — Acquisition of Water Rights — state, among other things, that "An application to the comptroller or regional water manager for a licence must be signed in duplicate by the applicant or his agent and shall include the quantity of water proposed to be diverted or stored, or diverted and stored, or the amount of power to be generated". However, this water act does not take the groundwater sources into consideration. As a result, a new water sustainability act (WSA) [British Columbia's Water Act Modernization, 2010] was proposed in December 2010 and is still, at the time of writing this thesis, under public discussion on Living Water Smart Blog [http://blog.gov.bc.ca/livingwatersmart/]. One of the proposed policies in the WSA is

regulation of groundwater use. Although such an approach of groundwater and surface water regulation (often termed as "watershed based approach for water management") is habitually suggested, implementation of the approach is rarely realized due to the difficulties to fully understand total water resources i.e., climate, surface water, shallow and deep aquifers as "one –water" [Wei, 2008] and their interactions at a watershed scale. In this thesis, I aim at demonstrating the need to conjunctively understand surface water resources and potential yields from shallow and deep aquifers in relation to agricultural water demand, climate change impact and pumping well network before devising water management strategies.

Recent studies in the North Okanagan have attempted to assess the water usage and available groundwater resources of the basin [Ping et al. 2010, DHI Cambridge, 2011]. According to these studies, total licensed surface water extraction, as obtained from the Ministry of Environment Water Stewardship office, is estimated at 3 Mm^3/year [Ping et al. 2010]. The total water withdrawal from deep aquifers was estimated at 1 Mm^3/year.

Building on previous studies by DHI Cambridge [2011] and Assefa et al. [2011], various scenarios of MIKESHE are setup here to hind cast the past hydrologic processes (1977 to 2006) and to assess future water resources availability for two bi-decade periods (2010-2029 and 2030-2049). This investigation is done by using projected climate data from the four GCM scenarios discussed in Chapter 6 (CGCM3A2, CM2.1-B1, ECHAM5-B1, and HadCM3-B2), as well as by accounting for potential anthropogenic impacts of land use changes on hydrological processes. Land use change impacts on surface hydrology was

studied by several previous studies [e.g., Jones and Grant, 1996; Gebremeskel et al., 2005]. This study looks at the combined consequences of climate and land use change on surface and groundwater resources, and the implication of unregulated water withdrawal on the environment in relation to water use policies. The impacts of land use changes on hydrological processes are described here in terms of potential changes in hydrological model parameters as well as variations in agricultural water demand.

7.1.1 Land Use Change and Hydrologic Modelling

The current land use map for the Deep Creek watershed was modified for land use simulation by re-classifying the different types of land uses into five major categories [Figure 7-1] [Janmaat and Anputhas, 2010] . These are cultivation, pasture, forest, farm land and residential areas. In projecting the land use maps, Janmaat and Anputhas [2010] assumed that the different land use categories in the study area will continue to change at the present rate with no restriction on land use categories. The land use change simulation results were obtained in ASCII files categories, converted here to the raster maps shown in Figures 7-1, 7-2, and 7-3.

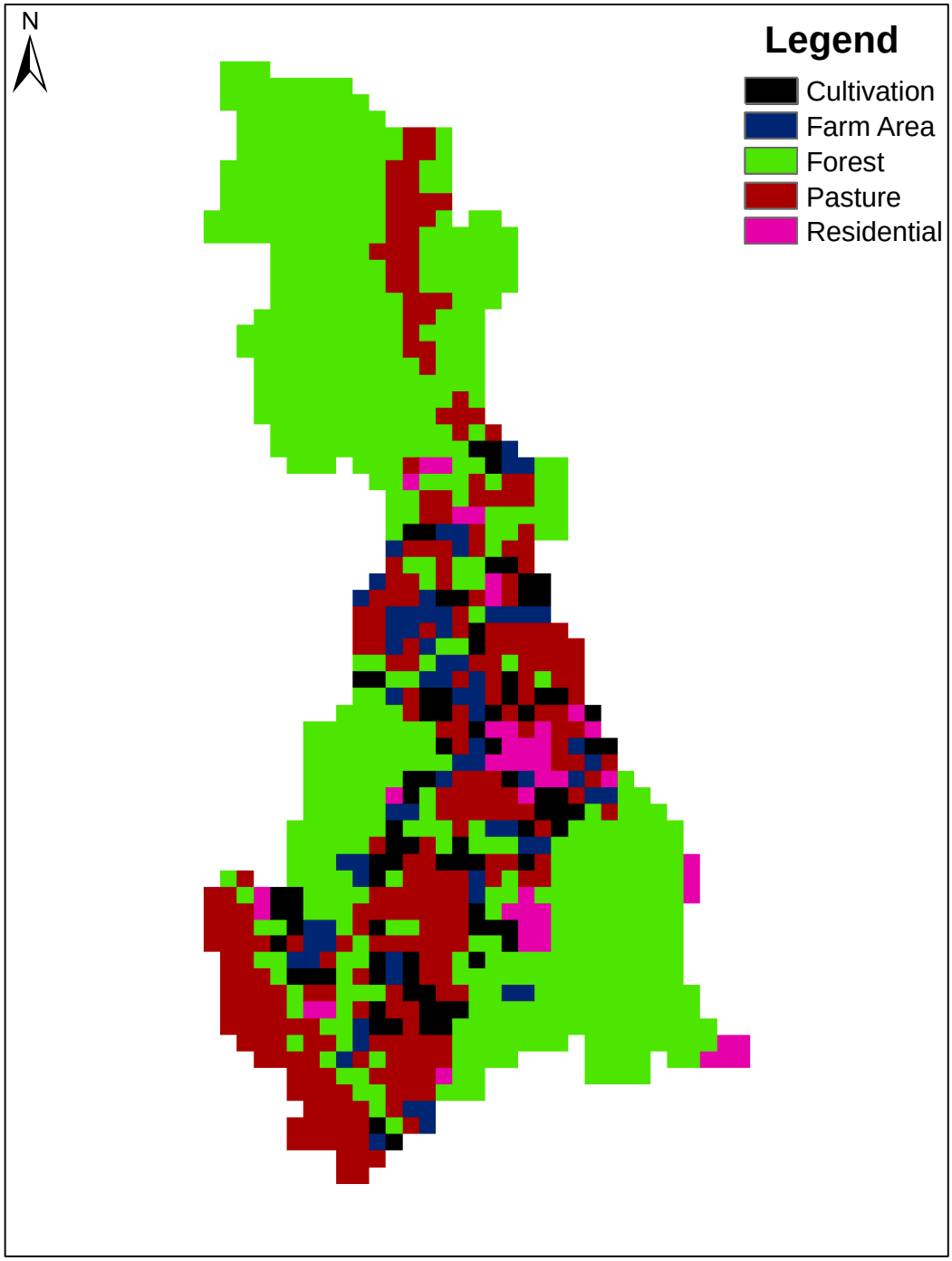

Figure 7-1 Current land use map

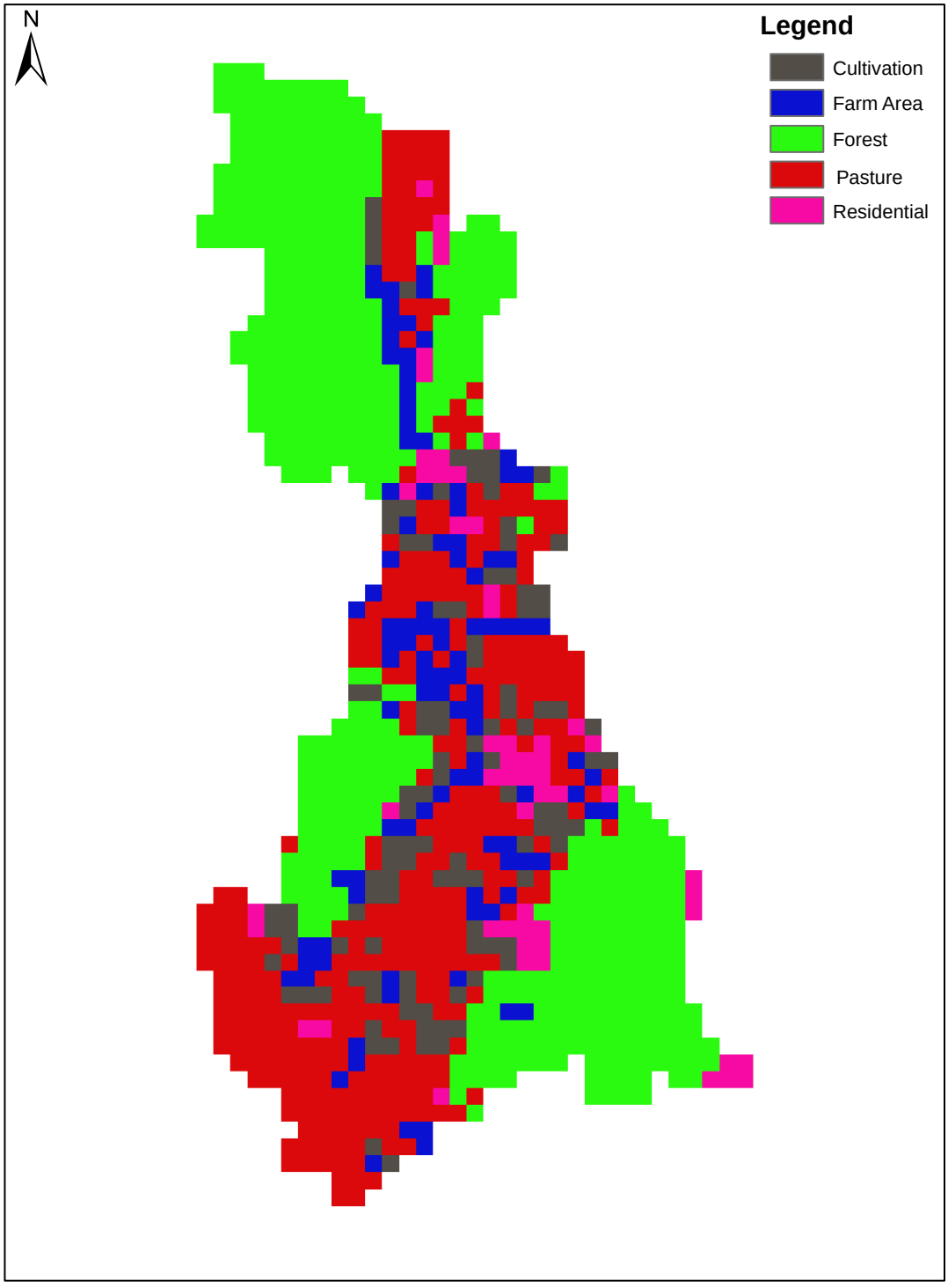

Figure 7-2 Projected land use map for year 2030.

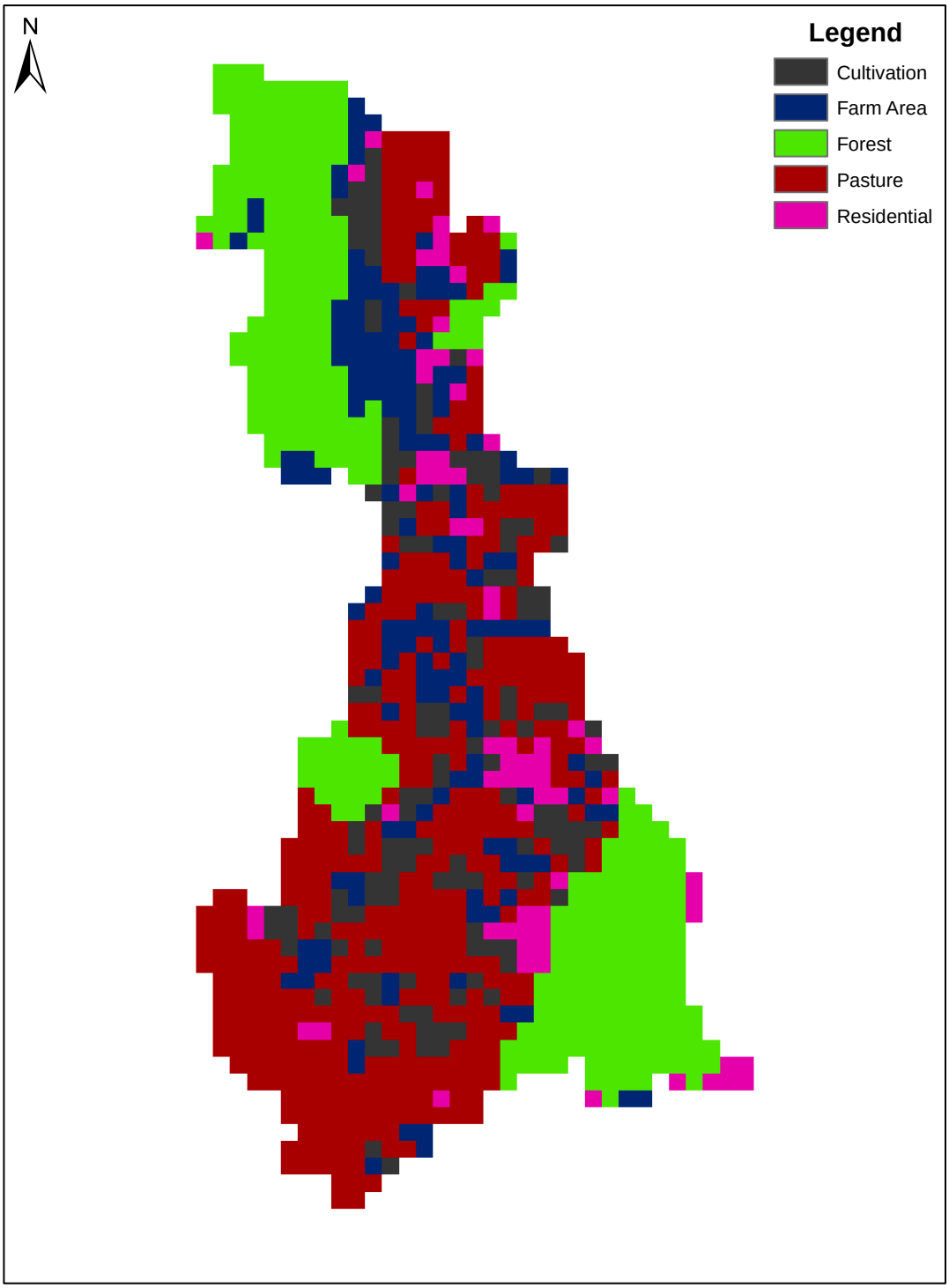

Figure 7-3 Projected land use map for year 2050.

According to the projected land use maps, an expansion of agricultural area, farm area and residential areas is anticipated to occur in the Deep Creek watershed at the expense of forest land. The percentage of areal changes in land use category and land use codes are shown in [Table 7-1]. Therefore, the spatial distribution of future hydrologic model parameters cannot be the same as the once used for the historical simulation. Figure 7-4 and Figure 7-5 below show the change in parameter distribution for a randomly selected land use category (Forest). The legends LAI and RD in the figures represent leaf area index and root depth respectively. The orange and blue colours therefore represent root depths and leaf area index values for the forest land use category. Note in the figures that the percentage of the area that has the LAI and RD values indicated in Figure 7-4 (1977-2006) is reduced in the future scenario (2030-2049) according to the anticipated areal changes in land use categories [Table 7-1].

Table 7-1 Percentage changes in land use category within the Deep Creek watershed

Year/ Land use category	Cultivation [%]	Farm Area [%]	Forest [%]	Pasture [%]	Residential [%]
Land use codes	0	1	2	3	4
2030	27	48.5	-21.30	22.09	24.9
2050	60	120.80	-49.05	51.26	56.13

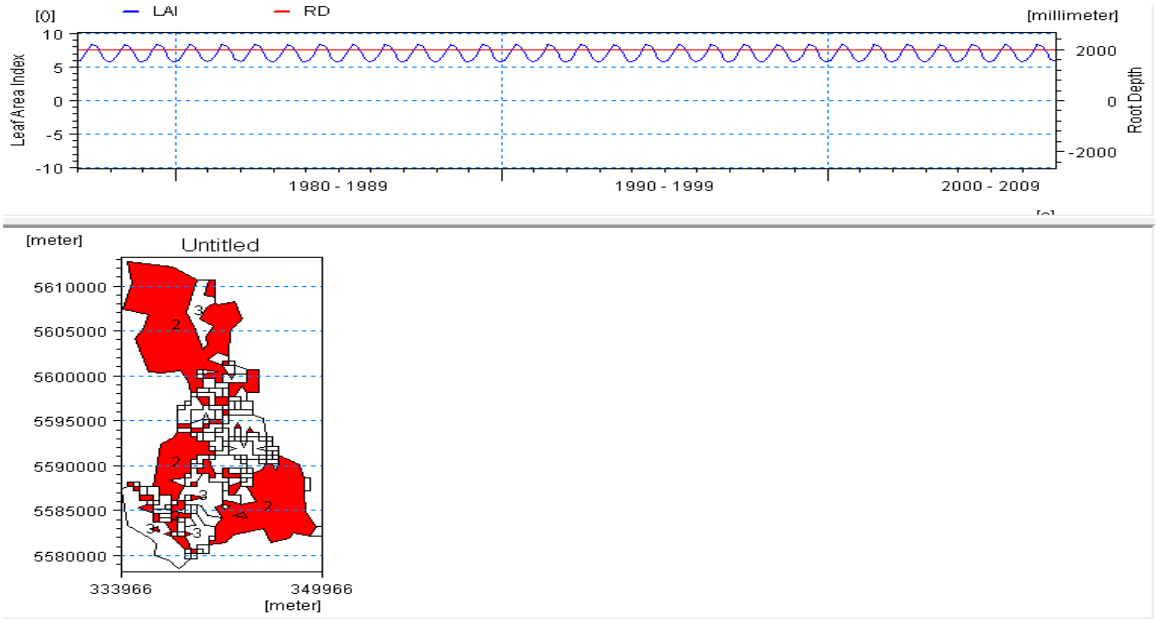

Figure 7-4 Spatial distribution of leaf area index and root depth for forest land use category (1977-2006)

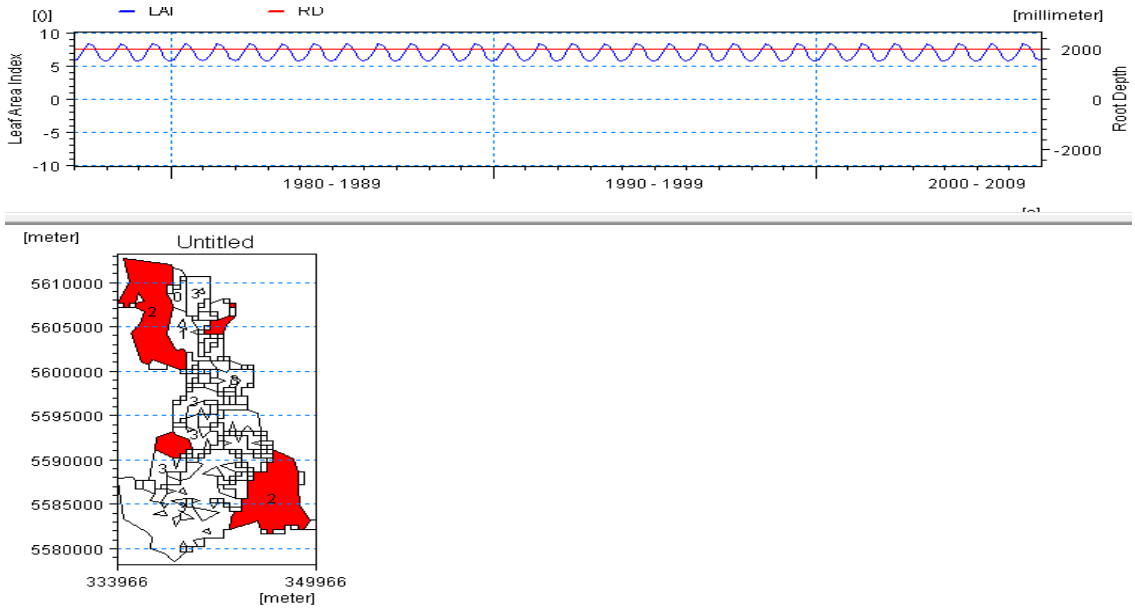

Figure 7-5 Spatial distribution of leaf area index and root depth for projected forest land use (2030- 2049)

Table 7-2 Annual agricultural water demand

Year	Annual agricultural water demand [Million m^3/year]
2006	3
2030	3.7
2050	4.8

The spatially and temporally varied land use simulation results were used in the study by Janmaat and Anputhas [2010] to estimate daily agricultural water demands. Average annual agricultural water demand estimates are shown in Table 7-2. As the current water resource policy restricts abstraction from surface water sources, the projected agricultural water demand are expected to be fully supplied by the groundwater resources - and thus are represented as sinks in the MIKESHE saturated zone groundwater model.

In summary, the impacts of land use change on water resources is simulated here by considering potential changes in hydrological model parameters as well as the additional stress in groundwater resources due to the increasing agricultural water demand.

7.2 Results: Water Resources Sustainability

7.2.1 Current Water Resources Potential

The MIKESHE simulation results, which consist of all the major water balance components totalled for 30 years (1977 to 2006), are shown in Figure 7-6 below. The average annual surface runoff volume from the Deep Creek watershed is calculated to be 10.9 Mm^3/year, 37% of which is base flow from groundwater aquifers. Additional

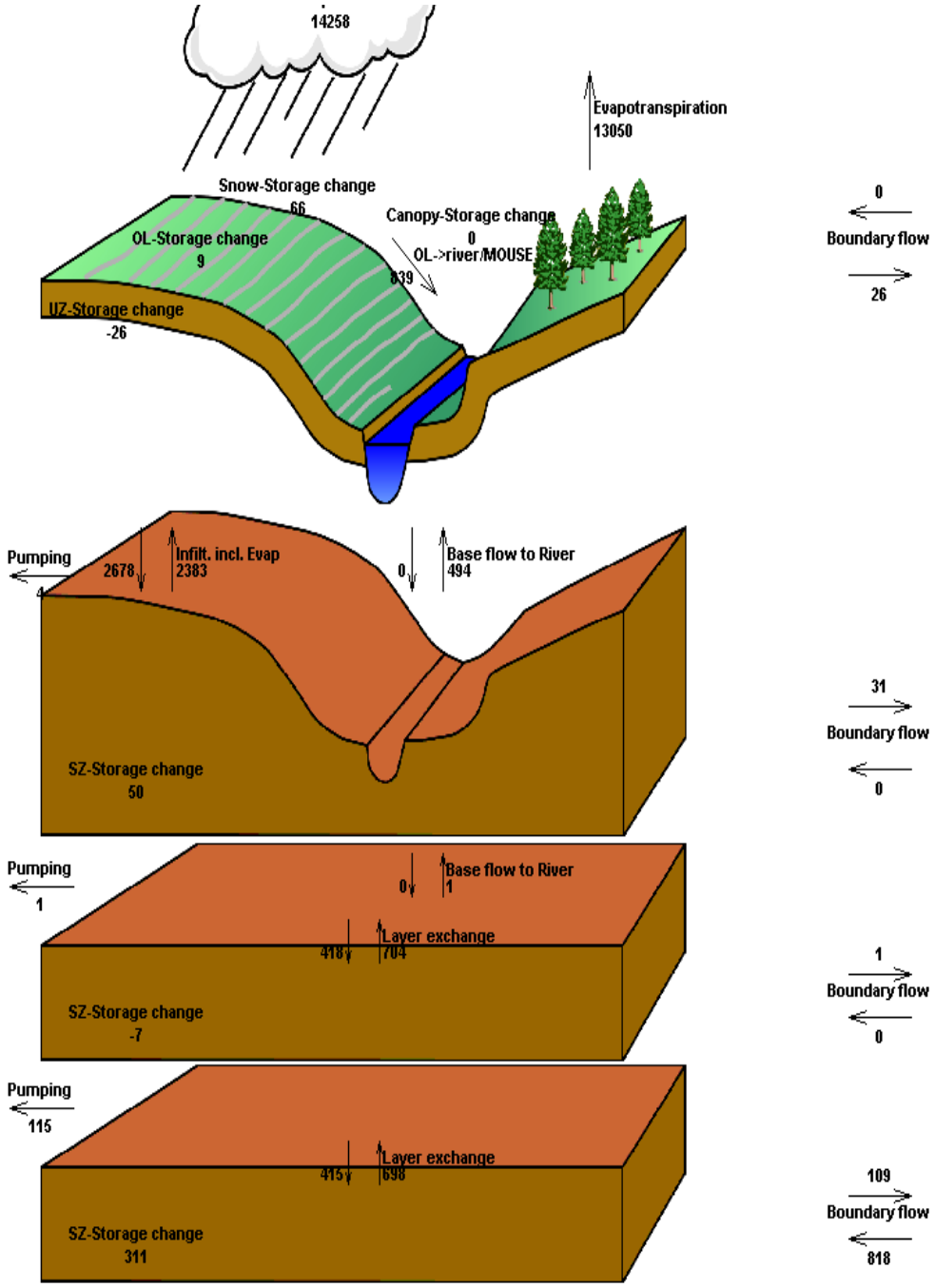

Figure 7-6 Total water budget (1977 to 2006). All values are in mm.

analysis (seasonal) is conducted in order to estimate the surface water volume than can actually supplement the agricultural water demand during the period of irrigation (June to September). Analysis of the results show that, even though the surface runoff yield from the catchment is 10.9 Mm^3/year, the average annual surface water available for supplementary irrigation is only about 2 Mm^3/year [Section 7.2.3]. Monthly average overland and base flows are shown in Figure 7-7.

On the other hand, the average yield that can be obtained from the groundwater aquifers is estimated at about 1 Mm^3/year. The groundwater level would drop below the screen level if more than 1 Mm^3/year were extracted [Section 7.2.2]. Thus, the total amount of water that can possibly be used for agricultural purposes is about 3 Mm^3/year (2M from surface and 1M from groundwater sources). Although this amount seems to be just enough to satisfy the current agricultural water demand in the watershed [Table 7-1], the simulation results raises the question whether climate and land use change would allow additional pumping from the groundwater aquifers [Section 7.2.3]. Note that the current water policy relies on groundwater source to meet the future agricultural water demand.

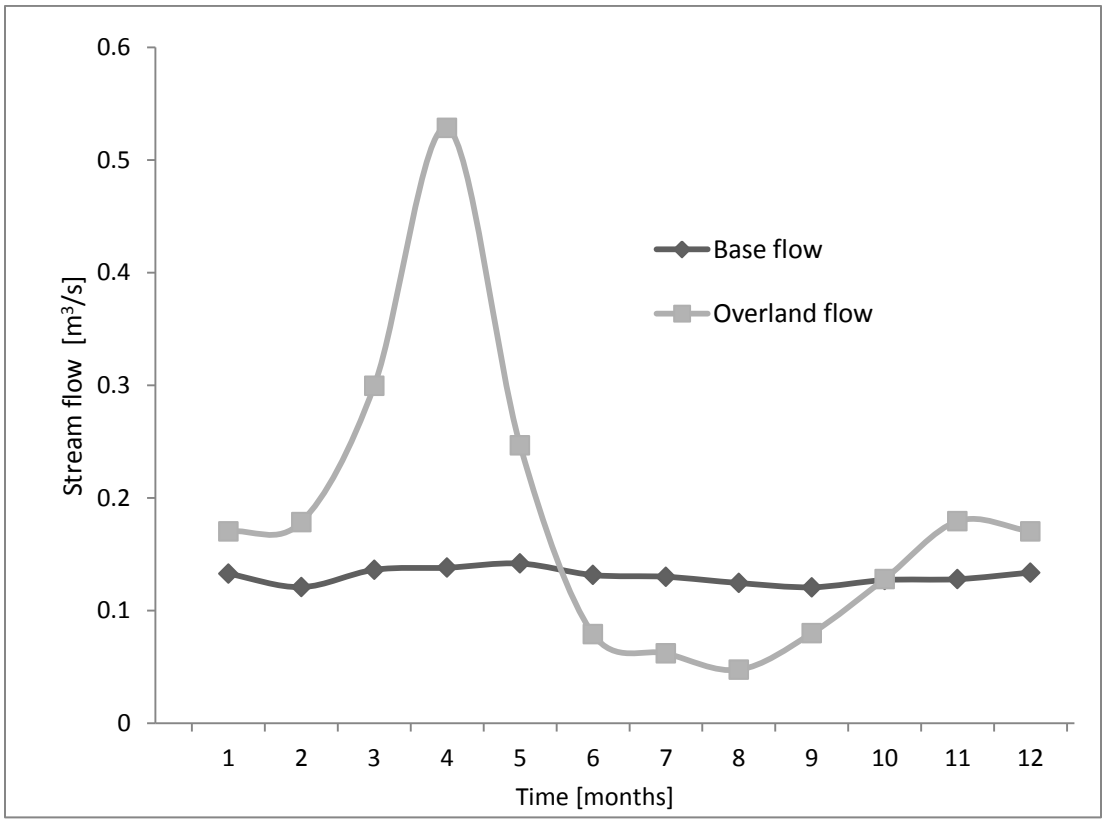

Figure 7-7 Average monthly over land and base flow (1977-2006)

7.2.2 Hydraulic head and Groundwater extraction

The relationship between pumping well screen levels and saturated zone elevation head is studied here by extracting model results. To this end, a snapshot of the 3D groundwater head map is taken on a randomly selected date (July 25, 2001) within the pumping period (May-August). Two cross sections are selected in the spatial map based on the pumping well characteristics shown in Table 7-3 (Figure 7-8 and Figure 7-10). While the cross sectional profile shown in Figure 7-9 is selected to analyse the relationship between well screen levels and groundwater levels in the relatively shallow unconfined aquifer in the Hullcar area, the profile extracted along axis B-B of Figure 7-10, shown in [Figure 7-11]

is used to compare and contrast saturated zone elevation heads and screen levels of the relatively deep wells in the Spallumcheen aquifer. Note that the cross sectional profiles shown in Figure 7-9 and Figure 7-11 are also snapshots of the water level on the same summer day (July 25, 2001) in the supplementary irrigation season.

The relatively shallow wells in the Hullcar area are designated with the following well ID: Q1, Q2, Q3, Q4, Q5, Q6 and Q7 [Table 7-3]. These wells are located at distance of 2000 - 3000 meters, as measured in ArcGIS, from the west boundary of the Deep Creek Watershed on Axis A-A [Figure 7-8] . Figure 4-16 shows the Northing and location of the pumping wells. The screen levels of these wells are in the range of 507 to 515 meter above sea level (m a.s.l). Whereas, as can be seen in Figure 7-9, the saturated head elevation at the chainage of 2000 – 3000 meters, on axis A-A, is about 500 m a.s.l. It can be seen here that the groundwater level is below the screen levels of the wells. Thus, no water can actually be extracted from the existing shallow wells at-least on this particular day (July 25, 2001) of the supplementary irrigation season. To further evaluate the situation in the existing deep wells, a similar cross sectional profile is analysed at and near the locations of the deepest well (140 meters deep) in the study watershed (Well ID - C4). The wells in this part of the watershed are located at a distance of 4000 - 7000 meters, as measured in ArcGIS, from the west boundary of the Deep Creek Watershed on Axis B-B [Figure 7-10]. Figure 4-15 shows the Northing and location of the pumping wells on the Spallumcheen Aquifers. The screen levels of this deep well (C4), and similar other wells along section B-B (C1, C2, C3) are in the range of 388 to 443 m a.s.l. [Table 7-3]. However, the water levels in the confined aquifer are estimated only at about 360 m

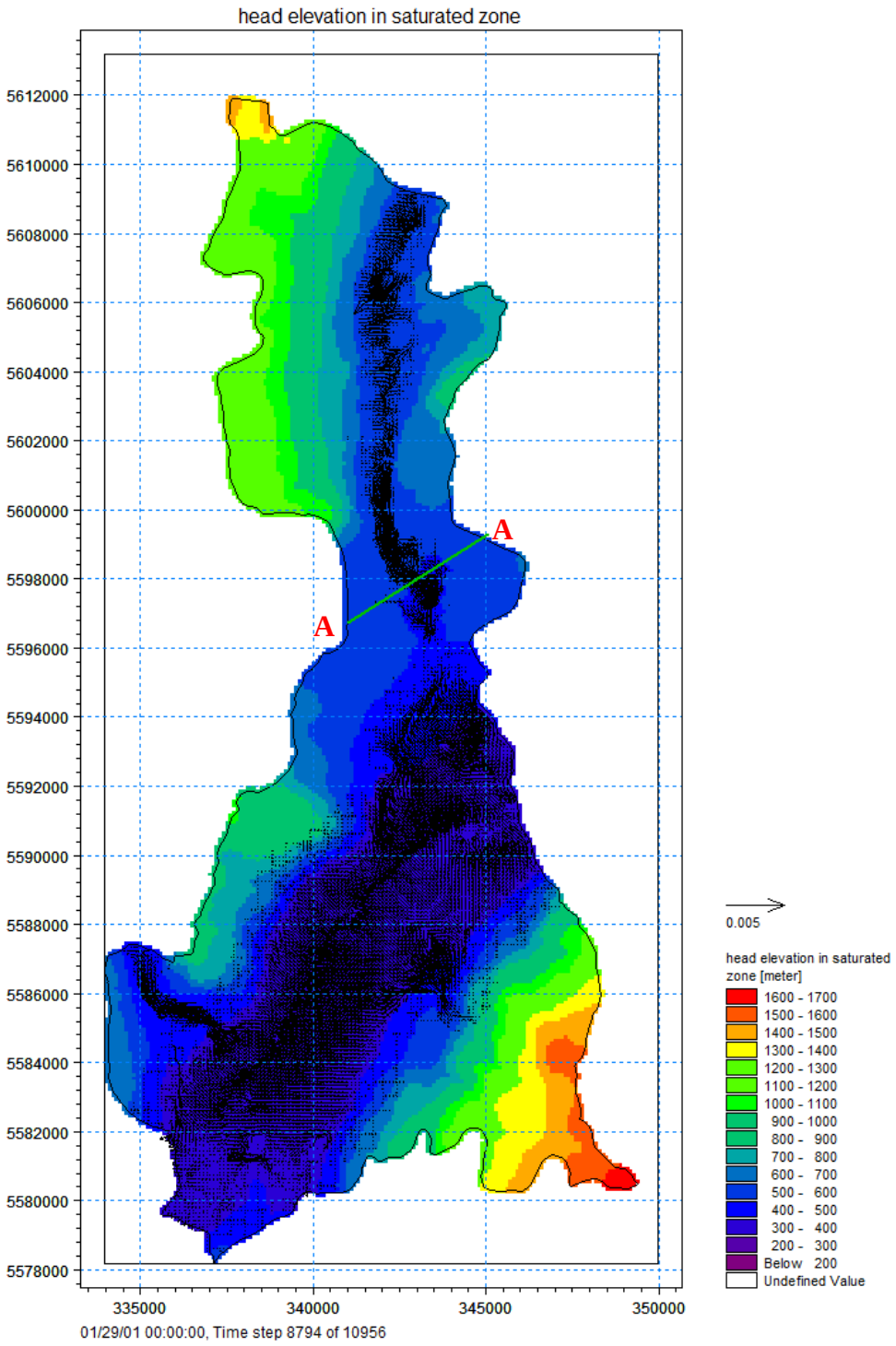

Figure 7-8 Hydraulic head elevation in saturated zone – Axis A-A

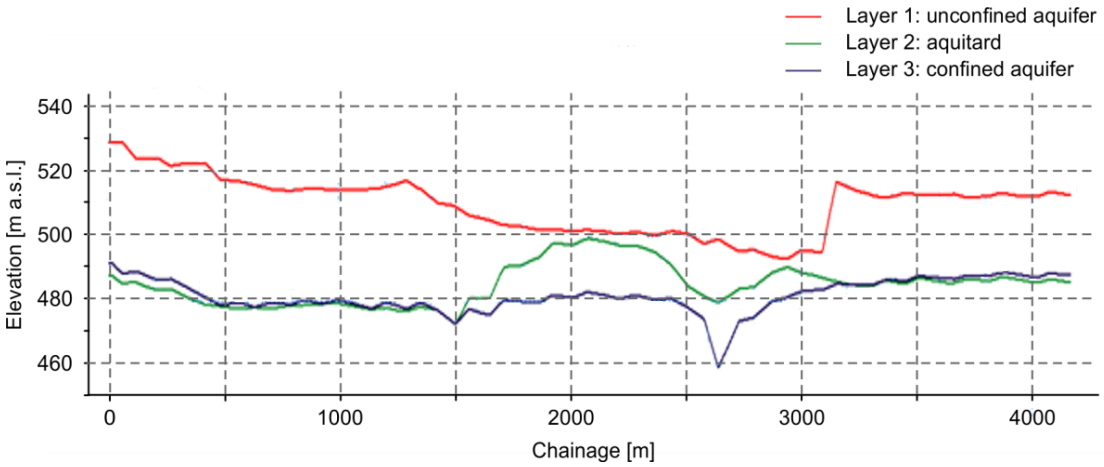

Figure 7-9 Section A-A: saturated zone elevation head on July 25, 2001

a.s.l. - which is far below the screen levels of all the four wells. The results of this modelling attempt thus suggest that the limited yield from the groundwater aquifers may not just be due to groundwater resource scarcity but also to the position of the groundwater wells in the aquifers – highlighting the need for detailed investigation of deep aquifers for any possibilities of deeper well installation.

Table 7-3 Attributes of Pumping Wells [DHI Cambridge, 2011]

WELL ID	Latitude [N] [UTM]	Longitude [W] [UTM]	Screen level [m asl]	Depth [m below OGL]
L9	341446	5597375	516	67
L10	341386	5597381	516	67
Q1	342642	5597771	515	38
Q2	342391	5597775	513	47
Q3	342299	5597779	513	37
Q4	343248	5598420	508	60
Q5	343255	5598516	507	44
R1	342883	5596832	509	93
R2	342835	5596863	508	93
W1	343078	5598870	520	35
Q6	343031	5597761	509	42
Q7	342007	5598212	509	34
G1	341846	5592538	447	40
F1	340242	5593725	573	63
C1	337203	5584533	443	129
C2	337578	5584521	410	91
C3	337653	5584457	394	90
C4	337266	5584467	449	140
D4	339427	5581277	388	27
K1	344450	5589236	388	85
K2	344438	5589276	388	85
M1	3461082	5591459	364	62
V1	340567	5588150	358	53
J1	343765	5587528	394	81
J2	343728	5587531	394	87

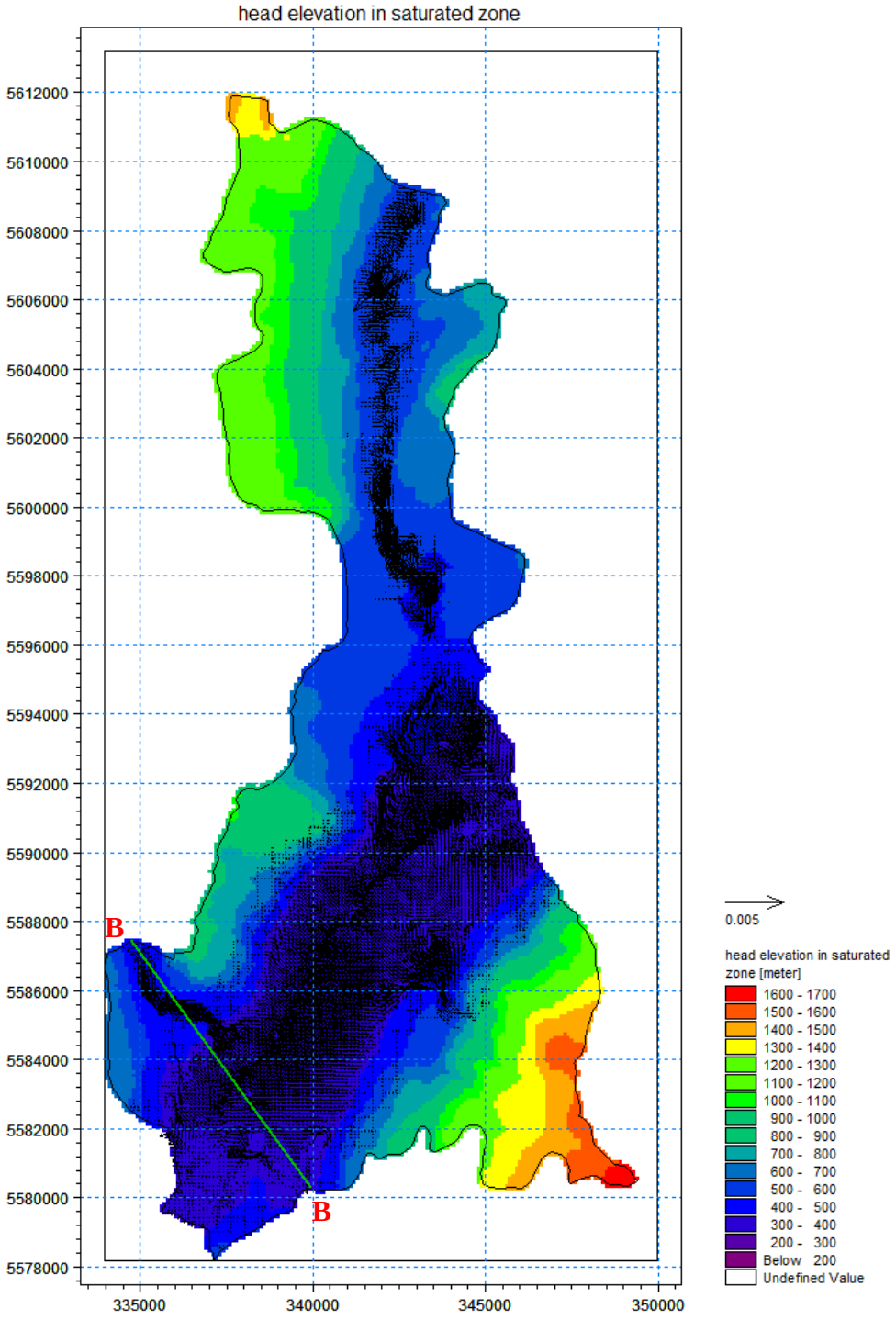

Figure 7-10 Hydraulic head elevation in saturated zone – Axis B-B

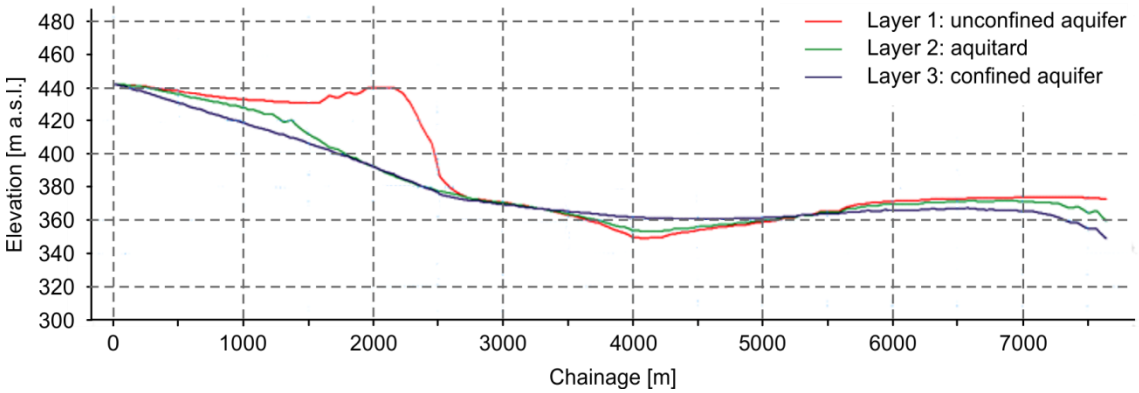

Figure 7-11 Section B-B - Saturated zone hydraulic head elevation on July 25, 2001

7.2.3 Future Water Resource Potential

As discussed, four GCM scenarios are used to evaluate water resource sustainability under the impacts of climate change and land use change. As each GCM projection is grouped into two future periods ranging from 2010 – 2029 and 2030 – 2049, a total of eight future climate scenarios are prepared. The MIKESHE simulation was done on a 12.0 GB RAM, 64-bit OS, 3.07 GHz dual core machine. Each scenario took over 12 hours to run, and over 300 GB of data were produced. The results were summarised by performing additional sets of model runs to produce the water balance charts shown in Appendix B as well as time series outputs. The results so obtained pertaining the major water balance components are summarised in Table 7-4 and Table 7-5.

Table 7-4 Average annual water budget, (2010-2029) and (1977-2006)

	1977 - 2006	2010 - 2029			
		ECHAM5B1	H3B2	CGC3A2	CM21B1
Net Recharge [Mm^3]	6.9	15.4	10.7	13.7	9.5
Runoff [Mm^3]	6.9	16.1	12.1	17.2	10.6
Base flow [Mm^3]	4.0	4.9	4.5	5.0	4.3
Total surface runoff [Mm^3]	10.9	21.0	16.6	22.2	14.9
Groundwater flow to Lake Okanagan [Mm^3]	1.2	1.3	1.2	1.3	1.2
Maximum yield from groundwater aquifers [Mm^3]	1.0	1.6			

Table 7-5 Average annual water budget, (2030-2049) and (1977-2006)

	1977- 2006	2030 - 2049			
		ECHAM5B1	H3B2	CGC3A2	CM21B1
Net Recharge [Mm^3]	6.9	15.3	12.4	15.5	10.9
Runoff [Mm^3]	6.9	17.5	11.1	17.2	10.7
Base flow [Mm^3]	4.0	5.0	4.4	5.1	4.4
Total surface runoff [Mm^3]	10.9	22.5	15.4	22.3	15.1
Groundwater flow to Lake Okanagan [Mm^3]	1.2	1.3	1.2	1.3	1.2
Maximum yield from groundwater aquifers [Mm^3]	1.0	1.6			

It can be seen from the above summery tables that the water resources in the Deep Creek watershed is anticipated to increase in the future periods. For instance, surface water resource is expected to double in the future climates. However, as discussed in section 7.2.1, this water resource cannot be fully used in the supplementary irrigation season for two major reasons. First, the current water resource policy does not allow additional

water abstraction from surface water sources beyond the licensed amount. Secondly, about 82% of the surface water is received during the periods when there is no need for supplementary irrigation. As a result, groundwater resources are expected to cover the additional demand. As can be seen in Tables 7-4 and 7-5, the amount of water that can possibly be extracted from the groundwater aquifers is projected to increase by 0.6 Mm^3/year. This is made possible due to the anticipated increment in net recharge by about 6.6 Mm^3/year – which is equivalent to 27mm/year. However, the additional groundwater yield obtained due to the increase in net recharge is still not sufficient to meet the future agricultural water demand. As water demand is projected to increase by 1.8 Mm^3/year in 2050 [Table 7-1], there will still be a deficit of about 1.2 Mm^3/year if the current water policy remains in place.

In addition to the above water balance analyses, surface runoff and base flow projected using the four GCM scenarios are also analysed to study seasonal variation of surface and groundwater flow. Long term monthly average overland and base flows are shown in Figures 7-12 and 7-13..

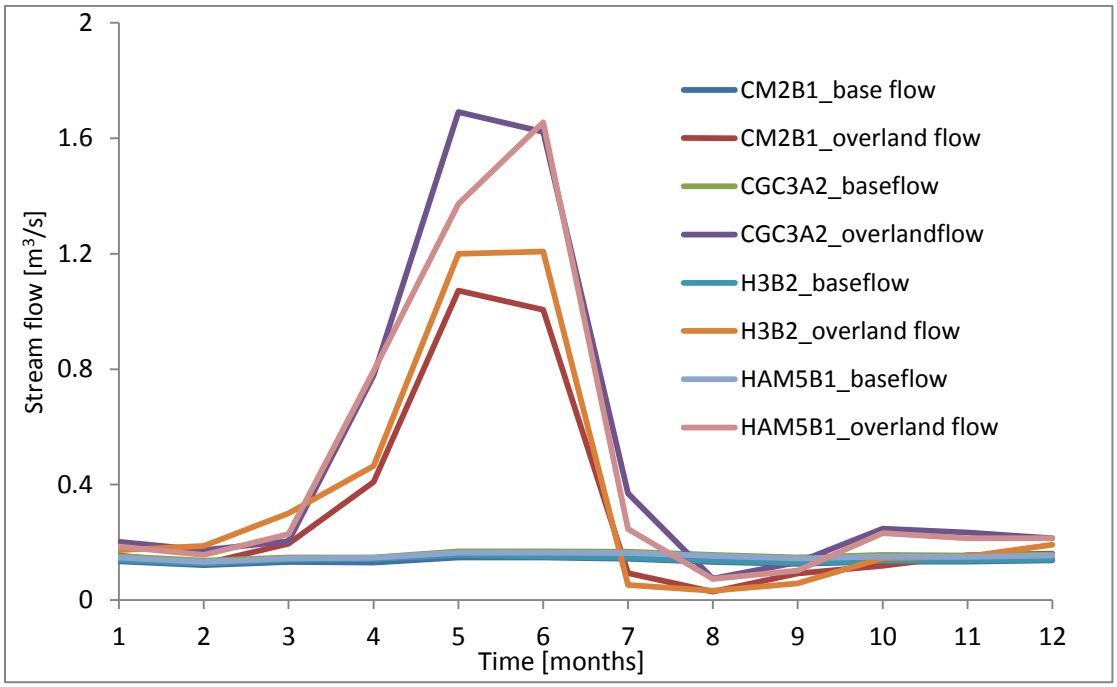

Figure 7-12 Long term monthly average overland and base flow (2010-2029)

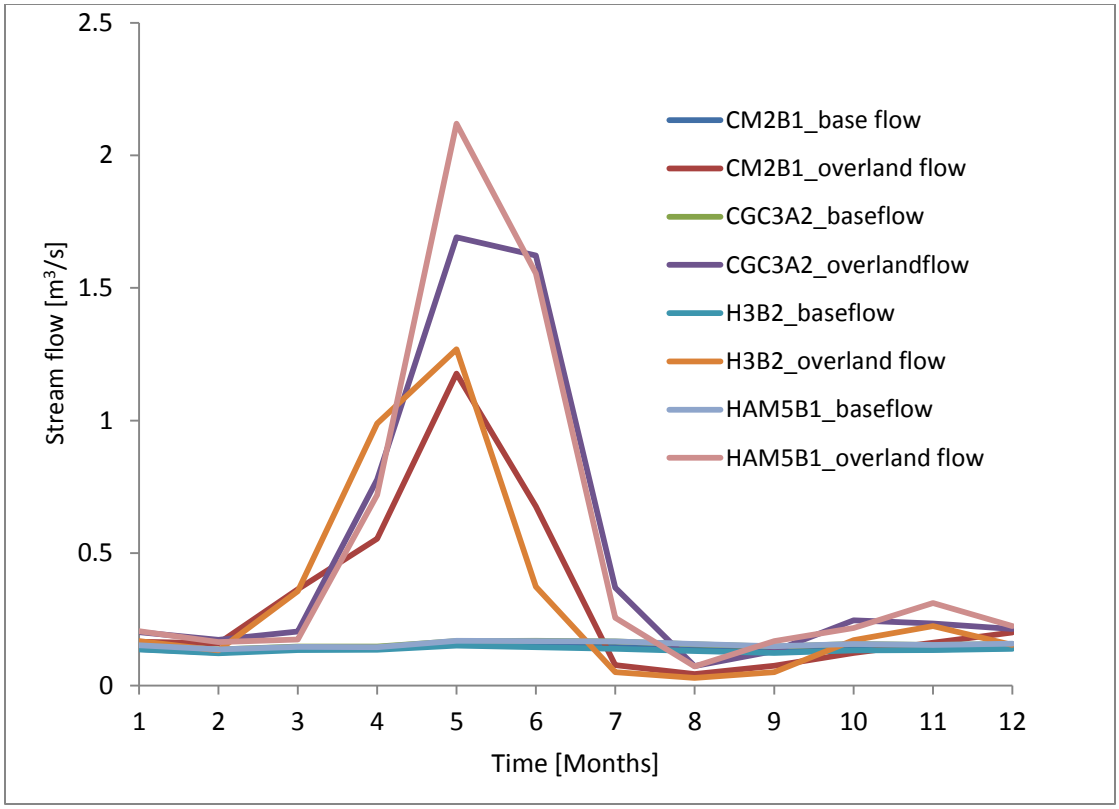

Figure 7-13 Long term monthly average overland and base flow (2030-2049)

It can be discerned from Figures 7-12 and 7-13 that groundwater is a significant contribution to the river flow, particularly over the months of July, August, and September. Additional analyses of the average monthly flow data in these three months show that about 45% to 75% of the total flow is coming from the groundwater aquifers as base flow. This means that the groundwater abstraction from the unregulated shallow wells is actually extracting the base flow that might otherwise help fulfill environmental requirements. The existing water policy is hence encouraging farmers to continue the unregulated pumping near streams, probably in an accelerated rate to cover the increasing demands. This problem could be minimised, if not solved, by conducting a detailed investigation of deep aquifers and installing wells deeper than the existing pumping wells [Table 7-3], and by building appropriate water storage structures that can store the excess water in spring [Figures 7-7, 7-12, and 7-13] and use it during the irrigation period when it is needed most, especially July, August and September.

In summary, the above results show that the primary problem in the study area is not water resource scarcity but lack of detailed information on the groundwater aquifers and the water policy that separates the two water sources. Therefore the primary solution that should be taken as a key adaptation strategy, hand in hand with the detailed investigation of aquifers and installation of deeper wells, is to devise a new water use policy that considers the dynamic interaction of all water sources in the basin. In addition, it is always necessary to make continued attempts to optimise water use efficiency, implement appropriate water harvesting structures across the watershed and perhaps, restrict land use expansion.

7.2.4 Changes in Flood Frequency

In investigating the impact of climate change on stream flow, changes in the rate and magnitude of floods should be considered. To this end, a preliminary attempt at flood frequency analyses is made here for the baseline and future periods of all the four GCM scenarios. This is done by sorting annual maximum daily stream flow values of the historical and the future climate scenarios in descending order, and plotting these according to the percentage of exceedence. The percentage of exceedence is calculated as $m/(n+1)$, where $m$the rank with one is assigned to the highest flow and n to the lowest, and n is the number of maximum stream flow. The probability of exceedences so calculated and the corresponding extreme events for the historical and future scenarios are shown in Table 7-6. Note in Table 7-6 that the lowest and highest probabilities of exceedence values are 4.8 % and 95%, respectively. Thus, events that correspond to "1%" and "100%" probabilities may be estimated by fitting a trendline to the data points (extrapolation). Figure 7-14 shows a plot of peak steam flow events against the percentage of the time the flood is exceeded using the historical (1977-2006) and projected (2030-2049) climate of two GCM scenarios (CM21-B1 and ECHAM5-B1). The dashed lines represent the fitted trend lines (logarithmic for the historical data and exponential for the two future conditions). Note in Figure 7-14 that the fit is slightly better for the historical data than for the two GCM scenarios. These differences in the degree of fit can be attributed, besides possible biases in climate models, to one of the

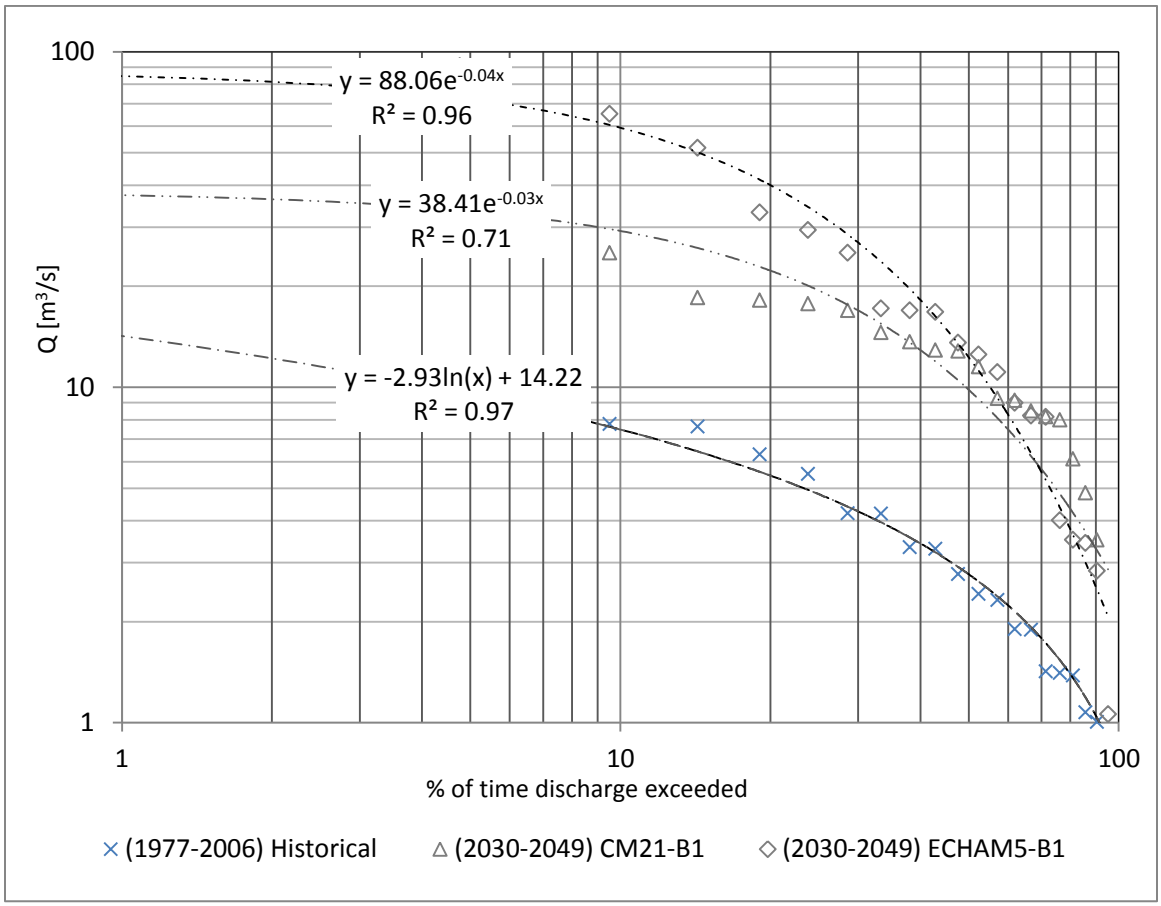

Figure 7-14 Percentage of exceedence of annual daily maximum flood: historical (1977-2666) and projected (2030-2049) climate of two GCM scenarios (CM21-B1 and ECHAM5-B1). The dashed lines represent the fitted trendlines.

major limitations in procedure of synthesising future climates - i.e., the assumption that the statistical relationship formulated for the historical climate would remain valid under the future climate conditions [Fowler et al., 2007].

Changes in the probability of occurrence of extreme events between the base period and future scenarios are analysed by selecting a 20 year and 2 year return period annual maximum stream flow. These events correspond to a magnitude of 8.4 m^3/s and 2.3 m^3/s with a percentages of exceedence estimated at 4.8% and 57.1%, respectively (Table 7-6).

However, it can be discerned from Table 7-6 that 8.4 m^3/s (4.8% probability of exceedence in the base period) may have a probability of exceedence of about 65% (in the case of ECHAM5B1 scenario), 67% (CGC3A2), 71% (CM2B1), and 85% (HADCM3B2) in the future climate (2030 - 2049). These results may be translated to potential reduction in return period of about 13, 14, 15, and 18, respectively. The reduction in return periods are estimated as the ratio of probability exceedence under the future climate to that of the historical climate. On the other hand, the 2 years return period event (or 57.1% percentage exceedence) is expected to be exceeded between 86 and 95% of the time in the future climate. In this case, the potential reduction in return period is only about 2.

The wide range of variation in "changes in return periods" (2 in the case of the relatively low event, and as high as 18 in the case of the largest flow event) may be attributed to the uncertainty involved in the empirical frequency analyses technique. Although it is difficult to make quantitative conclusion based this preliminary analysis, the results remain indicative of the potential increase in the magnitude and frequency of flow events in the Okanagan.

Table 7-6 Changes in flood frequency for historical climate and three tri- decade projections of four GCM scenarios

Probability of exceedence [%]	Historical (1977-2006)	CGC3A2 2050's	CM2B1 2050's	HADCM33B2 2050's	ECHAM5B1 2050's
4.8	8.3	60.6	33.8	47.2	90.6
9.5	7.8	53.7	25.2	40.8	65.4
14.3	7.6	45.5	18.5	38.9	51.8
19.0	6.3	30.6	18.2	38.2	33.2
23.8	5.5	18.5	17.8	29.6	29.4
28.6	4.2	17.8	17.0	28.4	25.2
33.3	4.2	16.4	14.6	25.9	17.2
38.1	3.3	13.3	13.7	23.4	17.0
42.9	3.3	12.8	12.9	22.8	16.8
47.6	2.8	12.8	12.8	22.8	13.6
52.4	2.4	12.3	11.5	22.7	12.5
57.1	2.3	10.1	9.3	19.2	11.1
61.9	1.9	9.7	9.1	16.2	9.0
66.7	1.9	8.3	8.5	16.1	8.2
71.4	1.4	7.5	8.2	15.2	8.2
76.2	1.4	7.0	8.0	15.0	4.0
81.0	1.4	5.2	6.1	12.2	3.5
85.7	1.1	3.4	4.9	7.0	3.4
90.5	1.0	1.7	3.5	1.2	2.8
95.2	0.9	1.1	0.4	0.6	1.1

Chapter 8

Conclusion and Discussion

8.1.1 Groundwater Recharge Estimation

This study has developed and tested a new methodology for recharge estimation by using various modelling tools including ArcGIS [ESRI, 2011], field data (in situ observations of soil water content and soil temperature), and soil physics as represented by a physically-based finite element code (HYDRUS-1D) [Simunek et al., 2005].

The HYDUS-1D model, both with and without a freezing and thawing module, is first used to simulate soil temperature, snow pack and soil moisture over a one year experimental period. Comparison between simulated results from both versions of HYDRUS-1D and in situ observations of soil temperature and soil moisture are made by using various statistical measures. Analysis of the results shows both versions of HYDRUS-1D reproduce the observed data to the same degree, proving the hypothesis that rigorously accounting for freezing and thawing will not change subsurface water and

heat movement in semi-arid study area. The statistical comparison is performed at two different locations in the Deep Creek watershed (Valley bottom and Silver Star Mountain) in order to assess the degree to which the field site results can be extrapolated to the other areas of the basin with different soil type and land cover. Results of the statistical analyses show good performance of the model at both locations suggesting the robustness of the methodology developed. The results also support conclusions made by previous studies about the code deployed to determine unsaturated hydraulic properties, namely that ROSETTA is a reliable tool for estimating soil hydraulic properties.

After evaluating the performance of HYDRUS-1D and ROSETTA at the experimental sites, the HYDRUS-1D code is coupled with ArcGIS^{TM} to produce spatially and temporally variable recharge maps throughout the Deep Creek watershed. Fourteen unique HYDRUS columns are identified across the watershed after discretizing model inputs into 500 m × 500 m cells in ArcGIS^{TM}. A total of more than 46 years simulation is completed at each of the fourteen columns, and the recharge results from each column are used to produce a raster map of recharge. Averaged spatially and temporally, the mean annual recharge throughout the Deep Creek watershed is estimated at 77.8 ± 50.8 mm /year. As evident from the large standard deviation, recharge in the Deep Creek watershed is found to exhibit significant spatial and temporal variation**.**

As discussed earlier, groundwater recharge estimation has been attempted in the Okanagan Basin and other parts of Canada by making use of the HELP code. However, HELP consists of several empirical relationships which may not be appropriate in some

applications [Schroeder and Ammon, 1994]. The limitations are even more pronounced in semi-arid areas like the Okanagan Basin where upward fluxes of water can be high, because HELP assumes that water below the evaporative zone simply drains to the base of a soil column without accounting for upward fluxes. HELP is also limited by boundary conditions as well as spatial and temporal discretization options, and thus cannot simulate highly variable fluxes near boundaries. In addition to these limitations, previous studies that used HELP for recharge estimation did not attempt to verify model performance in their study area [Toews and Allen, 2009; Jyrkama and Sykes, 2007]. On the other hand, HYDRUS-1D, being a Richards equation-based finite element code, provides flexibility in defining physically realistic boundary conditions. Also, the model provides the option for variable temporal and spatial discretization and allows water to move up or down depending on the pressure head gradient. Although as stated by Jyrkama and Sykes [2007] the direct comparison of model estimated recharge to field observations is challenging and expensive, this current study has conducted a one-year field study at our experimental sites and verified that HYDRUS-1D can, in fact, simulate heat and water movement in the vadose zone, and thus groundwater recharge. Unfortunately, HELP has not been used in the Deep Creek watershed to quantitatively compare results although it has been used in the Vernon area (south of the Deep Creek watershed) where average annual recharge was estimated at 109 mm/year [Liggett and Allen, 2010]. To their credit, Liggett and Allen [2010] acknowledged the fact the HELP over predicts recharge. Note that Liggett and Allen [2010] used the most recent version of HELP [Version 3.80D]. Their result is significantly higher than the mean annual recharge estimated at the

southern part of the Deep Creek watershed (19 mm/year) as well as the watershed average (77.8 mm/year).

8.1.2 Significance of the Method for Watershed Scale Transient Groundwater Modelling

The benefit of the recharge estimation method for catchment scale groundwater modelling is demonstrated by applying the spatially and temporally varying recharge results as upper boundary condition to MIKESHE model. The spatial boundary of the groundwater model was set to match the boundary of the Deep Creek watershed by representing lateral transfer of water from adjacent aquifers as outer boundary condition [Assefa et al., 2011]. The water table simulated using the variable recharge estimate is found to be within 0.6 m of the observed values, whereas the water levels estimated using uniform recharge boundary condition can fluctuate by as much as 1.6 m. Root mean square errors are estimated at 0.3 m and 0.94 m respectively. These results highlight the importance of the method in improving calibration of groundwater models. Note that previous groundwater modelling studies in the Okanagan assume constant percentage of precipitation to crudely estimate recharge as a lumped fitting parameter [e.g., Ping et al., 2010]. The results from such modelling attempts can lead to erroneous groundwater level information as demonstrated by the groundwater model calibration results, and thus to wrong decisions about pumping well depths and screen level positions. For instance, Chapter 7 of this thesis has showed that previously installed pumping wells in the Deep Creek watershed are not likely properly positioned. In fact, the potential water resources

problem in the study watershed is partly accounted for the inappropriate pumping well network (Chapter 7). In summary, this comparative study has demonstrated that such problems related to aquifer yield and inappropriate well design can greatly be minimised with the use of the novel recharge estimation methodology developed here.

8.1.3 Significance of the Method for Plot Scale Vadose Zone Hydrologic Modelling

The significance of the recharge estimation method for plot scale vadose zone hydrologic modelling is further demonstrated at the experimental site in the valley bottom. In addition to the soil hydraulic parameters derived from ROSETTA and government soil texture data [Assefa and Woodbury, 2013], a different set of model parameters are estimated by calibration using observed transient soil moisture data (Chapter 5). A first hand assessment of the two set of parameters (calibration and ROSETTA) is made by producing retentively and conductivity functions. Moisture content values at field capacity and wilting point are compared, and the results suggest reasonably acceptable errors for a variable which is generally known to exhibit significant spatial variability [Hillel, 2004]. This preliminary assessment about the soil hydraulic parameters is further assessed by simulating soil moisture and comparing that with observed values. Analysis of the results suggest promising performance of the ROSETTA derived parameters for plot scale modelling, with correlation coefficient and RMSE estimated at 0.84 and 0.036 cm^3cm^{-3}, respectively. Besides, the two set of parameters (ROSETTA and calibration) are used in HYDRUS-1D to simulate groundwater recharge for the past climate (1982-2006).

The results show that the differences in annual recharge values due to model parameterization is negligible compared to the significant differences due to temporal variability.

While the above results indicate the reliability of the government soil data for vadose zone hydrologic modelling, additional effort is expended to verify the results under different climate. To this end, downscaled climate data are forced to HYDRUS-1D, and recharge is simulated. Analyses of the results also confirm that the gridded soil data developed by Agriculture and Agri-Food Canada [Kenney and Frank, 2010] can be taken as a reliable resource for vadose zone hydrologic modelling. In addition, this research has demonstrated the application of the recharge estimation method as a "base model" for climate change studies. Note that previous climate change studies in the Okanagan Basin [Towes and Allen, 2009] used HELP without any attempt of model performance evaluation, notwithstanding its inherent limitations.

8.1.4 Water Resources Management and Policy

This research investigates the implication of inappropriate pumping well screen levels on aquifer yield in an evolving climate, and water resources potential in relation to climate change impact, increasing agricultural water demand, and the provincial water use policy. The climate change data, namely the daily maximum temperature, daily minimum temperature, and total daily precipitation are first analysed for changes in variability and extremes using frequency analysis techniques and STARDEX weather extreme indices. Analyses of the results suggest a warmer and wetter future climate in the Okanagan Basin

(Chapter 6). Next, the downscaled climate data are forced to MIKESHE and model outputs are analysed. The results show a drastic increase in surface runoff (35 to 100%) and a relatively milder increase in base flow (7 to 25%). However, the anticipated abundant water resource cannot be efficiently used for supplementary irrigation for two major reasons: i) the current water policy restricts surface water extraction ii) about 82% of the surface water is received during the periods when there is no need for supplementary irrigation. Therefore, according to the current water resource policy, the additional future agricultural water demand (1.8 Mm^3/year in the year 2050) should be covered by groundwater only. Although climate change is anticipated to positively impact the groundwater yield (an increase of about 0.6 Mm^3/year is expected), the increment is, unfortunately, not high enough to cover the projected agricultural water demand. Had it not been for the water policy in place however, this demand could have been supplied with the available surface water resource. In an attempt to explain why the groundwater aquifers are not yielding sufficient water to cover the increasing agricultural water demand, the saturated zone hydraulic head elevation are extracted at two different cross sections in the Deep Creek watershed during a typical pumping season. The groundwater levels so extracted are compared and contrasted with the screen levels of the existing pumping well networks in the confined and unconfined aquifer sections. The results suggest that the limited yield from the groundwater aquifers may not just be due to groundwater resource scarcity but due to the position of the groundwater wells in the aquifers – highlighting the need for detailed investigation of deep aquifers and deeper well installation. Hand in hand with the required aquifer investigation, continuous experimentation with more GCM and land use change scenarios is necessary to better

understand the water resource challenges in the basin, and thus to make a well informed decision about the necessary adaptation measures. It is important to note here that model results should always be interpreted in the eyes of the various uncertainties discussed in Section 2.2.3 (input data, model parameters and structure) as well as the lateral flux boundary conditions obtained from previous geochemistry studies [Nichol et al., 2011] (Section 4.4).

In summary, the findings of this study suggest that the water resources in the basin can sustainably be used provided that the water resource policy is changed. Construction of appropriate water harvesting structures and installation of pumping wells in the deep aquifers may also be taken as potential adaptation measures. The general message emphasizes the need to conjunctively understand surface water and potential yield from shallow and deep aquifers in relation to water demand, climate change impact, all sources and sinks including pumping well network conditions before devising water management strategies. The recharge estimation method developed here can be taken as a reliable platform to link groundwater and surface water, and thus to assist decision making related to water resources management and policy. The method can also play a key role in optimising aquifer yield, particularly in an evolving climate.

Reference List

Abbasi, F., J. Feyen, and M. T. Van Genuchten [2004], Two-dimensional Simulation of Water Flow and Solute Transport Below Furrows: Model Calibration and Validation, Journal of Hydrology 290 [1]: 63–79.

Abbaspour, K. C. [2008], SWAT-CUP2: SWAT Calibration and Uncertainty Programs - A User Manual. Department of Systems Analysis, Integrated Assessment and Modelling [SIAM], Eawag, Swiss Federal Institute of Aquatic Science and Technology, Duebendorf, Switzerland, 2008, 95pp.

Abbott, M. B., J. C. Bathurst, J. A. Cunge, P. E. O'Connell, and J. Rasmussen [1986], An Introduction to the European Hydrological system–Systeme Hydrologique Europeen, Journal of Hydrology 87 [1-2]: 45–59.

Alfonso R., M. A. Diana, and M. Harm [2004], Climate Variability and Change-Groundwater Resources. In: Threats to Water Availability in Canada [NWRI Scientific Assessment Report Series No 3 and ACSD Science Assessment Series No 1]. National Water Research Institute and Meteorological Service of Canada, Environment Canada -Science Liaison Branch, 128 p.

Assefa, K. A, A.Wei, and A. D. Woodbury [2011], The Impacts of Climate Change and Increasing Agricultural Demand on Water Resources in Deep Creek Watershed: MIKE SHE, submitted to: NSERC Strategic Project

Assefa, K. A., and A. D. Woodbury [2013], Transient, Spatially varied Ground water Recharge Modelling, Water Resources Research, 49, doi: 10. 1002/wrcr.

.20332.

British Columbia's Water Act Modernization [2010], Policy Proposal on British Columbia's new Water Sustainability Act. [Online]. Available [March 2013]: http://www.livingwatersmart.ca/water-act/docs/wam_wsa-policy-proposal.pdf

Cannon, A.J., P.H. Whitfield, and E.R. Lord [2002], Synoptic Map-Pattern Classification using Recursive Partitioning And Principal Component Analysis. Monthly Weather Review. 130[5]:1187-1206.

Carrera-Hernández, J.J., B.D. Smerdon, and C.A. Mendoza [2012], Estimating Groundwater Recharge through Unsaturated Flow Modelling: Sensitivity to Boundary Conditions and Vertical Discretization. Journal of Hydrology 452–453 [0] [July 25]: 90–101. doi:10.1016/j.jhydrol.2012.05.039.

Celia, M. A., E. T. Bouloutas, and R. L. Zarba [1990], A General Mass-conservative Numerical Solution for the Unsaturated Flow Equation, Water Resources Research 26 [7]: 1483–1496.

Chen, J., F. P. Brissette, and R. Leconte [2011], Uncertainty of Downscaling Method in Quantifying the Impact of Climate Change on Hydrology, Journal of Hydrology 401 [3]: 190–202.

Chung, S. O., and R. Horton [1987], Soil Heat and Water Flow with a Partial Surface Mulch, Water Resources Research 23 [12]: 2175–2186.

Déqué, M., D. Rowell, D. Luthi, F. Giorgi, J. Christensen, B. Rockel, D. Jacob, E. Kjellstrom, M. de Castro, and B. van den Hurk [2007], An Intercomparison of Regional Climate Simulations for Europe: Assessing Uncertainties in Model Projections, Climate Change, 81[S1], 53–70,doi:10.1007/s10584-006-9228-x.

De Vries, J. J., and I. Simmers [2002], Groundwater Recharge: An Overview of Processes and Challenges, Hydrogeology Journal 10 [1]: 5–17.

Durner, W. [1994], Hydraulic Conductivity Estimation for Soils with Heterogeneous Pore Structure, Water Resources Research 30 [2]: 211–224.

DHI [2007], MIKE 11 A Modelling System for Rivers and Channels User Guide Danish Hydraulic Institute, Denmark. [Online]. Available [November, 2012]: http://www.hydroeurope.org/jahia/webdav/site/hydroeurope/shared/Teams-2011/team1/Manuals/MIKE11_UserManual.pdf

DHI Cambridge [2011], Deep Creek Watershed Hydrologic Modelling, Cambridge, ON, Canada. Submitted to : NSERC Strategic Project

Environment Canada (2002), Canadian daily climate data, CDCD V1.01, Climate Information Branch, Atmospheric Environment Service, Ottawa, Ont.,Canada.

ESRI [2011], ArcGIS Desktop: Release 10. Redlands, CA: Environmental Systems Research Institute.

Feddes, R. A., P. J. Kowalik, and H. Zaradny [1978], Simulation of Field Water Use and Crop Yield. John Wiley & Sons, New York, NY.

Ferguson, G., A. D. Woodbury, and G.L. D. Matile [2003], Estimating Deep Recharge Rates Beneath an Interlobate Moraine Using Temperature Logs, Ground Water 41 [5] [October]: 640–646.

Fowler, H. J., S. Blenkinsop, and C. Tebaldi [2007], Linking Climate Change Modelling to Impacts Studies: Recent Advances in Downscaling Techniques for Hydrological Modelling, International Journal of Climatology 27 [12]: 1547–1578.

Flower, A., T. Q. Murdock, S. W. Taylor, and F. W. Zwiers [2013], Using an Ensemble of Downscaled Climate Model Projections to assess impacts of Climate Change on the Potential Distribution Of Spruce And Douglas-Fir Forests in British Columbia, Journal of Environmental Science 26 [63-74]:1462-9011.

Fulton, R. J. [2006], Geological Depositional Interpretations and the Impact of these on Trends in Hydraulic Properties of Identified Aquifers in the Deep Creek Drainage Basin, North Okanagan Valley. Contract Report with Ministry of Environment, BC, Canada.

Gardner, W. R [1962], Approximate Solution of a Non-Steady-State Drainage Problem, Soil Science Society of America Journal, 26, 129-132, 10.2136/sssaj1962.03615 9950026-00020011x.

Gebremeskel, S., Y. B. Liu, F. de Smedt, L. Hoffmann, and L. Pfister [2004], Analysing the Effect of Climate Changes on Streamflow Using Statistically Downscaled GCM Scenarios. International Journal of River Basin Management 2 [4] [December]: 271–280. doi:10.1080/15715124.2004.9635237.

Gebremeskel, S., Y.B. Liu, F. de Smedt, L. Hoffmann, and L. Pfister [2005]: Assessing the Hydrological Effects of Land Use Changes Using Distributed Hydrological Modelling and GIS, International Journal of River Basin Management, 3:4, 261-271

Gogolev, M. I. [2002], Assessing Groundwater Recharge with Two Unsaturated Zone Modelling Technologies., Environmental Geology 42 [2]: 248–258.

Gordon, C., C. Cooper, C. A., Senior, H. Banks, , J. M. Gregory, T. C. Johns, J. F. B. Mitchell and R.A Wood, [2000], The Simulation of SST, Sea Ice Extents and

Ocean Heat Transports in a Version of the Hadley Centre Coupled Model without Flux Adjustments , Clim. Dyn.16,147–168

Hansson, K., J. Simunek, M. Mizoguchi, L. C. Lundin, and M. T. Van Genuchten [2004], Water Flow and Heat Transport in Frozen Soil Numerical Solution and Freeze–Thaw Applications, Vadose Zone Journal 3 [2]: 693–704.

Hargreaves, G. H. [1994], Defining and Using Reference Evapotranspiration, Journal of Irrigation Drainage Engineering., 120[6], 1132–1139.

Hawkins, E., and R. Sutton [2009], The potential to narrow uncertainty in regional climate predictions, Bull. Am. Meteorol. Soc., 90(8), 1095–1107.

Hay, L. E., and M. P. Clark [2003], Use of Statistically and Dynamically Downscaled Atmospheric Model Output For Hydrologic Simulations in three Mountainous Basins in the Western United States, Journal of Hydrology, 282 [1-4] : 56–75.

Hayse, J. W. [2000], Using Monte Carlo Analysis in Ecological Risk Assessments. Interstate Technology, Regulatory Cooperation Work Group, and DNAPLs/Chemical Oxidation Work Team, Dense Non-Aqueous Phase Liquids [DNAPLs]: Review of Emerging Characterization and Remediation Technologies.

Hejazi, A., and A. D. Woodbury [2011], Evaluation of Land Surface Scheme SABAE-HW in Simulating Snow Depth, Soil Temperature and Soil Moisture Within the BOREAS Site, Saskatchewan, Atmosphere-Ocean 49 [4]: 408–420.

Hendriks, M.R. [2010]: Introduction to Physical Hydrology, Oxford University Press, Utrecht, The Netherlands, 331p.

Hillel, D. [2004]: Introduction to Soil Physics, Academic Press, New Delhi, India, 364 p.

Hollaender, H. M., T.Blume, H. Bormann, W. Buytaert, G.B. Chirico, J.F. Exbrayat, D. Gustafsson, H. Hölzel, P.Kraft, C. Stamm , S. Stoll, G. Blöschl, and H. Fluhler [2009a], Comparative Predictions of Discharge from an Artificial Catchment [Chicken Creek] using Sparse Data, Hydrology and Earth System Sciences, 13, 2069-2094, 10.5194/hess-13-2069-2009.

Hollaender, H. M., R. Mull and S.N. Panda [2009b], A Concept for Managed Aquifer Recharge Using ASR-Wells for Sustainable Use of Groundwater Resources in an Alluvial Coastal Aquifer In Eastern India, Physics and Chemistry of the Earth, Parts A/B/C, 34, 270-278, 10.1016/j.pce.2008.05.001.

IPCC [2000]: Emission Scenarios. Nakicenivic, N. and Swart, R. [Eds.], Cambridge University Press, Cambridge, UK, pp 570.

IPCC [2001], The scientific basis - Contribution of Working Group I to the Third Assessment Report Of The Intergovernmental Panel on Climate Change [IPCC], Cambridge University Press, Cambridge, United Kingdom and New York, NY, USA, pp 944. [Online]. Available [April 2012]: http://www.grida.no/climate/ipcc_tar/wg1/index.htm.

IPCC [2007], Climate change 2007: the physical science basis. In: Solomon S, Qin D, Manning M, Chen Z, Marquis M, Averyt, KB, Tignor M, Miller HL (eds) Contribution of working group I to the fourth assessment report of the intergovernmental panel on climate change. Cambridge University Press, Cambridge.

Janmaat, J., and M. Anputhas [2010], Land Use Change and Water Demand Estimation in Deep Creek Watershed, Irving K. Barber School of Arts and Sciences, University Of British Columbia, Okanagan.

Jimenez-Martinez, J., T.H. Skaggs, M.Th. van Genuchten, and L. Candela [2009] , A Root Zone Modelling Approach to Estimating Groundwater Recharge from Irrigated Areas. Journal of Hydrology 367: 138-149.

Jun, M., R. Knutti, and D. W. Nychka [2008], Spatial Analysis to Quantify Numerical Model Bias and Dependence: How many climate models are there?, Journal of the American Statistical Association, 103, 934–947.

Jyrkama, M. I., J. F. Sykes, and S. D. Normani [2002], Recharge Estimation for Transient Ground Water Modelling, Ground Water 40 [6]: 638–648

Jyrkama, M. I., and J. F. Sykes [2007], The Impact of Climate Change on Spatially Varying Groundwater Recharge in the Grand River Watershed [Ontario], Journal of Hydrology 338 [3-4]: 237–250.

Katz, R.. W., Brown, and G. Barbara [1992], Extreme Events in a Changing Climate: Variability is more important than Averages, Climate Change 21, Kluwer Academic Publishers, p289-302.

Kenney, E., and G. Frank [2010], Creating a Seamless Soil Data Set - Okanagan British Columbia, Western Region National Cooperative Soil Survey Conference, Las Vegas, Nevada, June 21-24.

Khire, M. V., C. H. Benson, and P. J. Bosscher [1997], Water Balance Modelling of Earthen Final Covers, Journal of Geotechnical and Geoenvironmental Engineering 123 [8]: 744–754.

Kleinen T, and Petschel-Held G [2007], Integrated Assessment of Changes in Flooding Probabilities due to Climate Change, Climate Change 81[3-4]:283–312.

Kosugi, K. [1994], Three-parameter Lognormal Distribution Model for Soil Water, Water Resources Research 30 [4]: 891–901.

Kundzewicz, Z. W., L. J. Mata, N. W. Arnell, P. D. O. Ll, B. Jimenez, K. Miller, T. Oki, Z. S. En, and I. Shiklomanov [2008], The Implications of Projected Climate Change for Freshwater Resources and their Management, Hydrological Sciences Journal, 53[1], 3–10.

Kunkel, R., and F. Wendland [2002], The GROWA98 Model for Water Balance Analysis in Large River Basins—The River Elbe Case Study, Journal of Hydrology, 259, 152-162, http://dx.doi.org/10.1016/S0022-1694[01]00579-0

Kurtzman, D., and B.R. Scanlon [2011], Groundwater Recharge through Vertisols: Irrigated Cropland vs. Natural Land, Israel, Vadose Zone Journal, 10[2], 662-674.

Lerner, D. N., A. S. Issar, and I. Simmers [1990], Groundwater Recharge: a Guide to Understanding and Estimating Natural Recharge. Heise Hannover, Germany.

Lettenmaier, D.P., K.L. Brettman, L.W. Vail, S.B. Yabusaki, and M.J. Scott [1992], Sensitivity of Pacific Northwest Water Resources to Global Warming, Northwest Environmental Journal 8[2]: 265-283.

Liggett, J. E., and D. M. Allen [2010], Comparing Approaches for Modelling Spatially Distributed Direct Recharge in a Semi-arid Region [Okanagan Basin, Canada], Hydrogeology Journal 18 [2]: 339–357.

Loukili, Y., A. D. Woodbury, and K. R. Snelgrove [2008], SABAE-HW: An Enhanced Water Balance Prediction in the Canadian Land Surface Scheme Compared with Existing Models, Vadose Zone Journal, 7, 865-877, 10.2136/vzj2007.0081.

Lu, X., M. Jin, M.Th. van Genuchten, and B. Wang [2011], Ground Water Recharge at Five Representative Sites In The Hebei Plain Of China: Case study. Ground Water 49[2]: 286-294.

Mastrociccoa, M., N. Colombania, E. Salemia, and G. Castaldelli [2010], Numerical Assessment of Effective Evapotranspiration From Maize Plots to estimate Groundwater Recharge in Lowlands, Agricultural Water Management: 97, 1389-1398.

McDonald, M.G., and A.W. Harbaugh [1988], A Modular Three-Dimensional Finite-Difference Ground-Water Flow Model: Techniques of Water-Resources Investigations of the United States Geological Survey, Book 6, Chapter A1, 586 p.

Meehl, G.A., W.M. Washington, C.A. Ammann, J.M. Arblaster, T.M.L. Wigleym and C. Tebaldi [2004], Combinations of Natural and Anthropogenic Forcings in Twentieth-Century Climate , Journal of Climate 17: 3721-3727.

Meehl, G.A., T. Karl, D.R. Easterling, S. Changnon, R. Pielke, Jr., D.Changnon, J. Evans, P.Ya. Groisman, T.R. Knutson, K.E. Knukel, L.O. Mearns, C. Parmesan, R. Pulwarty, T. Root, R.T. Sylves, P.Whetton, and F. Zwiers [2000], An Introduction To Trends In Extreme Weather And Climate Events: Observations, Socioeconomic Impacts, Terrestrial Ecological Impacts, And Model Projections. Bull. Am. Met.Soc., 81, 413-416.

Merritt, W. S., Y. Alila, M. Barton, B. Taylor, S. Cohen, and D. Neilsen [2006], Hydrologic Response to Scenarios of Climate Change in Sub Watersheds of the Okanagan Basin, British Columbia, Journal of Hydrology, 326[1–4]:79-108.

Miller K., D. Yates, C. Roesch, and D. J. Stewart [2005], Climate Change and Water Resources: A Primer for Municipal Water Providers, Boulder, USA: National for Atmospheric Research, Boulder CO, 83pp.

Mirza MMQ [2003], Climate Change and Extreme Weather Events: Can Developing Countries Adapt? Climate Policy Journal 3[3]:233–248.

Mualem, Y. [1976], A New Model for Predicting the Hydraulic Conductivity of Unsaturated Porous Media. Water Resources Research 12 [3]: 513–522.

Monahan, P. A. [2006], North Okanagan Aquifer Mapping Project. Unpublished report to water stewardship division of B.C. Ministry of Environment, Canada.

Monteith, J. L. (1965), Evaporation and Environment, in: Fogg, G.E. (Editor), The State and Movement of Water in Living Organisms, Symp. Soc. Exp. Biol., vol. 19, pp. 205–234, The Company of Biologists, Cambridge, U. K.

Neilsen, D., G. Duke, W. Taylor, J. Byrne, S. Kienzle, and T. Van der Gulik [2010], Development and Verification of Daily Gridded Climate Surfaces in the Okanagan Basin of British Columbia. Canadian Water Resources Journal 35 [2]: 131–154.

Nichol, C., J. Ping, S. Kneisel, A.Collins,and N. Pyett [2011], Surface water–groundwater interactions and aquifer geochemical characterization. Earth and Environmental Sciences,Irving K. Barber School of Arts and Sciences,UBC Okanagan.

Obeysekera, J., M. Irizarry, J. Park, J. Barnes, and T. Dessalegne [2011], Climate Change And its Implications for Water Resources Management In South Florida, stochastic environmental research risk assessment journal, 25[4], 495–516.

Pancura, M., and G. S. Lines [2005], Variability and Extremes in Statistically Downscaled Climate Change Projections at Greenwood Nova Scotia. Meteorological Service of Canada, Atlantic Region Science Report Series 2005-10.

Ping, J., C. Nichol, and X. Wei [2010], Numerical groundwater modelling in the Deep Creek watershed [Final]. Report to BC Ministry of Environment. 208p.

Power, S. B., F. Delage, R. Colman, and A. Moise [2012], Consensus On Twenty-First-Century Rainfall Projections In Climate Models More Widespread Than Previously Thought, Journal of Climate, 25[11], 3792–3809.

Refsgaard, J. C. [1996], Terminology, Modelling Protocol and Classification of Hydrological Model Codes. In: M.B. Abbott and J.C. Refsgaard [Editors], Distributed hydrological modelling. Kluwer, Dordrecht, The Netherlands, pp. 77-39.

Samani, Z. [2000], Estimating Solar Radiation and Evapotranspiration using Minimum Climatological Data [Hargreaves-Samani Equation], Journal of Irrigation and Drainage Engineering 126 [4]: 265–267.

Sanford, W. [2002], Recharge and Groundwater Models: An Overview, Hydrogeology Journal 10 [1]: 110–120.

Scanlon, B. R., R. W. Healy, and P. G. Cook [2002], Choosing Appropriate Techniques for Quantifying Groundwater Recharge, Hydrogeology Journal 10 [1]: 18–39.

Scanlon, B. R., K. Keese, R. C. Reedy, J. Simunek, and B. J. Andraski [2003], Variations in Flow and Transport in Thick Desert Vadose Zones in Response to Paleoclimatic Forcing [0–90 Kyr]: Field Measurements, Modelling and Uncertainties, Water Resources Research 39 [7]: 1179.

Schaap, M. G., F. J. Leij, and M. T. van Genuchten [2001], ROSETTA: A Computer Program for Estimating Soil Hydraulic Parameters with Hierarchical Pedotransfer Functions, Journal of Hydrology 251 [3]: 163–176.
Scharnagl, B., J. A. Vrugt, H. Vereecken, and M. Herbst [2011], Bayesian Inverse Modelling of in Situ Soil Water Dynamics: Using Prior Information About the Soil Hydraulic Properties, Hydrology and Earth System Sciences Discussions 8 [1] [February 23]: 2019–2063. doi:10.5194/hessd-8-2019-2011.

Schoof, J. T., and S.C. Pryor [2005], Downscaling Temperature And Precipitation: A Comparison of Regression-Based Methods and Artificial Neural Networks, International Journal of Climatology, 21, 773-790, 10.1002/joc.655, 2001.

Schroeder, P. R., and D. C. Ammon [1994], The Hydrologic Evaluation of Landfill Performance [HELP] Model: User's Guide for Version 1. Risk Reduction Engineering Laboratory, Office of Research and Development, US Environmental Protection Agency.

Scott, R. L., W. J. Shuttleworth, T. O. Keefer, and A. W. Warrick [2000], Modelling Multiyear Observations of Soil Moisture Recharge in the Semiarid American Southwest, Water Resources Research 36 [8]: 2233–2247.

Seiler, KP, and J. GAT [2007], Groundwater Recharge from Run-off, Infiltration and Percolation [Water Science and Technology Library, Vol. 55], Recherche 67: 02.

Simmers, I. [Ed.] [1997], Recharge of Phreatic Aquifers In [Semi-] Arid Areas, IAH International Contributions to Hydrogeology, 19, AA Balkema, Rotterdam.

Simunek, J., M. Th. Van Genuchten, and M. Sejna [2005], The HYDRUS-1D Software Package for Simulating the One-dimensional Movement of Water, Heat, and Multiple Solutes in Variably-saturated Media. University of California, Riverside, Research Reports 240.

Simunek, J., M.Th. van Genuchten, and M. Sejna [2008], Development and Applications of the HYDRUS and STANMOD Software Packages and Related Codes. Vadose Zone Journal 7: 587-600.

Simunek, J., M.Th. van Genuchten, and M. Sejna [2012], HYDRUS: Model use, Calibration and Validation, American Society of Agricultural and Biological Engineers , 55[4]: 1261-1274.

Sivakumar, B. [2009], Nonlinear Dynamics and Chaos in Hydrologic Systems: Latest Developments and a Look Forward. Stochastic Environmental Research and Risk Assessment 23:1027–1036.

Sivakumar, B. [2011], Global Climate Change and its Impacts on Water Resources Planning and Management: Assessment and challenges, stochastic environmental research risk assessment journal, 25[4], 583–600

Smerdon, B. D., C. A. Mendoza and K. J. Devito [2008], Influence of Subhumid Climate and Water Table Depth on Groundwater Recharge in Shallow Outwash Aquifers, Water Resources Research 44 [8]: n/a–n/a.doi:10.1029/2007WR005950

Summit Environmental Consultants Inc. [2010], Okanagan Water Supply and Demand Project: Phase 2 Summary Report [Online] Available [May 2013]: http://www.obwb.ca

Toews, M. W. and D. M. Allen [2009], Evaluating Different GCMs for Predicting Spatial Recharge in an Irrigated Arid Region, Journal of Hydrology 374 [3]: 265–281.

Towler, E., B. Rajagopalan, E. Gilleland, R. S. Summers, D. Yates, and R. W. Katz [2010], Modelling Hydrologic and Water Quality Extremes in a Changing Climate: A Statistical Approach Based on Extreme Value Theory, Water Resources Research, 46[11]:]: n/a–n/a. doi:10.1029/2009WR008876.

Stahl, K., R. D. Moore, J. M. Shea, D. Hutchinson, and A. J. Cannon [2008], Coupled Modelling of Glacier and Stream Flow Response to Future Climate Scenarios. Water Resources Research., 44, W02422, doi: 1 0.1 029/2007WR005956.

STARDEX [2004], Statistical and Regional Dynamical Downscaling of Extremes for European Regions. [Online]. Available [June 2012]: http://www.cru.uea.ac.uk/cru/projects/stardex/

Valiantzas, J. D., and P. A. Londra [2008], Direct Determination of the Brooks-Corey Hydraulic Functions by Fitting an Extended Power Function to the Outflow Method Data, Journal of Hydrology 362 [1-2]: 128–133.

Vandenbohede, A. and E. Van Houtte [2012], Heat Transport and Temperature Distribution During Managed Artificial Recharge with Surface Ponds, Journal of Hydrology S0022169412008311.

Van der Gulik,T. and D.Neilson [2008], Agricultural Water Management in the Okanagan Basin, Presented at the One Watershed – One Water Conference, Kelowna, BC.

Van der Gulik, T., D. Neilson, and R. Fretwell [2010], Agriculture Water Demand Model, Report for the Okanagan Basin, BC.

Van Genuchten, M. T. [1980], A Closed-form Equation for Predicting the Hydraulic Conductivity of Unsaturated Soils, Soil Science Society of America Journal 44 [5]: 892–898.

Varni, M. R., and E. J. Usunoff [1999], Simulation of Regional-scale Groundwater Flow in the Azul River Basin, Buenos Aires Province, Argentina, Hydrogeology Journal 7 [2]: 180–187.

Wei, A. [2008], Water Sustainability under Climate Change and Increasing Demand: a One-Water Approach at the Watershed Scale, One Watershed – One Water Conference Abstracts, October 21 to 23, 2008, Kelowna, BC.

Wilby, R.L, L.E. Hay, and G.H. Leavesley [1999], A comparison of Downscaled and raw GCM output: Implications for Climate Change Scenarios in the San Juan River basin, Colorado, Journal of Hydrology 225: 67-91.

Wilby, R. L., C.W. Dawson, and E. M. Barrow [2002], SDSM—a Decision Support Tool for the Assessment of Regional Climate Change Impacts, Environmental Modelling and Software 17 [2]: 145–157.

Winter, T. C. [1999], Ground Water and Surface Water: a Single Resource, DIANE Publishing, Darby, PA.

Winter, T. C. [2001], The Concept of Hydrologic Landscapes, Journal of the American Water Resources Association 37 [2]: 335–349.

Woldemeskel, F. M., A. Sharma, B. Sivakumar, and R. Mehrotra [2012], An Error Estimation Method for Precipitation and Temperature Projections for Future Climates, Journal of Geophysical Research, 117, D22104.

Xu, C. [1999], Climate Change and Hydrologic Models: A review of Existing Gaps and Recent Research Developments, Water Resources Management 13 [5]: 369–382

APPENDICES

APPENDIX A: Variability and extremes

Appendix A -1 Statistics of daily maximum temperature

CGCM3-A2				
	1977-2006	2020's	2050's	2080's
Average	7.73	8.44	9.61	11.11
Std Deviation	10.29	10.31	10.65	10.99
Maximum	33.30	33.80	33.70	34.70
Minimum	-27.20	-27.30	-24.10	-24.50

HADCM3-B2				
	1977-2006	2020's	2050's	2080's
Average	7.73	9.19	8.41	11.48
Std Deviation	10.29	10.94	11.44	11.8
Maximum	33.3	33.3	35.8	35
Minimum	-27.2	-30.1	-28.9	-24

ECHAM5-B1				
	1977-2006	2020's	2050's	2080's
Average	7.73	8.16	8.84	9.90
Std Deviation	10.29	10.29	10.38	10.49
Maximum	33.30	33.00	34.30	35.80
Minimum	-27.20	-32.70	-30.00	-22.90

CGCM3-A2				
	1977-2006	2020's	2050's	2080's
Average	7.73	8.81	9.44	9.83
Std Deviation	10.29	10.66	10.63	11.12
Maximum	33.30	34.80	35.30	35.30
Minimum	-27.20	-25.80	-21.40	-20.20

Appendix A -2 Probability density functions for daily maximum temperature

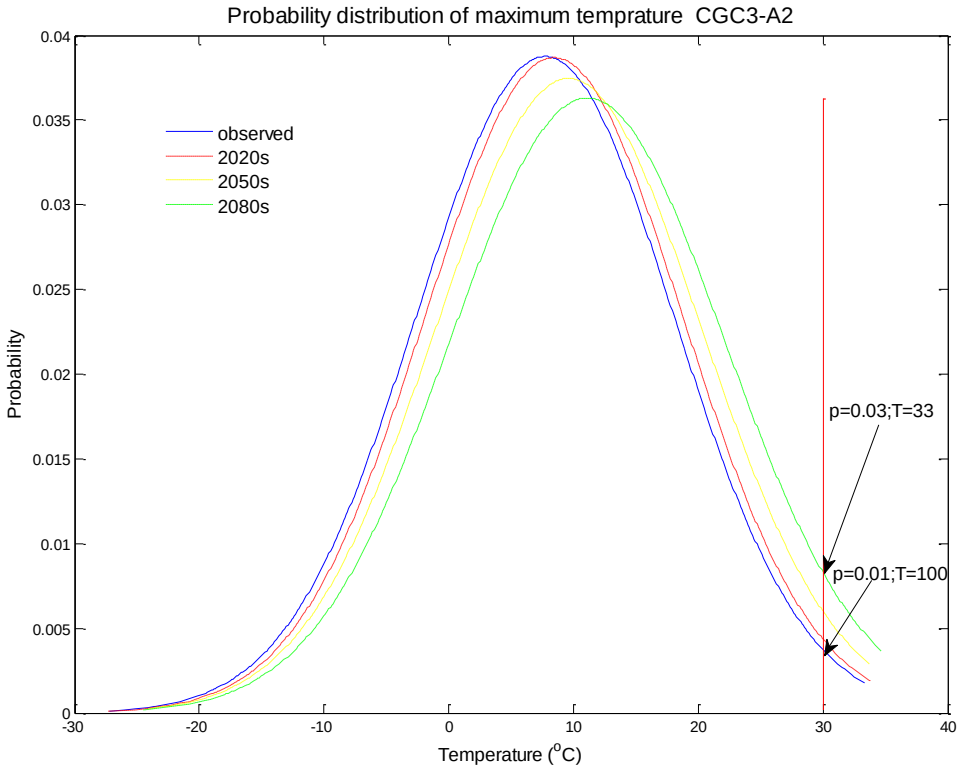

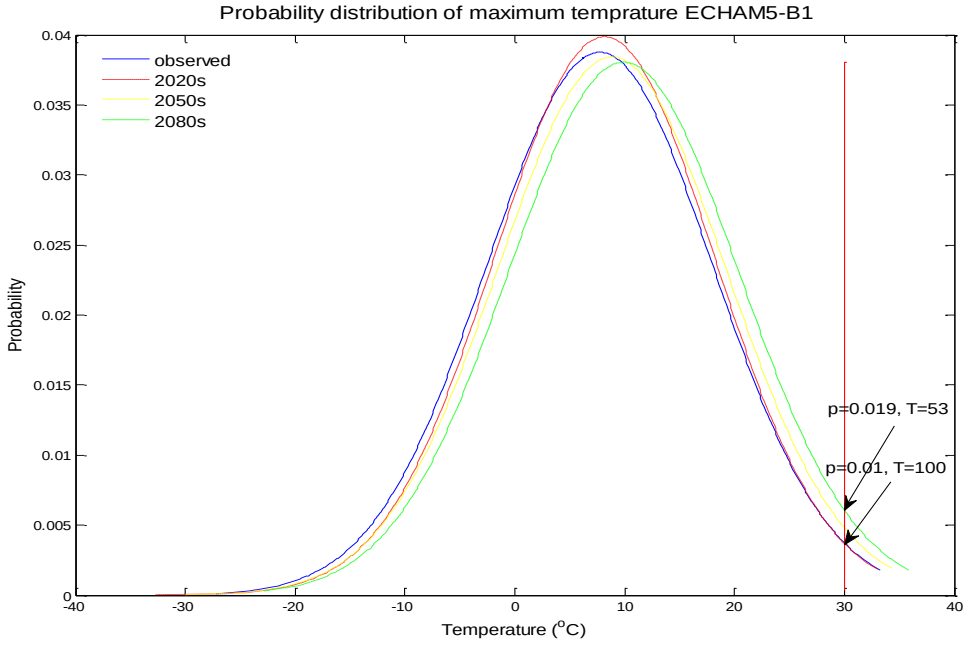

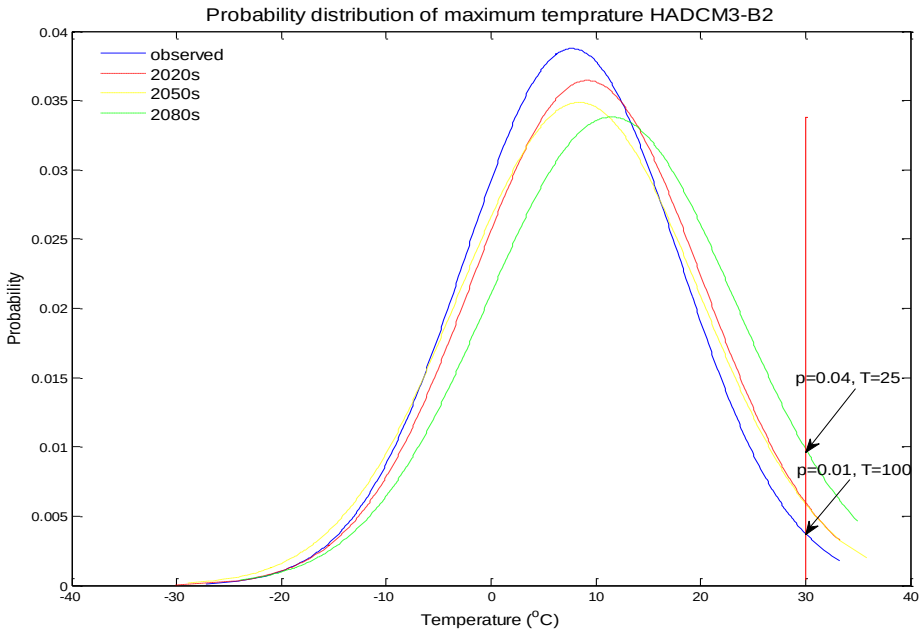
Probability distribution of maximum temprature HADCM3-B2
observed
2020s
2050s
2080s
p=0.04, T=25
p=0.01, T=100
Probability
Temperature (°C)

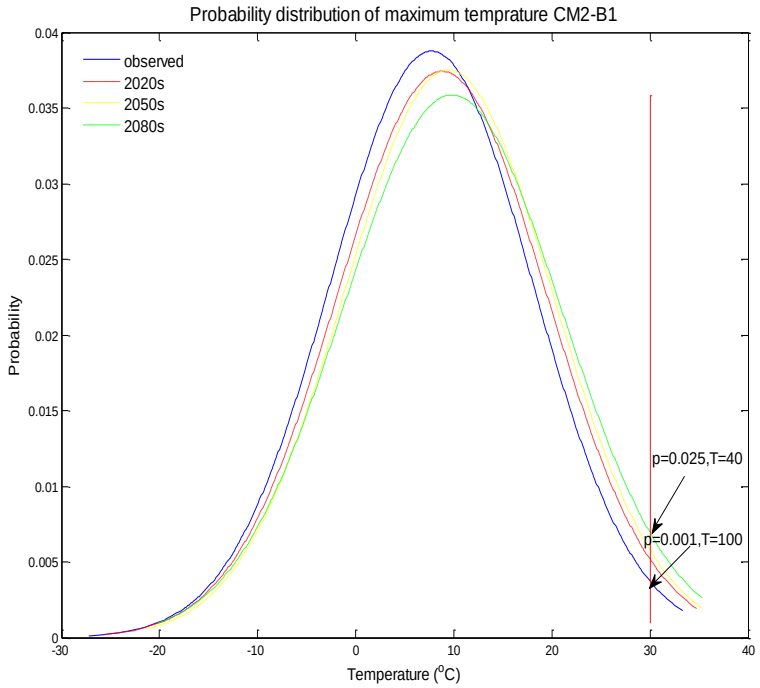
Probability distribution of maximum temprature CM2-B1
observed
2020s
2050s
2080s
p=0.025,T=40
p=0.001,T=100
Probability
Temperature (°C)

Appendix A -3 Statistics of daily minimum temperature

CGCM3-A2				
	1977-2006	2020's	2050's	2080's
Average	-2.1	-1.4	-0.4	0.9
Std Deviation	7.7	7.7	7.7	7.7
Maximum	19.9	20.8	20.3	23.6
Minimum	-39.0	-34.3	-34.7	-31.4

CM21-B1				
	1977-2006	2020's	2050's	2080's
Average	-2.08	-1.56	-0.97	-0.63
Std Deviation	7.67	7.74	7.69	8.14
Maximum	19.90	23.00	21.30	22.20
Minimum	-39.00	-35.10	-33.40	-32.10

HADCM3-B2				
	1977-2006	2020's	2050's	2080's
Average	-2.08	-1.12	-0.34	0.89
Std Deviation	7.67	8.27	9.13	9.05
Maximum	19.90	20.30	21.20	21.90
Minimum	-39.00	-36.60	-37.50	-34.30

ECHAM5-B1				
	1977-2006	2020's	2050's	2080's
Average	-2.08	-1.67	-1.01	-0.05
Std Deviation	7.67	7.67	7.67	7.75
Maximum	19.90	22.50	20.50	20.90
Minimum	-39.00	-39.50	-42.20	-34.50

Appendix A - 4 Probability density functions for daily minimum temperature

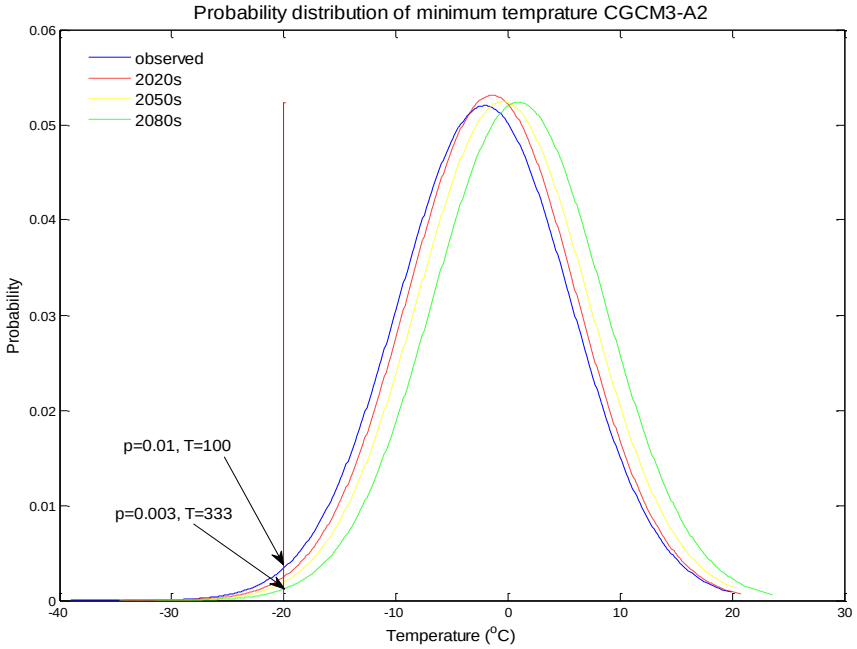

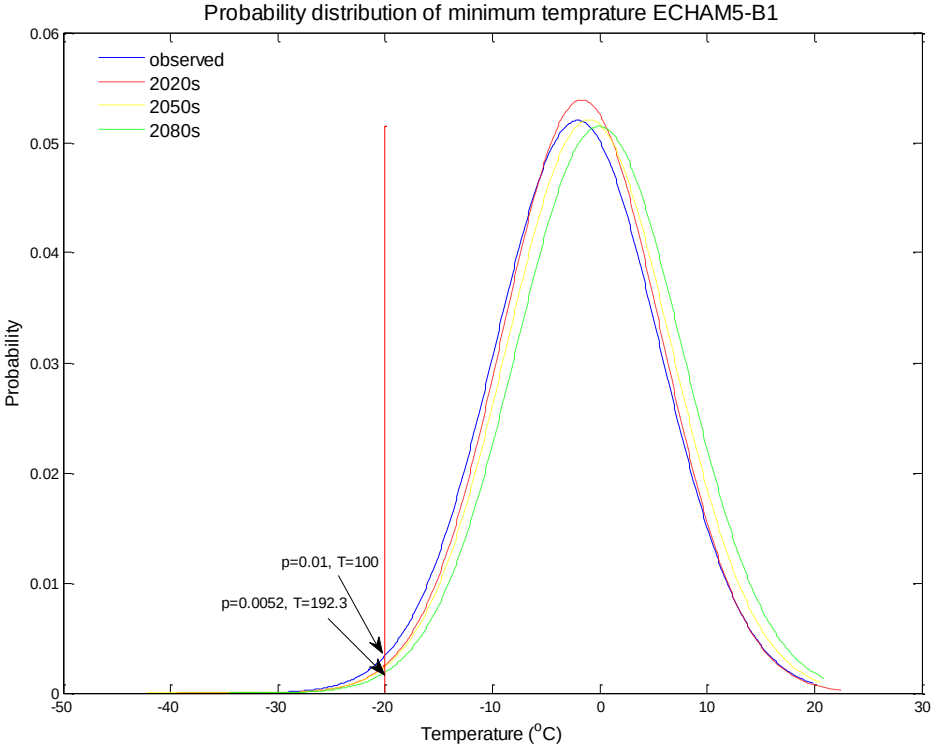

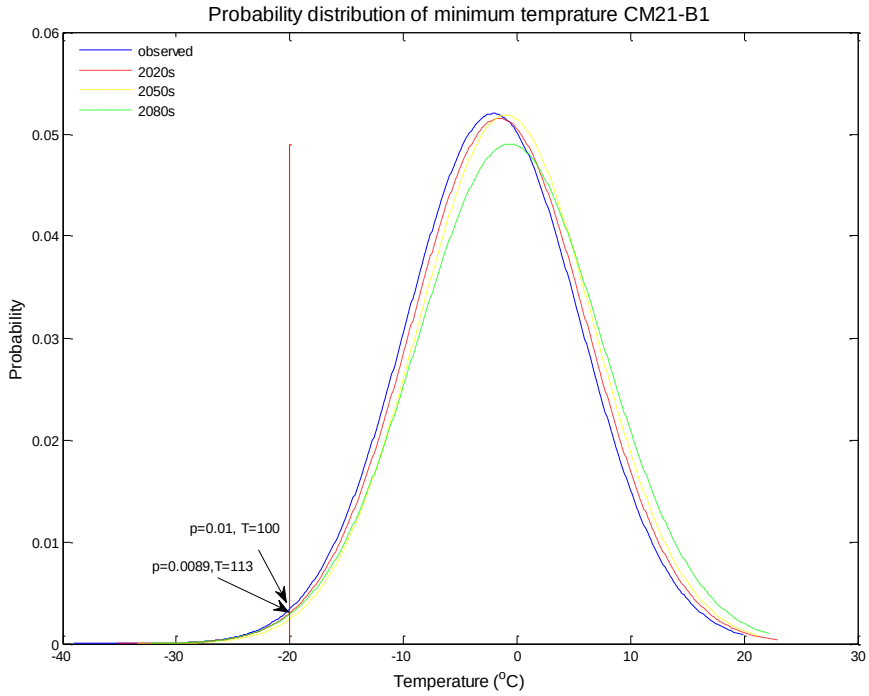
Probability distribution of minimum temprature CM21-B1
observed
2020s
2050s
2080s
p=0.01, T=100
p=0.0089,T=113
Probability
Temperature (°C)
0.06
0.05
0.04
0.03
0.02
0.01
0
-40
-30
-20
-10
0
10
20
30

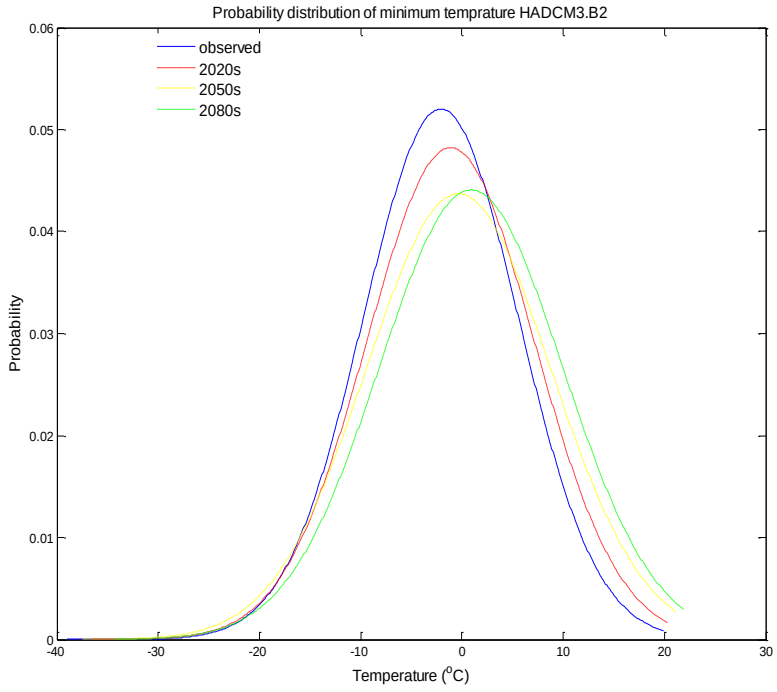
Probability distribution of minimum temprature HADCM3.B2
observed
2020s
2050s
2080s
Probability
Temperature (°C)
0.06
0.05
0.04
0.03
0.02
0.01
0
-40
-30
-20
-10
0
10
20
30

Appendix A– 5 Changes in projected number of cold days per year

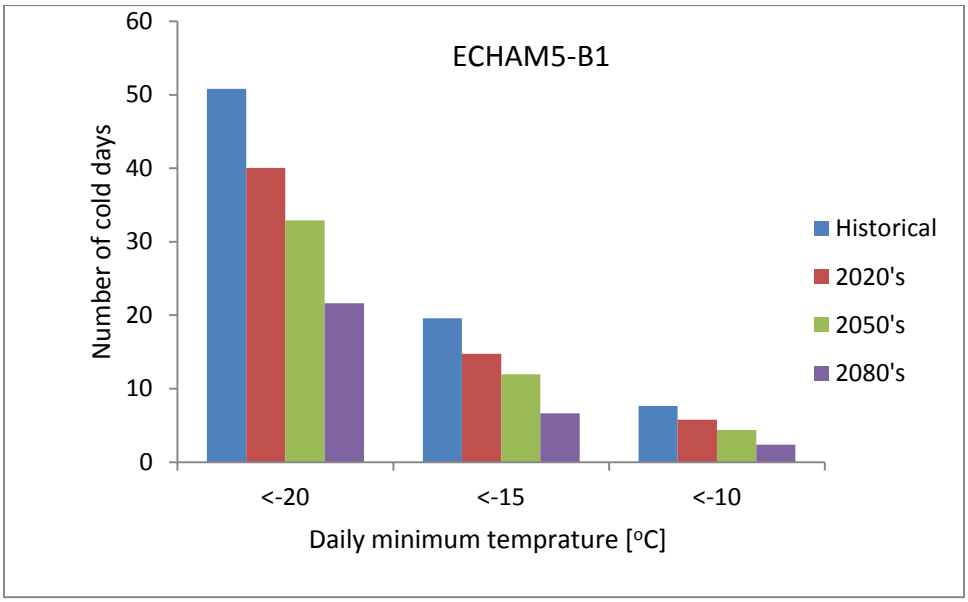

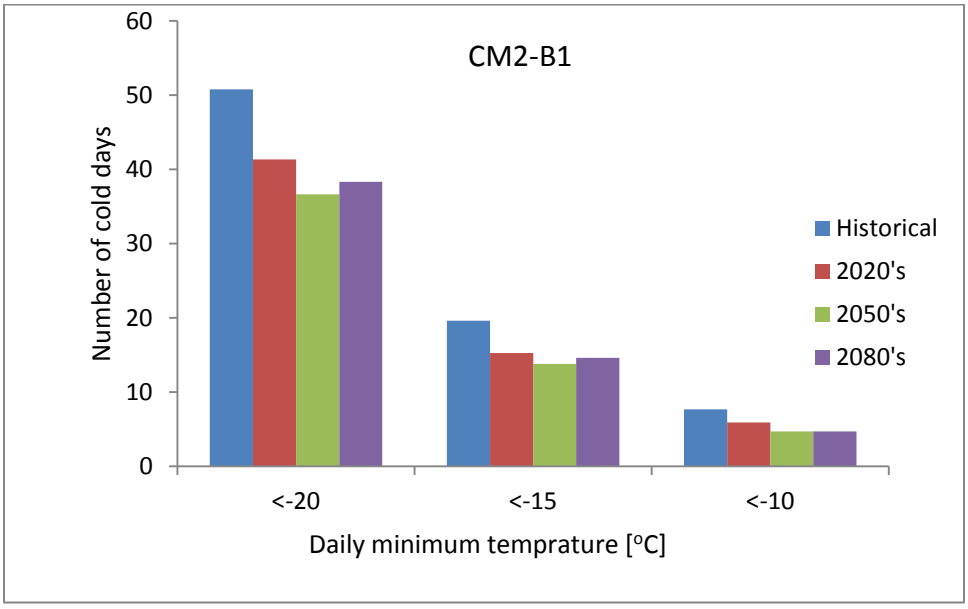

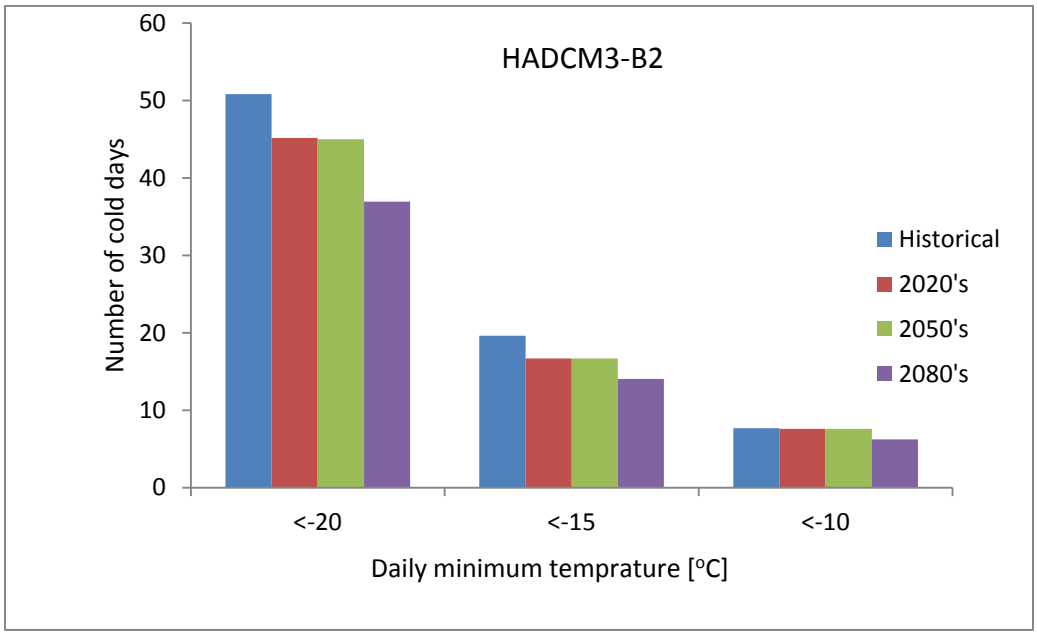
HADCM3-B2
Number of cold days
60
50
40
30
20
10
0
<-20
<-15
<-10
Daily minimum temprature [°C]
Historical
2020's
2050's
2080's

Appendix A– 6 Frequency analysis: annual daily maximum precipitation versus return period

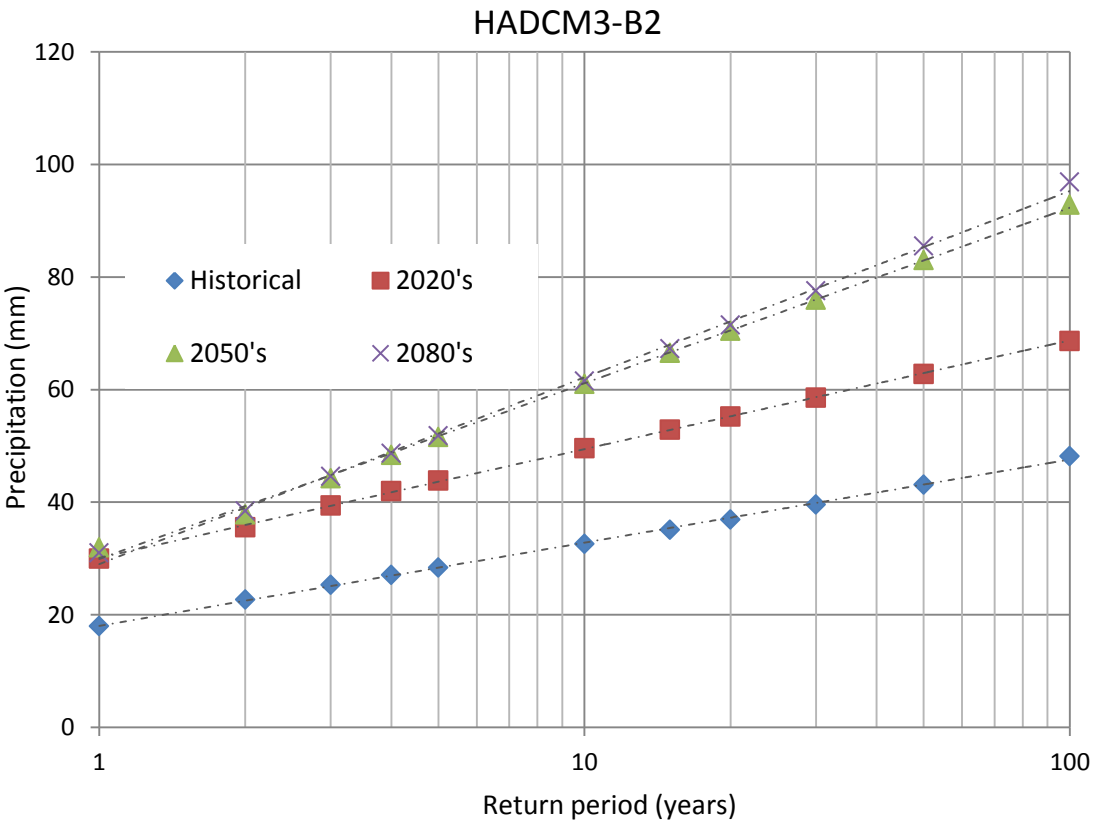

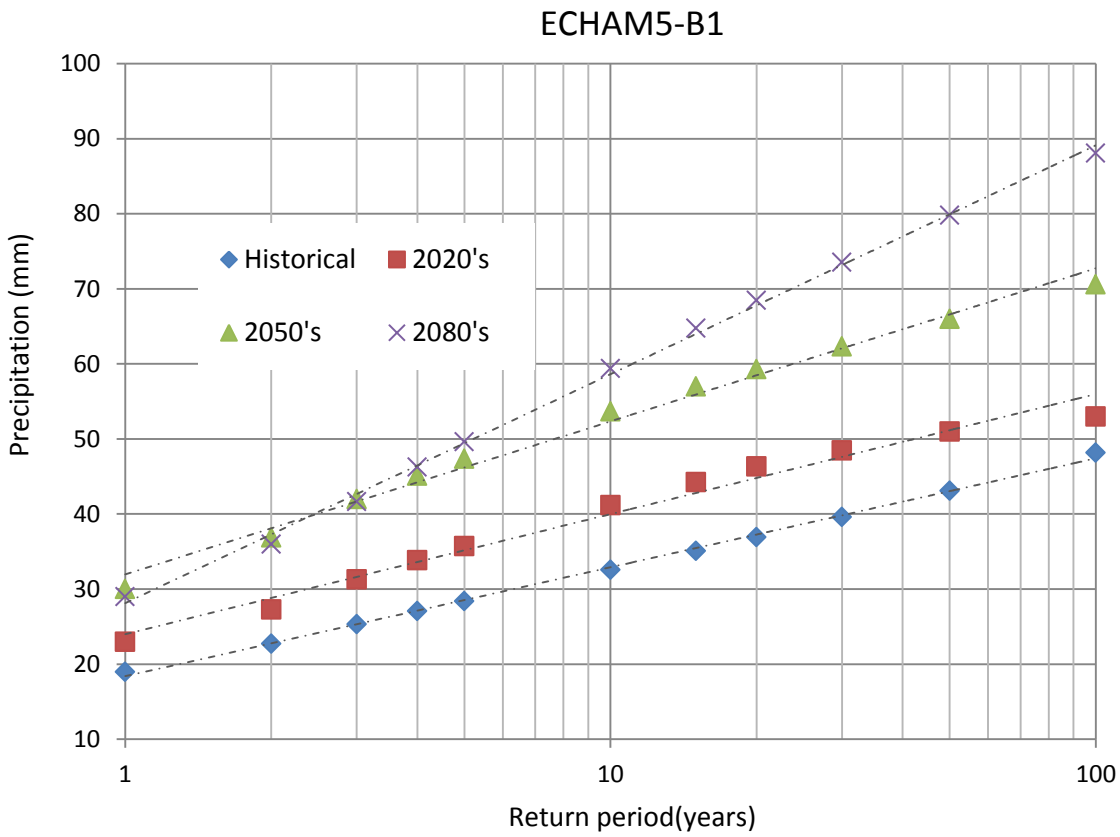
ECHAM5-B1
Precipitation (mm)
100
90
80
70
60
50
40
30
20
10
1
10
100
Return period(years)
Historical
2020's
2050's
2080's

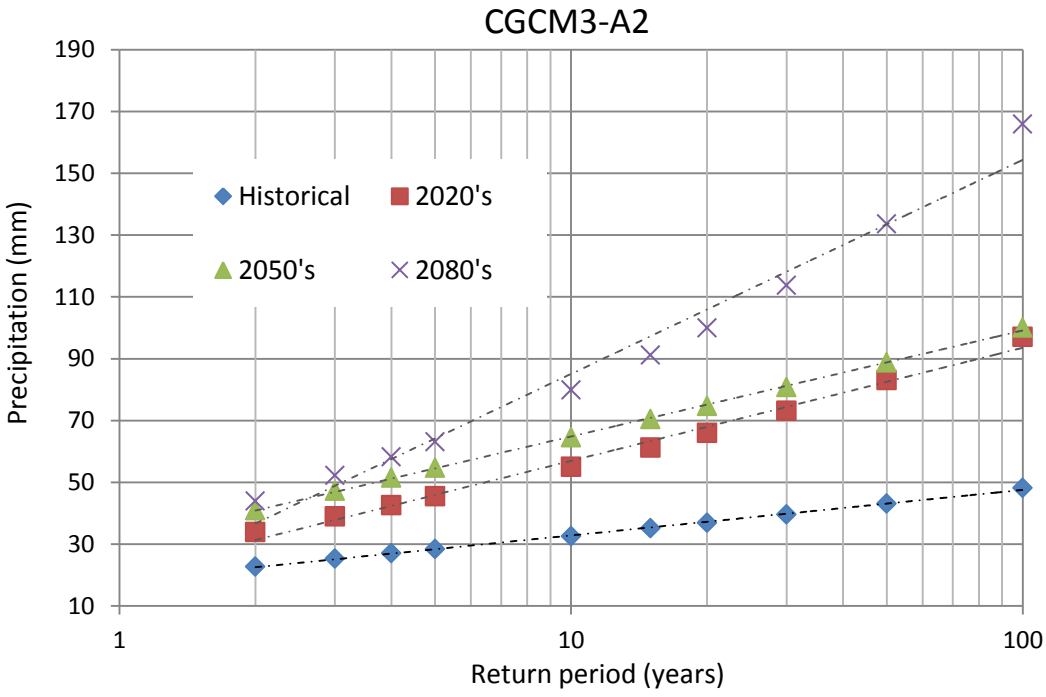
CGCM3-A2
Precipitation (mm)
190
170
150
130
110
90
70
50
30
10
1
10
100
Return period (years)
Historical
2020's
2050's
2080's

Appendix A– 7 Statistics of STARDEX extreme index [Tmax90p]

CGCM3-A2				
	1977 to 2006	2020's	2050's	2080's
Average	22.52	23.58	25.25	26.97
Std deviation	1.74	1.34	1.17	0.95
Maximum	26.32	26.10	27.35	28.20
Minimum	19.96	21.18	22.66	24.58

HADCM3-B2				
	1977 to 2006	2020's	2050's	2080's
Average	22.52	24.80	24.60	27.72
Std deviation	1.74	2.04	1.18	0.89
Maximum	26.32	18.96	22.36	24.80
Minimum	19.96	27.50	27.90	29.40

CM21-B1				
	1977 to 2006	2020's	2050's	2080's
Average	22.52	24.65	25.44	26.48
std Deviation	1.74	1.74	1.67	1.52
Maximum	26.32	27.26	27.90	29.90
Minimum	19.96	20.46	20.32	22.88

ECHAM5-B1				
	1977 to 2006	2020's	2050's	2080's
Average	22.52	22.62	24.19	25.13
std Deviation	1.74	1.47	1.63	1.63
Maximum	26.32	25.56	27.10	28.60
Minimum	19.96	20.35	20.00	21.60

Appendix A– 8 Statistics of STARDEX extreme index [Tmin10p]

CGCM3-A2				
	1977 to 2006	2020's	2050's	2080's
Average	-11.88	-10.52	-9.59	-7.88
std Deviation	1.54	1.63	1.10	1.09
Maximum	-9.10	-6.90	-7.66	-6.16
Minimum	-16.16	-15.90	-12.60	-10.50

HADCM3-B2				
	1977 to 2006	2020's	2050's	2080's
Average	-11.88	-11.07	-11.38	-10.14
std Deviation	1.54	1.37	1.58	1.5
Maximum	-9.1	-13.9	-15.42	-13.05
Minimum	-16.16	-8.5	-8.38	-6.75

CM21-B1				
	1977 to 2006	2020's	2050's	2080's
Average	-11.88	-10.88	-10.06	-10.39
std Deviation	1.54	1.87	1.65	1.79
Maximum	-9.1	-7.56	-7.16	-7.62
Minimum	-16.16	-14.84	-13.38	-14.32

ECHAM5-B1				
	1977 to 2006	2020's	2050's	2080's
Average	-11.88	-10.86	-10.56	-9.32
std Deviation	1.54	1.34	1.47	1.71
Maximum	-9.10	-8.40	-8.30	-5.50
Minimum	-16.16	-12.96	-13.76	-12.80

Appendix A–9 Statistics of STARDEX extreme index [125FD]

CGCM3-A2				
	1977 to 2006	2020's	2050's	2080's
Average	216.97	210.27	193.23	176.97
std Deviation	12.76	11.95	13.93	15.19
Maximum	241	234	228	226
Minimum	178	182	168	147

HAD3-B2				
	1977 to 2006	2020's	2050's	2080's
Average	216.97	201.2	190.23	171.77
std Deviation	12.76	13.67	15.48	14.89
Maximum	241	172	164	144
Minimum	178	230	222	208

ECHAM5-B1				
	1977 to 2006	2020's	2050's	2080's
Average	216.97	212.93	203	186.97
std Deviation	12.76	11.97	12.03	14.21
Maximum	241	234	230	213
Minimum	178	191	181	150

CM21-B1				
	1977 to 2006	2020's	2050's	2080's
Average	216.97	213.03	205.57	201.67
std Deviation	12.76	13.13	14.01	14.54
Maximum	241	241	233	229
Minimum	178	190	175	171

Appendix A–10 Statistics of STARDEX extreme index [Prec90p]

CGCM3-A2				
	1977 to 2006	2020's	2050's	2080's
Average [mm/day]	12.62	12.57	13.99	14.40
std Deviation	1.53	1.37	1.96	1.82
Maximum	17.14	16.42	18.60	17.95
Minimum	8.75	9.92	11.48	10.92

ECHAM5-B1				
	1977 to 2006	2020's	2050's	2080's
Average	12.62	13.07	13.69	14.51
std Deviation	1.53	1.53	1.61	2.13
Maximum	17.14	16.10	17.64	18.80
Minimum	8.75	9.80	10.63	9.42

CM21-B1				
	1977 to 2006	2020's	2050's	2080's
Average	12.62	12.30	12.61	13.26
std Deviation	1.53	1.77	1.24	1.46
Maximum	17.14	16.05	14.82	17.24
Minimum	8.75	7.60	10.14	10.80

HAD3-B2				
	1977 to 2006	2020's	2050's	2080's
Average	12.62	12.90	13.41	12.99
std Deviation	1.53	1.85	1.90	2.60
Maximum	17.14	9.82	9.90	8.06
Minimum	8.75	17.46	17.05	18.32

Appendix B: Projected total water budget using four GCM scenarios [mm]

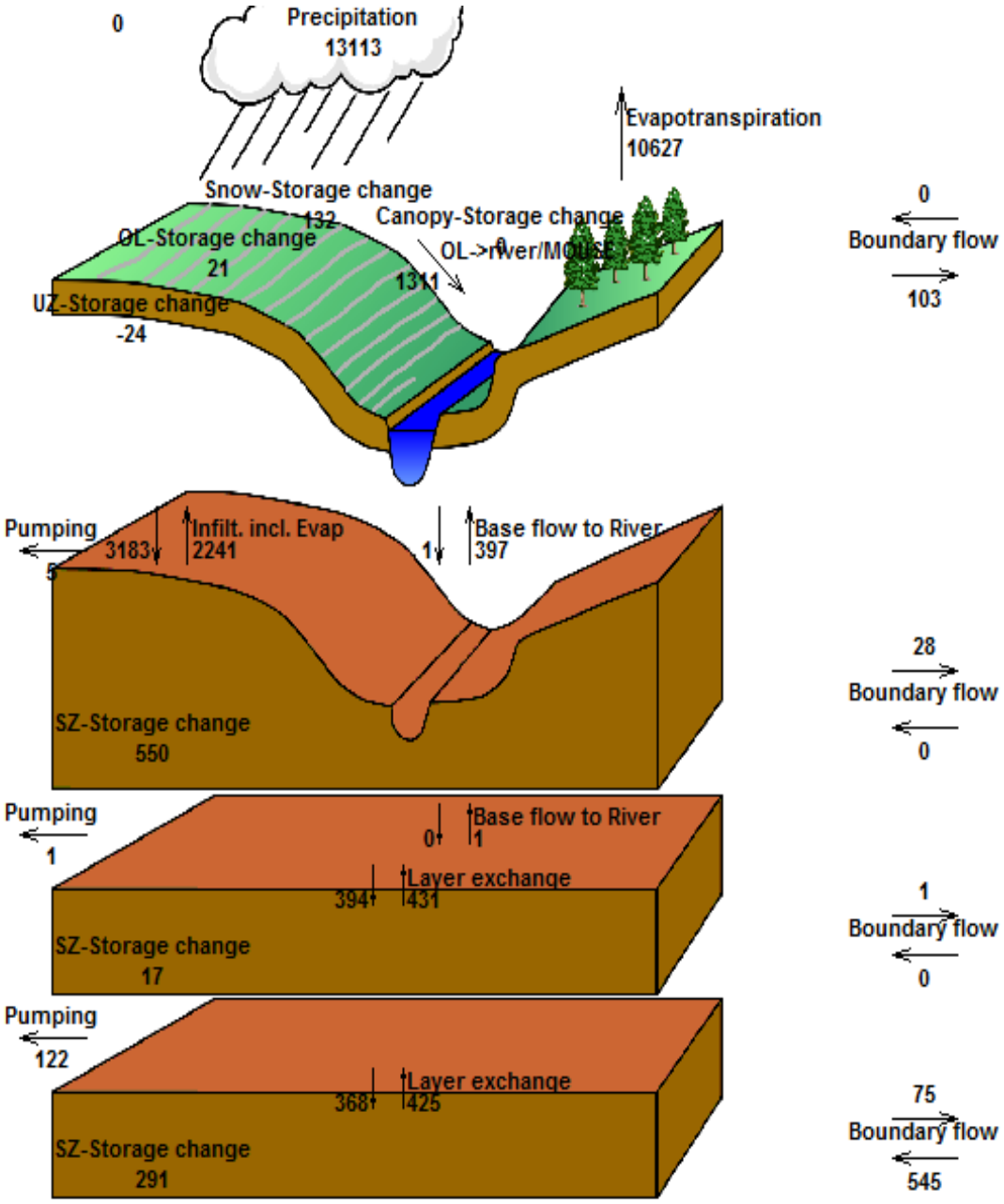

ECHAM5-B1: 2010 to 2029

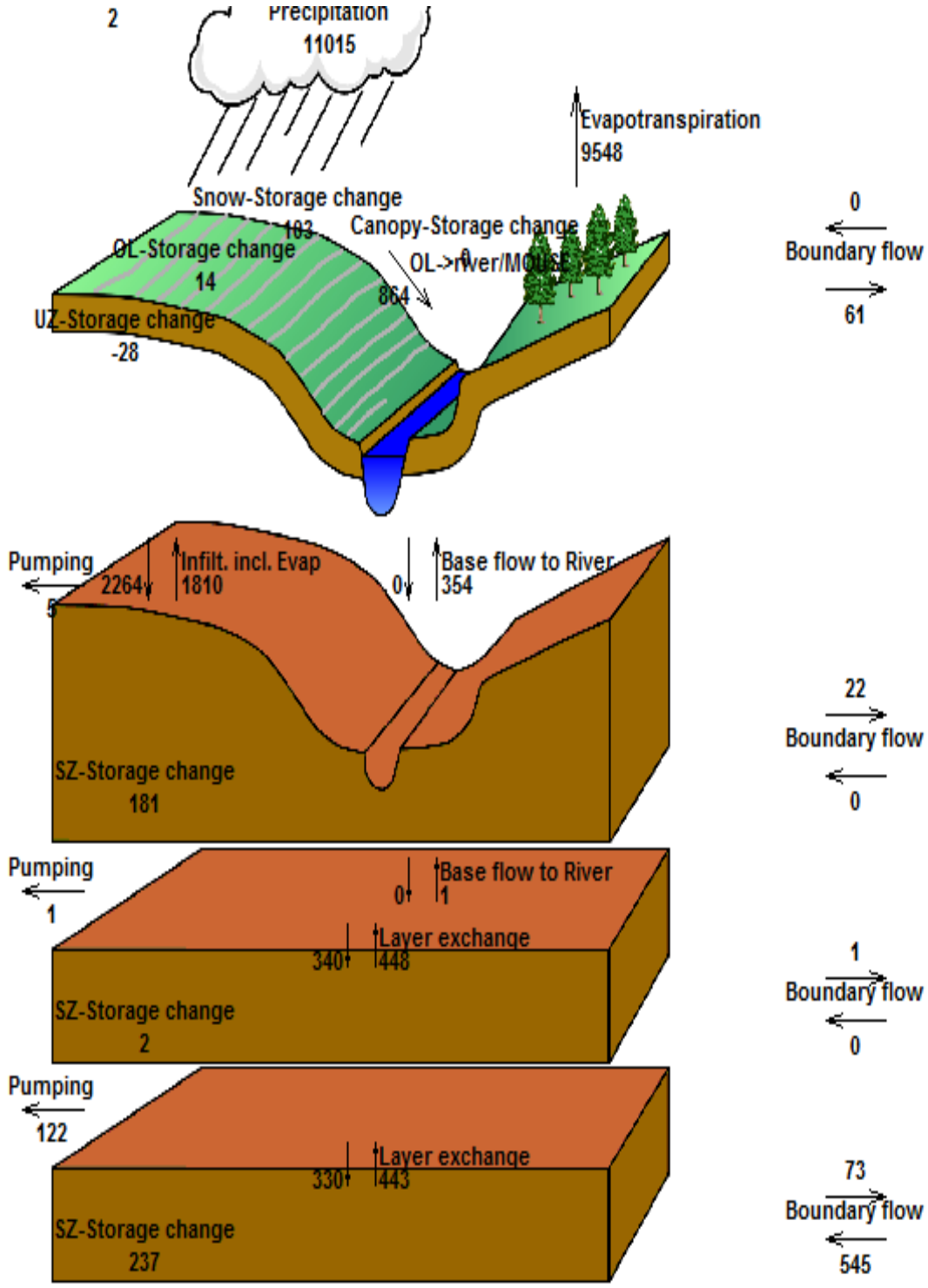

CM2-B1: 2010 to 2029

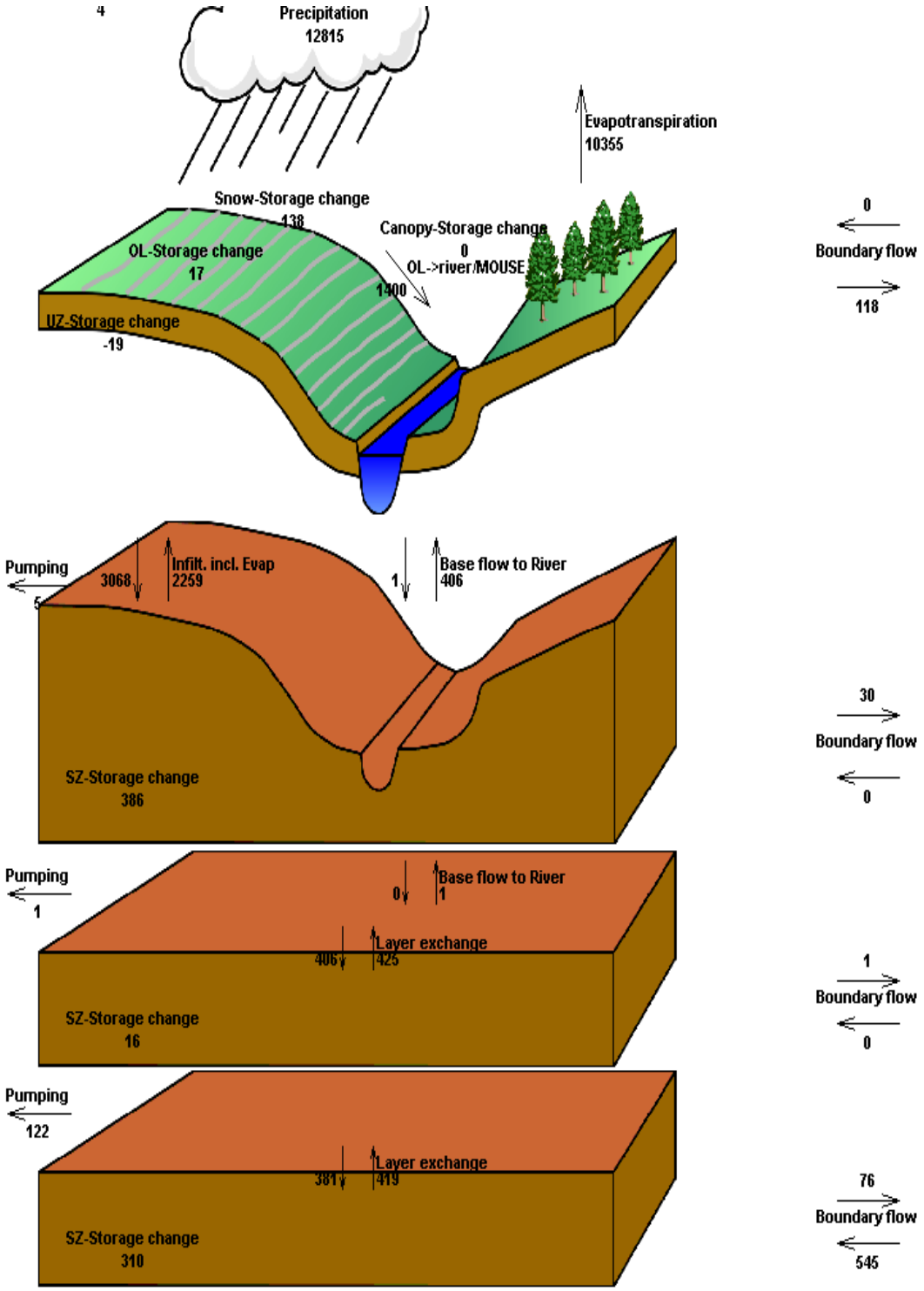

CGC3A2: 2010 to 2029

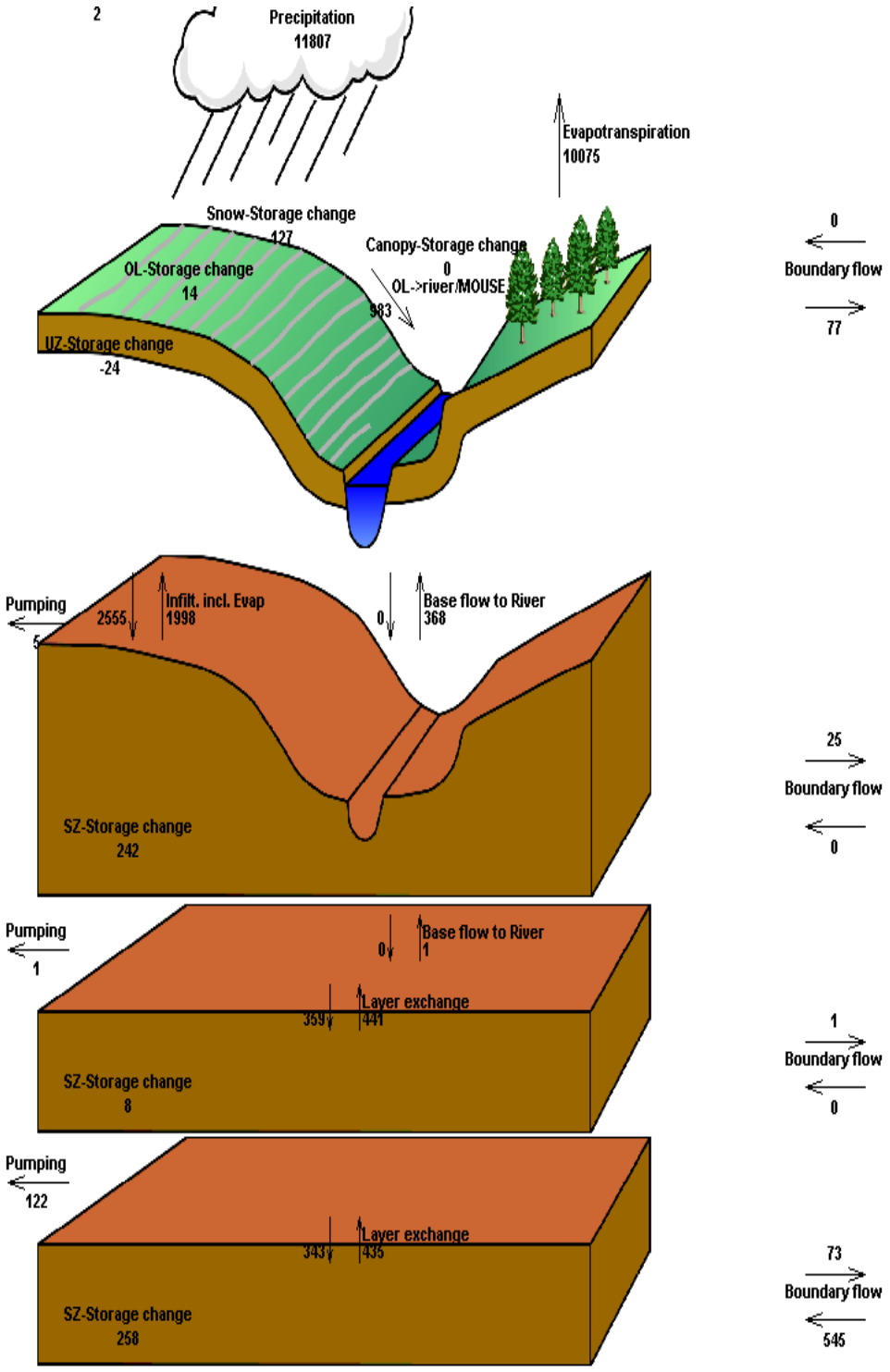

H3B2: 2010 to 2029

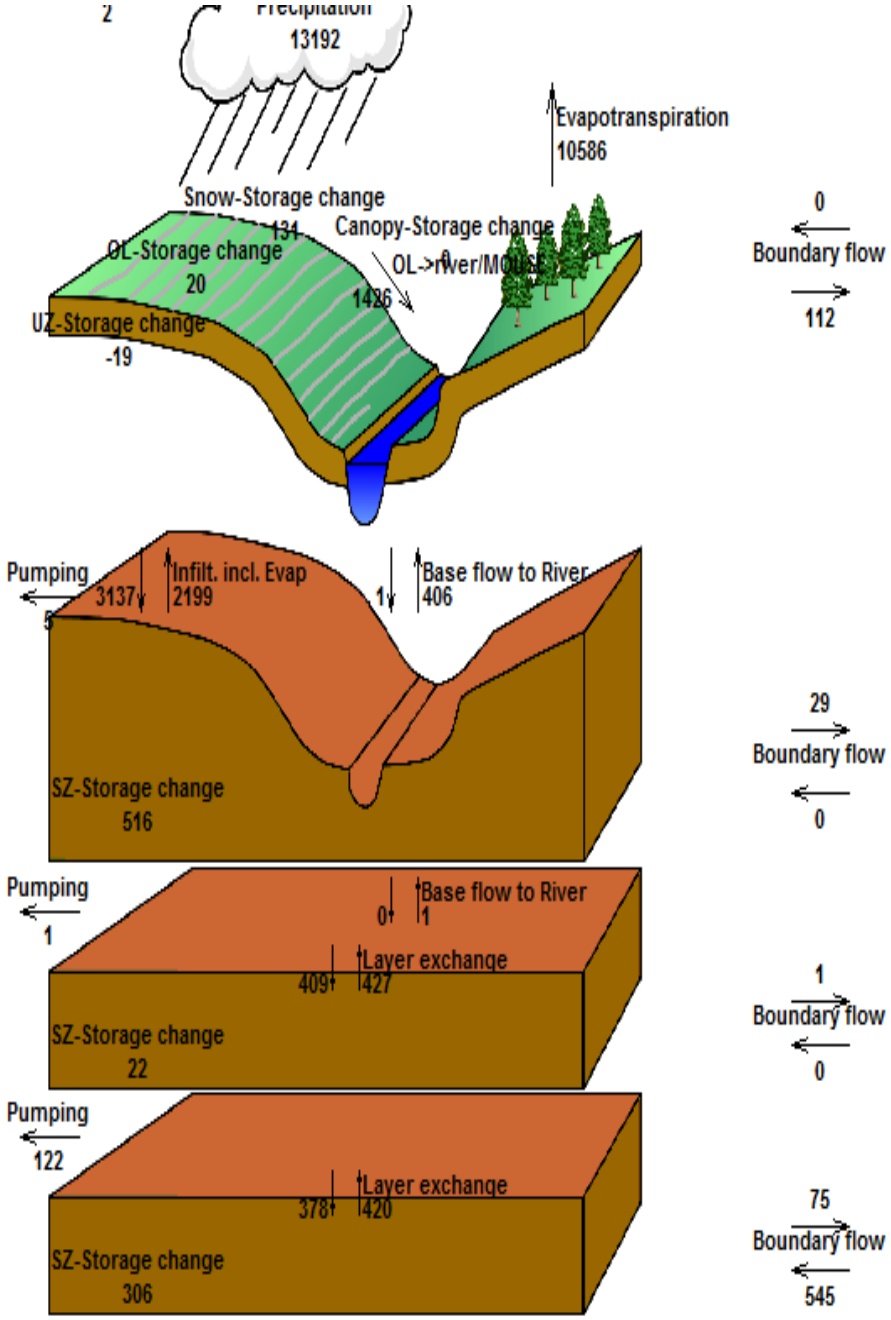

ECHam5B1: 2030 to 2049

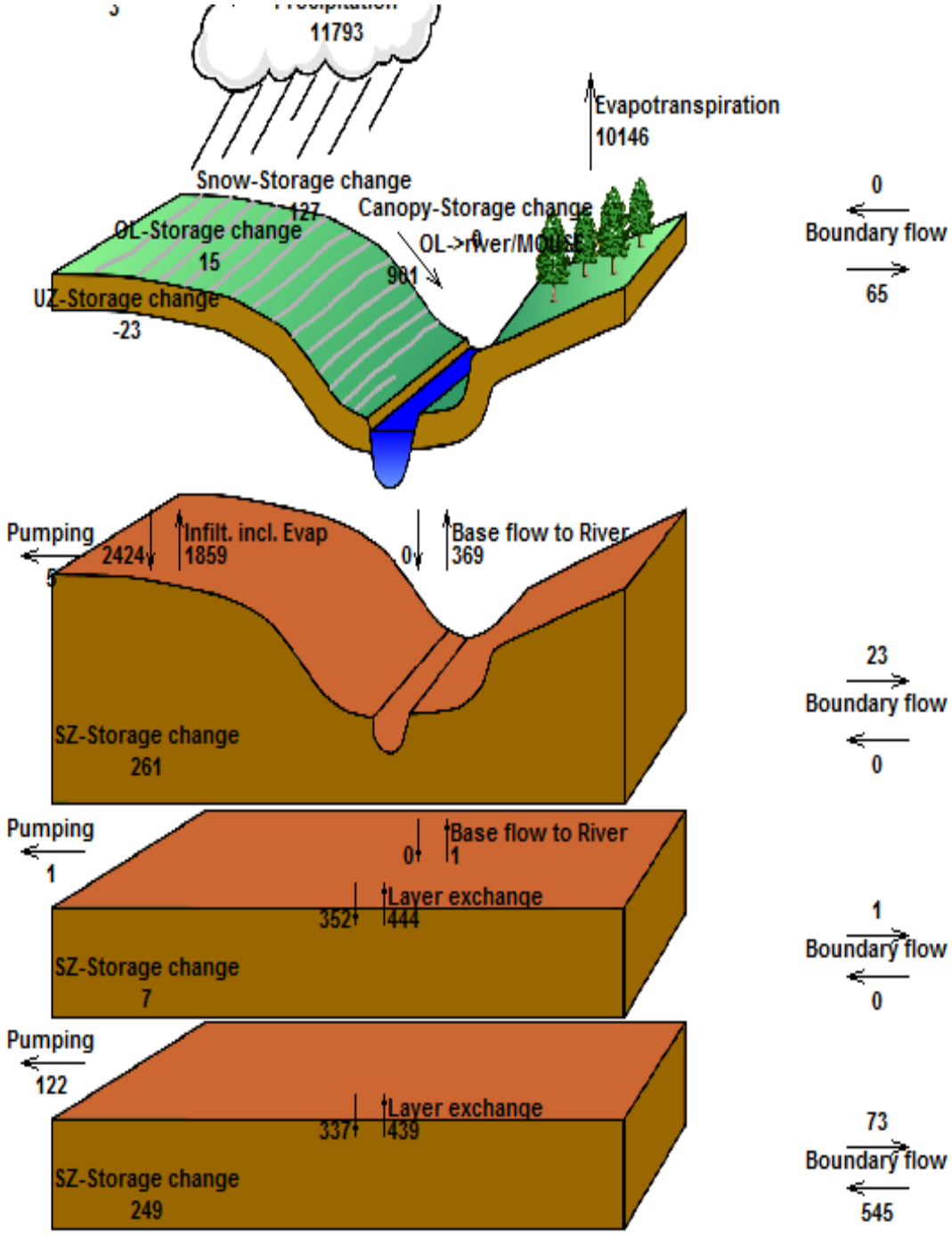

CM2B1: 2030 to 2049

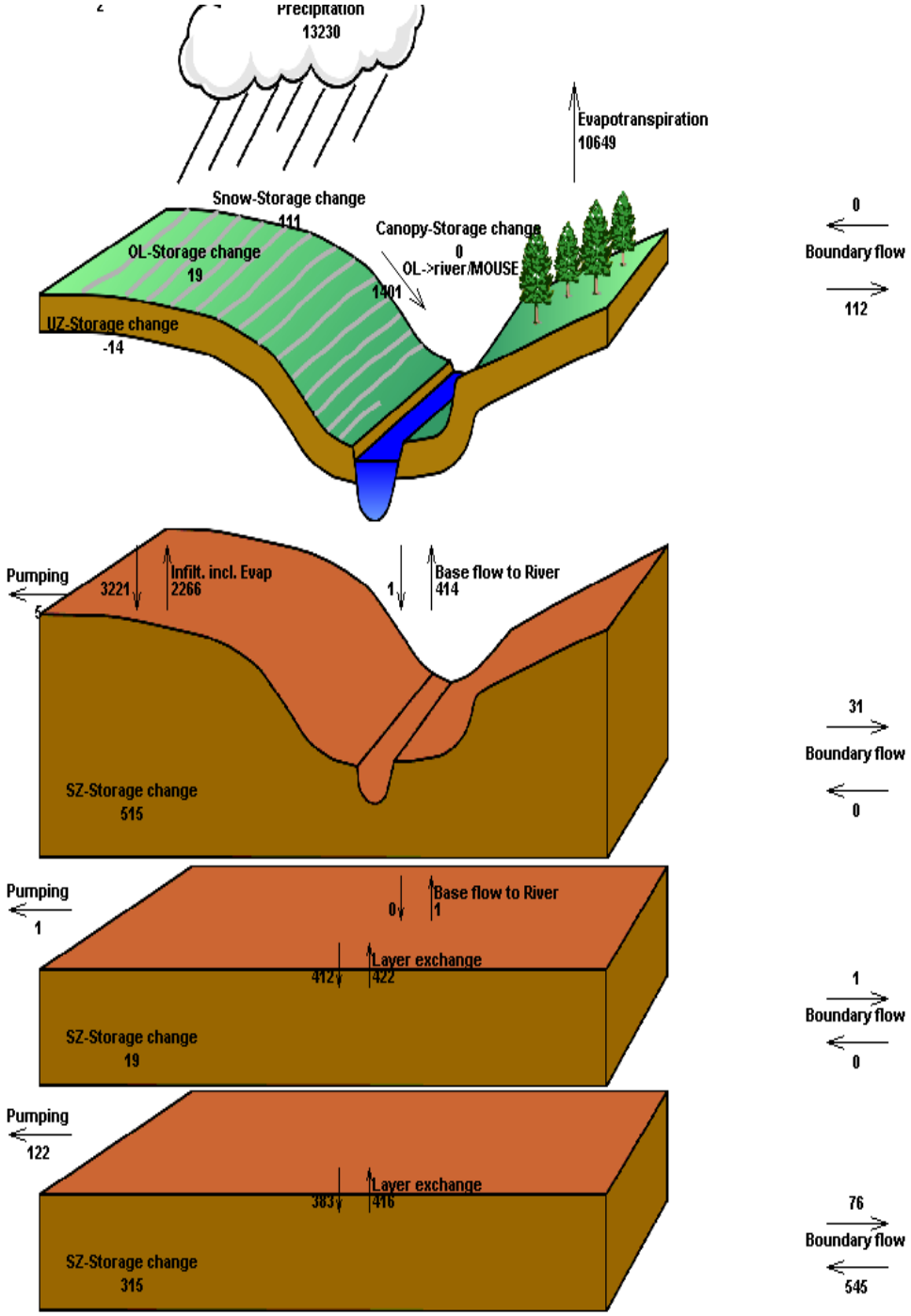

CG3A2: 2030 to 2049.

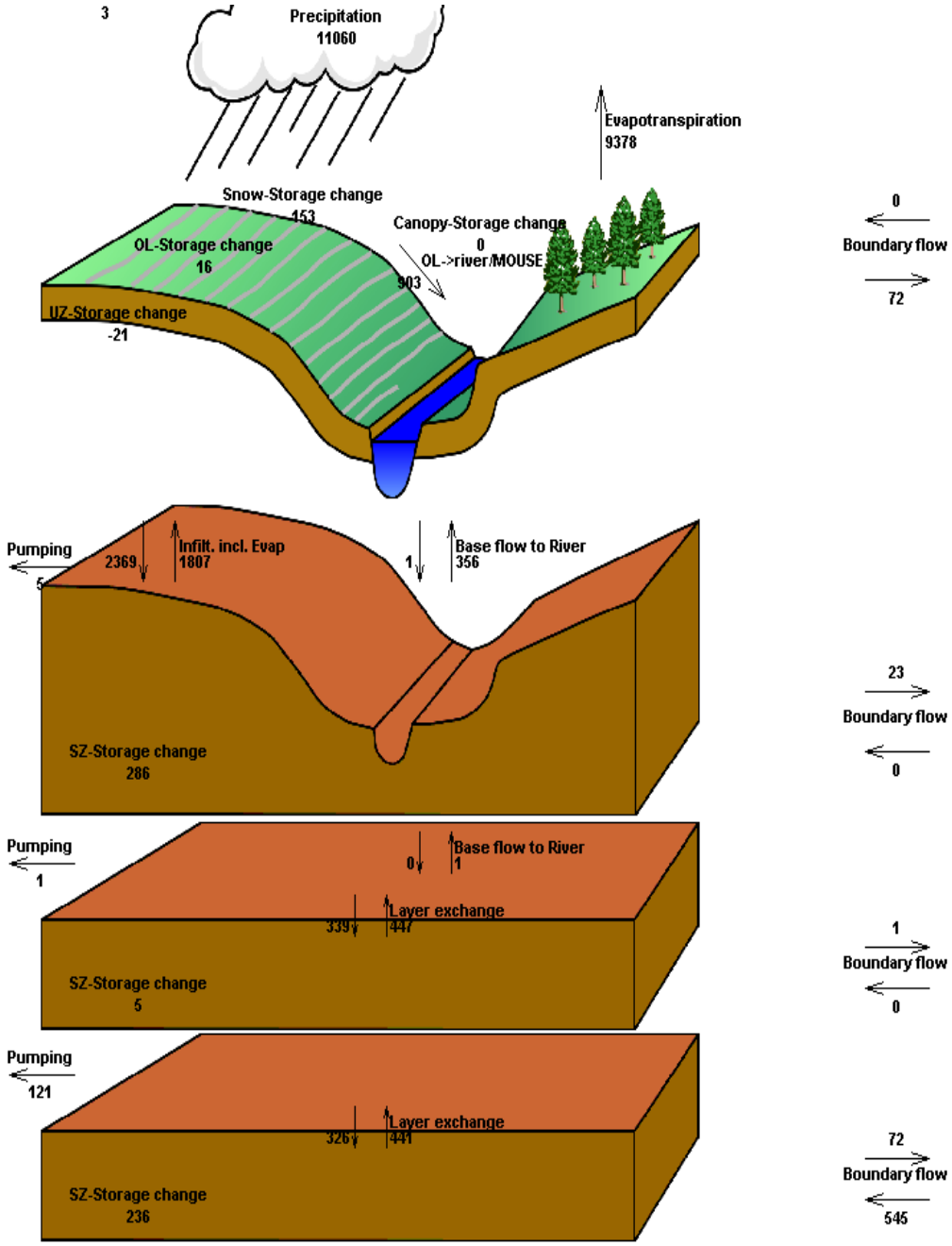

H3B2: 2030 to 2049